

Supplementary Information: The segregation of transition metals to iron grain boundaries and their effects on cohesion

Han Lin Mai ^{1,a}, Xiang-Yuan Cui ^{2,a}, Daniel Scheiber ^{3,b}, Lorenz Romaner ^{4,c},
Simon P. Ringer ^{5,a}

^a*The University of Sydney, Faculty of Engineering, School of Aerospace, Mechanical and Mechatronic Engineering & Australian Centre for Microscopy and Microanalysis, 2006 New South Wales, Australia*

^b*Materials Center Leoben Forschung GmbH, Roseggerstraße 12, 8700 Leoben, Austria*

^c*Department of Materials Science, University of Leoben, Franz-Josefstraße 18, 8700 Leoben, Austria.*

1. Functional selection

Functional	a_0 (Å)	bulk modulus (GPa)	magnetic moment (μ_B)
AM05	2.785	223	2.114
LDA	2.748	255	1.931
PBE	2.832	197	2.196
PBESol	2.787	228	2.105
Perdew-Zunger	2.751	247	1.937
PW91	2.829	181	2.156
Experimental	2.853	173	2.219

Table S1: DFT functional comparison for the bcc-Fe properties of lattice parameter, bulk modulus and magnetic moment against measured experimental values.

Here it is clear that PW91 and PBE functionals both reproduce the experimental properties closely. The choice between the two reduces down to whether we want to replicate the lattice parameter (PBE) or the bulk modulus (PW91) more accurately. Due to the abundance of results in the literature that have used the PBE functional, we have chosen to use it in this study for the practical comparison of results.

¹han.mai@sydney.edu.au

²carl.cui@sydney.edu.au

³daniel.scheiber@mcl.at

⁴lorenz.romaner@unileoben.ac.at

⁵simon.ringer@sydney.edu.au

2. Finalised calculation details

Almost all calculation results were attained by using cells that included a vacuum. The details of these cells are presented in Table S2. Only the calculations regarding the excess volume and GB energy were calculated using GB cells without vacuum. The details of these cells are presented in Table S3.

System	n _{GB}	n _{SLAB}	a (Å)	b (Å)	c (Å)	l _{vac} (Å)	k-points
$\Sigma 3[110](1\bar{1}1)$	72	72	4.005	6.937	41.144	>11.1	$6 \times 3 \times 1$
$\Sigma 3[110](1\bar{1}2)$	48	48	4.005	4.904	44.620	>16.6	$6 \times 6 \times 1$
$\Sigma 9[110](2\bar{2}1)$	68	108	4.005	6.332	50.973	>17.4	$6 \times 4 \times 1$
$\Sigma 11[110](3\bar{3}2)$	42	44	4.005	4.696	50.973	>25.1	$6 \times 6 \times 1$

Table S2: The sizes of the cells (with vacuum) used in this study and their corresponding k-point meshes. These cells were used for all calculations except for the GB quantities of excess volume v_{exc} and GB energy (γ_{GB}). The $\Sigma 9[110](2\bar{2}1)$ utilised a similarly dimensioned bulk-slab structure without vacuum, hence the higher atom count in the slab structure.

System	n _{SLAB}	n _{GB}	a (Å)	b (Å)	c _{GB} (Å)	c _{bulk} (Å)	k-points	v _{exc} (Å)	γ_{GB} (J/m ²)
$\Sigma 3[110](1\bar{1}1)$	72	72	4.005	6.937	30.032	29.429	$8 \times 4 \times 1$	0.301	1.58
$\Sigma 3[110](1\bar{1}2)$	24	24	4.005	2.452	27.995	27.746	$5 \times 10 \times 1$	0.124	0.45
$\Sigma 9[110](2\bar{2}1)$	72	68	4.005	6.332	33.595	33.982	$8 \times 2 \times 1$	0.279	1.77
$\Sigma 11[110](3\bar{3}2)$	44	42	4.005	4.696	25.838	26.565	$6 \times 6 \times 1$	0.240	1.45

Table S3: The sizes of the cells (no vacuum) used in this study and their corresponding GB quantities of excess volume v_{exc} and GB energy (γ_{GB}). Excess volume and GB energy calculations were conducted using GB cells without vacuum.

GB	γ_{GB} (J/m ²)			W_{sep} (J/m ²)	
	This work	Literature		This work	Literature
$\Sigma 3[110](1\bar{1}1)$	1.58	1.46 [1] 1.52 [2, 3], 1.56 [4], 1.57 [5–7], 1.60 [8, 9], 1.61 [10], 1.66 [11], 1.79 [12]		3.81	3.65 [11], 3.78 [5], 3.86 [2], 4.60 [12]
$\Sigma 3[110](1\bar{1}2)$	0.45	0.34 [3], 0.43 [13, 14], 0.44 [15], 0.46 [16], 0.47 [17]		4.71	4.79 [18]
$\Sigma 9[110](2\bar{2}1)$	1.77	1.71 [13]		3.60	3.56 [18]
$\Sigma 11[110](3\bar{3}2)$	1.45	1.43 [7], 1.49 [13]		3.83	

Table S4: A comparison of the γ_{GB} and W_{sep} quantities for our GBs compared to a compiled literature collection.

3. Convergence tests

The convergence tests mentioned in the main text are presented here. In all calculations, unless otherwise specified, we utilised the same calculation parameters (spin, ionic relaxation etc.) as mentioned prior in the calculation details. In total, we conducted three sets of convergence calculations to ensure our calculations excluded errors involved with:

1. a choice of plane wave energy cutoff being too low
2. a choice of \mathbf{k} -point mesh that was too coarse
3. interactions between the grain boundaries present in the cell did not occur due to insufficient separation to mimic bulk behaviour

3.1. Plane wave energy cutoff convergence

To investigate the effects of differing plane wave energy cutoffs, the quantities of grain boundary energy (γ_{GB}), free surface energy, (γ_{FS}), solution energy (E_{soln}) and segregation energy (E_{seg}) were calculated for the $\Sigma 3[110](1\bar{1}2)$ and its corresponding bulk slab structure. The solution and segregation energies were calculated for the element of Mo. A range of 300-500 eV was investigated, at 50 eV intervals. The details of the supercells used are tabulated in Table S5. The calculated quantities are presented in Table S6. It may be observed that our chosen value of 400 eV for the energy cutoff yields reasonably converged results. The errors associated with different cutoffs in the tested range is no more than 0.032 J/m² for γ_{GB} , 0.005 J/m² for γ_{FS} , 0.015 eV for E_{soln} , and 0.040 eV for E_{seg} .

System	$a \times b \times c$ (Å × Å × Å)	$\mathbf{k}_A \times \mathbf{k}_B \times \mathbf{k}_C$	Composition	Vacuum Size (Å)
GB-vac	$4.005 \times 4.905 \times 41.620$	$8 \times 6 \times 1$	Fe48	≈ 13.6
GB-vac-sol	$4.005 \times 4.905 \times 41.620$	$8 \times 6 \times 1$	Fe47 Mo1	≈ 13.6
slab-vac	$4.005 \times 4.905 \times 41.620$	$8 \times 6 \times 1$	Fe48	≈ 13.6
slab-vac-sol	$4.005 \times 4.905 \times 41.620$	$8 \times 6 \times 1$	Fe47 Mo1	≈ 13.6
slab-all	$4.005 \times 4.905 \times 41.620$	$8 \times 6 \times 1$	Fe72	0

Table S5: The details of the cells and calculations for the plane wave energy cutoff convergence testing conducted for the $\Sigma 3[110](1\bar{1}2)$ GB.

	Plane wave energy cutoff				
	300 eV	350 eV	400 eV	450 eV	500 eV
GB-vac (eV)	-388.94	-388.80	-388.59	-388.52	-388.56
GB-vac-sol (eV)	-391.62	-391.45	-391.24	-391.21	-391.23
slab-vac (eV)	-389.49	-389.31	-389.10	-389.07	-389.09
slab-vac-sol (eV)	-392.04	-391.87	-391.67	-391.63	-391.65
slab-all (eV)	-593.71	-593.45	-593.12	-593.07	-593.11
γ_{GB} (J/m ²)	0.446	0.420	0.414	0.444	0.430
γ_{FS} (J/m ²)	3.867	3.866	3.863	3.862	3.863
E_{soln} (eV)	-2.550	-2.555	-2.564	-2.565	-2.563
E_{seg} (eV)	-0.126	-0.095	-0.086	-0.123	-0.108

Table S6: The results of the plane wave energy cutoff convergence testing conducted for the $\Sigma 3[110](1\bar{1}2)$ GB.

3.2. \mathbf{k} -point convergence

The quantity which we benchmark our results to is the grain boundary energy (γ_{GB}). The calculations are deemed converged as long as deviations in this quantity between the selected mesh and a denser mesh are less than 0.01 J/m². As can be seen, the chosen \mathbf{k} -point meshes in our study all fulfil this requirement.

$a \times b \times c$ (Å × Å × Å)	$k_a \times k_b \times k_c$	E_{GB} (eV)	E_{slab} (eV)	$E_{\text{slab+vac}}$ (eV)	γ_{GB} (J/m ²)	γ_{FS} (J/m ²)
$4.005 \times 6.937 \times 44.144$	$4 \times 2 \times 1$	-581.29	-890.10	-584.04	1.583	2.700
$4.005 \times 6.937 \times 44.144$	$6 \times 3 \times 1$	-581.01	-889.65	-583.76	1.582	2.695
$4.005 \times 6.937 \times 44.144$	$8 \times 4 \times 1$	-581.05	-889.72	-583.79	1.584	2.698
$4.005 \times 6.937 \times 44.144$	$10 \times 5 \times 1$	-581.04	-889.75	-583.79	1.588	2.703
$4.005 \times 6.937 \times 44.144$	$11 \times 6 \times 1$	-581.02	-889.71	-583.77	1.586	2.702
$4.005 \times 6.937 \times 44.144$	$12 \times 6 \times 1$	-581.03	-889.73	-583.78	1.588	2.702

Table S7: The calculation details of the \mathbf{k} -point convergence testing conducted for the $\Sigma 3[110](1\bar{1}1)$ GB. The cells contain 72 atoms in the “slab+vac” and “GB” cells, 108 atoms in the space filling slab “slab”.

$a \times b \times c$ ($\text{\AA} \times \text{\AA} \times \text{\AA}$)	$k_a \times k_b \times k_c$	E_{GB} (eV)	E_{slab} (eV)	$E_{\text{slab+vac}}$ (eV)	γ_{GB} (J/m ²)	γ_{FS} (J/m ²)
$4.005 \times 4.905 \times 41.620$	$4 \times 4 \times 1$	-388.39	-592.75	-388.91	0.424	2.549
$4.005 \times 4.905 \times 41.620$	$5 \times 5 \times 1$	-388.60	-593.27	-389.16	0.454	2.592
$4.005 \times 4.905 \times 41.620$	$6 \times 6 \times 1$	-388.55	-593.13	-389.09	0.445	2.579
$4.005 \times 4.905 \times 41.620$	$8 \times 6 \times 1$	-388.56	-593.12	-389.10	0.444	2.576
$4.005 \times 4.905 \times 41.620$	$8 \times 8 \times 1$	-388.53	-593.08	-389.08	0.445	2.574
$4.005 \times 4.905 \times 41.620$	$9 \times 9 \times 1$	-388.57	-593.14	-389.10	0.436	2.579
$4.005 \times 4.905 \times 41.620$	$10 \times 10 \times 1$	-388.55	-593.14	-389.11	0.453	2.578

Table S8: The calculation details of the \mathbf{k} -point convergence testing conducted for the $\Sigma 3[110](1\bar{1}2)$ GB. The cells contain 48 atoms in the “slab+vac” and “GB” cells, 72 atoms in the space filling slab “slab”.

$a \times b \times c$ ($\text{\AA} \times \text{\AA} \times \text{\AA}$)	$k_a \times k_b \times k_c$	E_{GB} (eV)	E_{slab} (eV)	$E_{\text{slab+vac}}$ (eV)	γ_{GB} (J/m ²)	γ_{FS} (J/m ²)
$4.005 \times 4.905 \times 41.620$	$4 \times 4 \times 1$	-388.39	-592.75	-388.91	0.424	2.549
$4.005 \times 4.905 \times 41.620$	$5 \times 5 \times 1$	-388.60	-593.27	-389.16	0.454	2.592
$4.005 \times 4.905 \times 41.620$	$6 \times 6 \times 1$	-388.55	-593.13	-389.09	0.445	2.579
$4.005 \times 4.905 \times 41.620$	$8 \times 6 \times 1$	-388.56	-593.12	-389.10	0.444	2.576
$4.005 \times 4.905 \times 41.620$	$8 \times 8 \times 1$	-388.53	-593.08	-389.08	0.445	2.574
$4.005 \times 4.905 \times 41.620$	$9 \times 9 \times 1$	-388.57	-593.14	-389.10	0.436	2.579
$4.005 \times 4.905 \times 41.620$	$10 \times 10 \times 1$	-388.55	-593.14	-389.11	0.453	2.578

Table S9: The calculation details of the \mathbf{k} -point convergence testing conducted for the $\Sigma 9[110](2\bar{2}1)$ GB. The cells contain 72 atoms in the “slab+vac” cell, and “GB” cells, 108 atoms in the space filling slab “slab”.

$a \times b \times c$ ($\text{\AA} \times \text{\AA} \times \text{\AA}$)	$k_a \times k_b \times k_c$	E_{GB} (eV)	E_{slab} (eV)	$E_{\text{slab+vac}}$ (eV)	γ_{GB} (J/m ²)	γ_{FS} (J/m ²)
$4.005 \times 4.696 \times 50.973$	$4 \times 4 \times 1$	-338.09	-724.89	-356.27	1.695	2.629
$4.005 \times 4.696 \times 50.973$	$6 \times 6 \times 1$	-338.08	-724.82	-356.25	1.686	2.624
$4.005 \times 4.696 \times 50.973$	$8 \times 8 \times 1$	-338.10	-724.88	-356.27	1.689	2.626
$4.005 \times 4.696 \times 50.973$	$10 \times 10 \times 1$	-338.10	-724.91	-356.28	1.694	2.630

Table S10: The calculation details of the \mathbf{k} -point convergence testing conducted for the $\Sigma 11[110](3\bar{3}2)$ GB. The cells contain 44 atoms in the “slab+vac”, 42 atoms in the “GB”, 88 atoms in the space filling slab “slab”.

3.2.1. \mathbf{k} -point mesh choice on E_{seg}

For completeness, we demonstrate that the \mathbf{k} -point meshes are sufficient for calculating E_{seg} values which generate variations less than 0.03 eV [Table S11]. Here, we only perform this test for E_{seg} in the $\Sigma 3[110](1\bar{1}2)$ GB. The final \mathbf{k} -point mesh density used for this cell, with a smallest spacing between \mathbf{k} -points of $\approx 0.04 \text{ \AA}^{-1}$, is approximately the same across all the other GB models studied, and as such, the value differences in convergence here should transfer well to the other cells. For reference, the effects of other GB modelling choices, such as the chosen lattice parameter, or cell relaxations, can alter segregation energies by more than 0.05 eV. e.g. as demonstrated for Ni in [19, 20]. The difference of <0.03 eV attributed to differing \mathbf{k} -point meshes is effectively negligible for assessing absolute segregation tendency, e.g. as input to isotherm equations.

$a \times b \times c$ ($\text{\AA} \times \text{\AA} \times \text{\AA}$)	\mathbf{k} -point mesh $k_a \times k_b \times k_c$	E_{GB} (eV)	E_{GB+sol} (eV)	E_{slab} (eV)	$E_{slab+sol}$ (eV)	γ_{GB} (J/m ²)	γ_{FS} (J/m ²)	E_{seg} (eV)
$4.005 \times 4.905 \times 41.620$	$2 \times 2 \times 1$	-387.265	-389.921	-387.660	-390.328	0.32	2.46	0.012
$4.005 \times 4.905 \times 41.620$	$3 \times 3 \times 1$	-389.195	-391.855	-389.775	-392.267	0.47	2.60	-0.168
$4.005 \times 4.905 \times 41.620$	$4 \times 4 \times 1$	-388.426	-391.090	-388.915	-391.516	0.40	2.55	-0.063
$4.005 \times 4.905 \times 41.620$	$4 \times 4 \times 2$	-388.390	-391.090	-388.915	-391.517	0.43	2.55	-0.097
$4.005 \times 4.905 \times 41.620$	$5 \times 5 \times 1$	-388.625	-391.274	-389.161	-391.721	0.44	2.59	-0.090
$4.005 \times 4.905 \times 41.620$	$5 \times 5 \times 2$	-388.595	-391.273	-389.161	-391.720	0.46	2.58	-0.119
$4.005 \times 4.905 \times 41.620$	$6 \times 6 \times 1$	-388.574	-391.236	-389.095	-391.659	0.43	2.58	-0.097
$4.005 \times 4.905 \times 41.620$	$6 \times 6 \times 2$	-388.563	-391.235	-389.095	-391.658	0.43	2.58	-0.109

Table S11: The calculation details of the \mathbf{k} -point convergence testing conducted for the $\Sigma 3[110](1\bar{1}2)$ GB. The cells contain 48 atoms in the “slab+vac” and “GB” cells, 72 atoms in the space filling slab “slab”.

3.3. Length-convergence testing

We present the finalised values for the length-convergence testing. This was performed to exclude the interactions between the two interfaces. We use the quantity of GB energy to ensure this. The corresponding values of the fitted excess volume in each length-case are also presented. Do note that we use differing \mathbf{k} -point meshes here simply due to the absence of the vacuum that is used in all other calculations, thus reducing the c-length of the grains. Nevertheless, it may be observed that our chosen grain lengths tend to result in all GBs result in variance in γ_{GB} values of less than 0.023 J/m^2 . Ideally the chosen lengths would reduce the variance in γ_{GB} to less than 0.01 J/m^2 (as is the case for the $\Sigma 3[110](1\bar{1}1)$ and $\Sigma 3[110](1\bar{1}2)$ GBs). However, this is impractical due to the nature of our study, which has a permutational multiplier on computational cost due to the co-segregating interaction calculations.

system	n _{SLAB}	n _{GB}	a (Å)	b (Å)	c _{fit} (Å)	volume (Å ³)	v _{exc} (Å ³)	E _{SLAB} (eV)	E _{GB} (eV)	γ _{GB} (J/m ²)	k-points
$\Sigma 3[110](1\bar{1}1)$	36	36	4.005	6.937	15.285	424.61	0.285	-296.56	-291.22	1.539	$8 \times 4 \times 2$
	48	48	4.005	6.937	20.278	563.31	0.329	-395.23	-389.85	1.549	$8 \times 4 \times 1$
	60	60	4.005	6.937	25.108	697.51	0.292	-494.32	-488.76	1.602	$8 \times 4 \times 1$
	72	72	4.005	6.937	30.032	834.29	0.301	-593.12	-587.66	1.577	$8 \times 4 \times 1$
	84	84	4.005	6.937	34.968	971.42	0.317	-692.00	-686.51	1.581	$8 \times 4 \times 1$
$\Sigma 3[110](1\bar{1}2)$	12	12	4.005	2.452	14.128	138.76	0.128	-98.85	-98.30	0.449	$6 \times 12 \times 2$
	24	24	4.005	2.452	27.995	274.95	0.124	-197.74	-197.19	0.453	$5 \times 10 \times 1$
	36	36	4.005	2.452	41.856	411.10	0.118	-296.55	-295.99	0.453	$6 \times 12 \times 1$
$\Sigma 9[110](2\bar{2}1)$	72	68	4.005	12.015	16.605	798.98	0.279	-593.03	-549.48	1.767	$8 \times 2 \times 2$
	144	140	4.005	12.015	33.595	1616.47	0.278	-1186.04	-1142.56	1.754	$4 \times 2 \times 1$
$\Sigma 11[110](3\bar{3}2)$	44	42	4.005	4.696	25.838	485.95	0.240	-362.40	-342.53	1.450	$6 \times 6 \times 1$
	88	86	4.005	4.696	52.262	982.89	0.170	-724.88	-705.06	1.427	$4 \times 4 \times 1$

Table S12: The calculation details of the length convergence testing conducted for the $\Sigma 3[110](1\bar{1}1)$, $\Sigma 3[110](1\bar{1}2)$, $\Sigma 9[110](2\bar{2}1)$, and $\Sigma 11[110](3\bar{3}2)$ GBs.

4. Excess volume

system	a (Å)	b (Å)	c (Å)	$\mathbf{k}_a \times \mathbf{k}_b \times \mathbf{k}_c$	energy (eV)	volume (Å ³)				
GB-0.000	4.005	6.937	29.429	$8 \times 4 \times 1$	-587.3530	817.547				
GB-0.050	4.005	6.937	29.479	$8 \times 4 \times 1$	-587.4019	818.936				
GB-0.100	4.005	6.937	29.529	$8 \times 4 \times 1$	-587.4475	820.325				
GB-0.150	4.005	6.937	29.579	$8 \times 4 \times 1$	-587.4871	821.714				
GB-0.200	4.005	6.937	29.629	$8 \times 4 \times 1$	-587.5232	823.103				
GB-0.250	4.005	6.937	29.679	$8 \times 4 \times 1$	-587.5546	824.492				
GB-0.300	4.005	6.937	29.729	$8 \times 4 \times 1$	-587.5810	825.881				
GB-0.350	4.005	6.937	29.779	$8 \times 4 \times 1$	-587.6042	827.270				
GB-0.400	4.005	6.937	29.829	$8 \times 4 \times 1$	-587.6220	828.659				
GB-0.450	4.005	6.937	29.879	$8 \times 4 \times 1$	-587.6362	830.048				
GB-0.500	4.005	6.937	29.929	$8 \times 4 \times 1$	-587.6470	831.437				
GB-0.560	4.005	6.937	29.989	$8 \times 4 \times 1$	-587.6543	833.104				
GB-0.561	4.005	6.937	29.990	$8 \times 4 \times 1$	-587.6543	833.119				
GB-0.571	4.005	6.937	30.000	$8 \times 4 \times 1$	-587.6547	833.397				
GB-0.581	4.005	6.937	30.010	$8 \times 4 \times 1$	-587.6555	833.675				
GB-0.591	4.005	6.937	30.020	$8 \times 4 \times 1$	-587.6555	833.953				
GB-0.601	4.005	6.937	30.030	$8 \times 4 \times 1$	-587.6552	834.231				
GB-0.610	4.005	6.937	30.039	$8 \times 4 \times 1$	-587.6553	834.493				
GB-0.611	4.005	6.937	30.040	$8 \times 4 \times 1$	-587.6556	834.508				
GB-0.621	4.005	6.937	30.050	$8 \times 4 \times 1$	-587.6551	834.786				
GB-0.631	4.005	6.937	30.060	$8 \times 4 \times 1$	-587.6552	835.064				
GB-0.641	4.005	6.937	30.070	$8 \times 4 \times 1$	-587.6545	835.342				
GB-0.651	4.005	6.937	30.080	$8 \times 4 \times 1$	-587.6539	835.620				
GB-0.660	4.005	6.937	30.089	$8 \times 4 \times 1$	-587.6535	835.882				
GB-0.661	4.005	6.937	30.090	$8 \times 4 \times 1$	-587.6534	835.897				
GB-0.710	4.005	6.937	30.139	$8 \times 4 \times 1$	-587.6483	837.271				
GB-0.760	4.005	6.937	30.189	$8 \times 4 \times 1$	-587.6386	838.660				
GB-0.810	4.005	6.937	30.239	$8 \times 4 \times 1$	-587.6255	840.049				
SLAB	4.005	6.937	29.429	$8 \times 4 \times 1$	-593.1226	817.547				
Finalised details	n _{GB}	n _{SLAB}	a (Å)	b (Å)	c _{fit} (Å)	k-points	E _{GB} ^{fit} (eV)	γ_{GB} (J/m ²)	volume (Å ³)	v_{exc} (Å)
	72	72	4.005	6.937	30.032	$8 \times 4 \times 1$	-587.6555	1.577	834.292	0.301

Table S13: The data used to calculate the excess volume for the $\Sigma 3[110](1\bar{1}1)$ GB.

system	a (Å)	b (Å)	c (Å)	$\mathbf{k}_a \times \mathbf{k}_b \times \mathbf{k}_c$	energy (eV)	volume (Å ³)				
GB-0.00	4.005	2.452	27.746	$5 \times 10 \times 1$	-197.165	272.5156				
GB-0.10	4.005	2.452	27.846	$5 \times 10 \times 1$	-197.178	273.4978				
GB-0.20	4.005	2.452	27.946	$5 \times 10 \times 1$	-197.185	274.4800				
GB-0.201	4.005	2.452	27.947	$5 \times 10 \times 1$	-197.185	274.4865				
GB-0.211	4.005	2.452	27.957	$5 \times 10 \times 1$	-197.185	274.5847				
GB-0.221	4.005	2.452	27.967	$5 \times 10 \times 1$	-197.185	274.6829				
GB-0.231	4.005	2.452	27.977	$5 \times 10 \times 1$	-197.186	274.7811				
GB-0.241	4.005	2.452	27.987	$5 \times 10 \times 1$	-197.185	274.8793				
GB-0.251	4.005	2.452	27.997	$5 \times 10 \times 1$	-197.185	274.9776				
GB-0.261	4.005	2.452	28.007	$5 \times 10 \times 1$	-197.185	275.0758				
GB-0.271	4.005	2.452	28.017	$5 \times 10 \times 1$	-197.185	275.174				
GB-0.281	4.005	2.452	28.027	$5 \times 10 \times 1$	-197.185	275.2722				
GB-0.291	4.005	2.452	28.037	$5 \times 10 \times 1$	-197.185	275.3704				
GB-0.30	4.005	2.452	28.046	$5 \times 10 \times 1$	-197.185	275.4622				
GB-0.301	4.005	2.452	28.047	$5 \times 10 \times 1$	-197.185	275.4686				
GB-0.40	4.005	2.452	28.146	$5 \times 10 \times 1$	-197.178	276.4443				
GB-0.50	4.005	2.452	28.246	$5 \times 10 \times 1$	-197.166	277.4265				
GB-0.60	4.005	2.452	28.346	$5 \times 10 \times 1$	-197.148	278.4087				
GB-0.70	4.005	2.452	28.446	$5 \times 10 \times 1$	-197.124	279.3908				
GB-0.80	4.005	2.452	28.546	$5 \times 10 \times 1$	-197.096	280.373				
GB-0.90	4.005	2.452	28.646	$5 \times 10 \times 1$	-197.062	281.3552				
GB-n0.10	4.005	2.452	27.646	$5 \times 10 \times 1$	-197.145	271.5335				
SLAB	4.005	2.452	27.746	$5 \times 10 \times 1$	-197.741	272.5156				
Finalised details	n _{GB} 24	n _{SLAB} 24	a (Å) 4.005	b (Å) 2.452	c _{fit} (Å) 27.995	\mathbf{k} -points $5 \times 10 \times 1$	E _{GB} ^{fit} (eV) -197.185	γ_{GB} (J/m ²) 0.453	volume (Å ³) 274.953	v _{exc} (Å) 0.124

Table S14: The data used to generate the $\Sigma 3[110](1\bar{1}2)$ GB.

system	a (Å)	b (Å)	c (Å)	$\mathbf{k}_a \times \mathbf{k}_b \times \mathbf{k}_c$	energy (eV)	volume (Å³)				
GB-0.00	4.005	12.015	16.991	$8 \times 2 \times 2$	-549.1964	817.547				
GB-0.10	4.005	12.015	17.091	$8 \times 2 \times 2$	-549.0458	822.359				
GB-0.20	4.005	12.015	17.191	$8 \times 2 \times 2$	-548.8649	827.170				
GB-0.30	4.005	12.015	17.291	$8 \times 2 \times 2$	-548.6537	831.982				
GB-0.40	4.005	12.015	17.391	$8 \times 2 \times 2$	-548.4132	836.793				
GB-0.50	4.005	12.015	17.491	$8 \times 2 \times 2$	-548.1442	841.605				
GB-0.60	4.005	12.015	17.591	$8 \times 2 \times 2$	-547.8469	846.417				
GB-0.70	4.005	12.015	17.691	$8 \times 2 \times 2$	-547.5238	851.228				
GB-0.80	4.005	12.015	17.791	$8 \times 2 \times 2$	-547.1740	856.040				
GB-0.90	4.005	12.015	17.891	$8 \times 2 \times 2$	-546.8022	860.852				
GB-n0.10	4.005	12.015	16.891	$8 \times 2 \times 2$	-549.3188	812.735				
GB-n0.20	4.005	12.015	16.791	$8 \times 2 \times 2$	-549.4076	807.924				
GB-n0.30	4.005	12.015	16.691	$8 \times 2 \times 2$	-549.4601	803.112				
GB-n0.333	4.005	12.015	16.658	$8 \times 2 \times 2$	-549.4704	801.520				
GB-n0.343	4.005	12.015	16.648	$8 \times 2 \times 2$	-549.4724	801.039				
GB-n0.353	4.005	12.015	16.638	$8 \times 2 \times 2$	-549.4739	800.557				
GB-n0.363	4.005	12.015	16.628	$8 \times 2 \times 2$	-549.4754	800.076				
GB-n0.373	4.005	12.015	16.618	$8 \times 2 \times 2$	-549.4762	799.595				
GB-n0.383	4.005	12.015	16.608	$8 \times 2 \times 2$	-549.4768	799.114				
GB-n0.393	4.005	12.015	16.598	$8 \times 2 \times 2$	-549.4762	798.633				
GB-n0.40	4.005	12.015	16.591	$8 \times 2 \times 2$	-549.4759	798.300				
GB-n0.403	4.005	12.015	16.588	$8 \times 2 \times 2$	-549.4756	798.152				
GB-n0.413	4.005	12.015	16.578	$8 \times 2 \times 2$	-549.4750	797.670				
GB-n0.423	4.005	12.015	16.568	$8 \times 2 \times 2$	-549.4738	797.189				
GB-n0.433	4.005	12.015	16.558	$8 \times 2 \times 2$	-549.4726	796.708				
GB-n0.50	4.005	12.015	16.491	$8 \times 2 \times 2$	-549.4495	793.489				
GB-n0.60	4.005	12.015	16.391	$8 \times 2 \times 2$	-549.3789	788.677				
SLAB	4.005	12.015	16.991	$8 \times 2 \times 2$	-593.0331	817.547				
Finalised details	n _{GB} 72	n _{SLAB} 68	a (Å) 4.005	b (Å) 12.015	c _{fit} (Å) 16.605	\mathbf{k} -points $8 \times 2 \times 2$	E _{GB} ^{fit} (eV) -362.403	γ_{GB} (J/m ²) 1.767	volume (Å ³) 798.975	v _{exc} (Å) 0.279

Table S15: The data used to generate the $\Sigma 9[110](2\bar{2}1)$ GB.

system	a (Å)	b (Å)	c (Å)	$\mathbf{k}_a \times \mathbf{k}_b \times \mathbf{k}_c$	energy (eV)	volume (Å ³)				
GB-0.000	4.005	4.696	26.565	$6 \times 6 \times 1$	-342.2641	499.612				
GB-0.100	4.005	4.696	26.665	$6 \times 6 \times 1$	-342.1927	501.493				
GB-0.200	4.005	4.696	26.765	$6 \times 6 \times 1$	-342.1141	503.373				
GB-0.300	4.005	4.696	26.865	$6 \times 6 \times 1$	-342.0285	505.254				
GB-0.400	4.005	4.696	26.965	$6 \times 6 \times 1$	-341.9356	507.135				
GB-0.500	4.005	4.696	27.065	$6 \times 6 \times 1$	-341.8364	509.016				
GB-0.600	4.005	4.696	27.165	$6 \times 6 \times 1$	-341.7305	510.896				
GB-0.700	4.005	4.696	27.265	$6 \times 6 \times 1$	-341.6179	512.777				
GB-0.800	4.005	4.696	27.365	$6 \times 6 \times 1$	-341.4994	514.658				
GB-n0.100	4.005	4.696	26.465	$6 \times 6 \times 1$	-342.3274	497.731				
GB-n0.200	4.005	4.696	26.365	$6 \times 6 \times 1$	-342.3827	495.851				
GB-n0.300	4.005	4.696	26.265	$6 \times 6 \times 1$	-342.4300	493.970				
GB-n0.400	4.005	4.696	26.165	$6 \times 6 \times 1$	-342.4687	492.089				
GB-n0.500	4.005	4.696	26.065	$6 \times 6 \times 1$	-342.4979	490.208				
GB-n0.600	4.005	4.696	25.965	$6 \times 6 \times 1$	-342.5162	488.328				
GB-n0.665	4.005	4.696	25.900	$6 \times 6 \times 1$	-342.5237	487.103				
GB-n0.675	4.005	4.696	25.890	$6 \times 6 \times 1$	-342.5238	486.915				
GB-n0.685	4.005	4.696	25.880	$6 \times 6 \times 1$	-342.5243	486.727				
GB-n0.695	4.005	4.696	25.870	$6 \times 6 \times 1$	-342.5248	486.539				
GB-n0.700	4.005	4.696	25.865	$6 \times 6 \times 1$	-342.5251	486.447				
GB-n0.705	4.005	4.696	25.860	$6 \times 6 \times 1$	-342.5253	486.351				
GB-n0.715	4.005	4.696	25.850	$6 \times 6 \times 1$	-342.5253	486.163				
GB-n0.725	4.005	4.696	25.840	$6 \times 6 \times 1$	-342.5254	485.975				
GB-n0.735	4.005	4.696	25.830	$6 \times 6 \times 1$	-342.5256	485.787				
GB-n0.745	4.005	4.696	25.820	$6 \times 6 \times 1$	-342.5255	485.599				
GB-n0.755	4.005	4.696	25.810	$6 \times 6 \times 1$	-342.5253	485.411				
GB-n0.765	4.005	4.696	25.800	$6 \times 6 \times 1$	-342.5248	485.223				
GB-n0.800	4.005	4.696	25.765	$6 \times 6 \times 1$	-342.5225	484.566				
GB-n0.900	4.005	4.696	25.665	$6 \times 6 \times 1$	-342.5078	482.686				
SLAB	4.005	4.696	26.565	$6 \times 6 \times 1$	-362.4038	499.612				
Finalised details	n _{GB}	n _{SLAB}	a (Å)	b (Å)	c _{fit} (Å)	\mathbf{k} -points	E ^{fit} _{GB} (eV)	γ_{GB} (J/m ²)	volume (Å ³)	v_{exc} (Å)
	42	44	4.005	4.696	25.838	$6 \times 6 \times 1$	-362.403	1.450	485.946	0.240

Table S16: The data used to generate the $\Sigma 11[110](3\bar{3}2)$ GB.

5. Structure files (GB+vac)

We provide the base structure files that were modified in the study to generate the various structures. Please note that the *sites* in Tables S25-S27 are zero-indexed. i.e. the first site is denoted as site 0.

5.1. $\Sigma 3[110](1\bar{1}1)$

GB-S3-RA110-S1-11.vasp

```
Fe72
1.0
4.004839 0.000000 0.000000
0.000000 6.936585 0.000000
0.000000 0.000000 44.144156
Fe
72
direct
0.500020 0.499865 0.174406 Fe
0.000020 0.999864 0.174406 Fe
0.000018 0.333206 0.192023 Fe
0.500018 0.833206 0.192023 Fe
0.000016 0.666432 0.207212 Fe
0.500016 0.166432 0.207212 Fe
0.500017 0.499846 0.227842 Fe
0.000018 0.999846 0.227842 Fe
0.000006 0.333167 0.246510 Fe
0.500006 0.833169 0.246511 Fe
0.500004 0.166563 0.264928 Fe
0.000002 0.666564 0.264928 Fe
0.499996 0.499844 0.283536 Fe
0.999996 0.999844 0.283536 Fe
0.999992 0.333274 0.302182 Fe
0.499992 0.833274 0.302182 Fe
0.999988 0.666648 0.320456 Fe
0.499987 0.166648 0.320456 Fe
0.499986 0.499993 0.339148 Fe
0.999986 -0.000007 0.339148 Fe
0.499982 0.833339 0.357718 Fe
0.999982 0.333339 0.357718 Fe
0.999982 0.666700 0.376090 Fe
0.499982 0.166698 0.376090 Fe
0.999978 0.000108 0.395020 Fe
0.499977 0.500108 0.395020 Fe
0.499980 0.833452 0.413457 Fe
```

0.999981 0.333452 0.413457 Fe
0.999980 0.666854 0.431511 Fe
0.499980 0.166855 0.431511 Fe
0.999981 0.000060 0.451243 Fe
0.499981 0.500060 0.451243 Fe
0.499979 0.833396 0.471109 Fe
0.999979 0.333396 0.471109 Fe
0.999978 0.666829 0.484584 Fe
0.499978 0.166829 0.484584 Fe
0.999998 0.000365 0.509449 Fe
0.499999 0.500365 0.509449 Fe
0.500023 0.166916 0.534317 Fe
0.000023 0.666916 0.534317 Fe
0.000025 0.333423 0.547997 Fe
0.500025 0.833423 0.547997 Fe
0.000026 0.000056 0.567672 Fe
0.500026 0.500056 0.567672 Fe
0.000029 0.666838 0.587404 Fe
0.500029 0.166838 0.587404 Fe
0.500033 0.833415 0.605344 Fe
0.000032 0.333415 0.605344 Fe
0.000036 0.000019 0.623791 Fe
0.500036 0.500018 0.623791 Fe
0.500038 0.166680 0.642703 Fe
0.000038 0.666680 0.642703 Fe
0.000047 0.333340 0.661100 Fe
0.500047 0.833340 0.661100 Fe
0.000044 0.999937 0.679572 Fe
0.500044 0.499937 0.679572 Fe
0.000046 0.666642 0.697998 Fe
0.500046 0.166642 0.697998 Fe
0.500051 0.833194 0.716553 Fe
0.000051 0.333194 0.716553 Fe
0.500050 0.499867 0.735116 Fe
0.000050 0.999867 0.735116 Fe
0.500050 0.166530 0.753562 Fe
0.000050 0.666530 0.753562 Fe
0.500048 0.833172 0.772186 Fe
0.000048 0.333172 0.772186 Fe
0.000046 0.999749 0.792716 Fe
0.500046 0.499749 0.792716 Fe
0.000049 0.666488 0.808004 Fe
0.500049 0.166488 0.808004 Fe
0.500049 0.833140 0.825542 Fe

0.000049 0.333140 0.825542 Fe

5.2. $\Sigma 3[110](1\bar{1}2)$

GB-S3-RA110-S1-12.vasp

```
Fe48
1.0
4.004839 0.000000 0.000000
0.000000 4.904906 0.000000
0.000000 0.000000 41.619509

Fe
48
direct
-0.000032 0.027731 0.179833 Fe
-0.000032 0.527732 0.179833 Fe
0.500066 0.330676 0.205695 Fe
0.500066 0.830675 0.205695 Fe
0.000005 0.168711 0.234560 Fe
0.000005 0.668711 0.234560 Fe
0.500017 0.500595 0.262485 Fe
0.500017 0.000595 0.262485 Fe
-0.000023 0.333753 0.290612 Fe
-0.000023 0.833754 0.290612 Fe
0.500018 0.165697 0.317980 Fe
0.500018 0.665697 0.317980 Fe
0.999983 0.498031 0.345981 Fe
0.999983 0.998031 0.345981 Fe
0.499932 0.335133 0.373491 Fe
0.499932 0.835132 0.373491 Fe
0.999980 0.169691 0.401247 Fe
0.999980 0.669691 0.401247 Fe
0.499977 0.001296 0.429178 Fe
0.499977 0.501295 0.429178 Fe
0.000013 0.332012 0.456982 Fe
0.000013 0.832012 0.456982 Fe
0.499943 0.173351 0.484747 Fe
0.499943 0.673351 0.484747 Fe
0.000005 0.478358 0.514052 Fe
0.000005 0.978358 0.514052 Fe
0.499978 0.156569 0.543367 Fe
0.499978 0.656569 0.543367 Fe
0.000034 0.323860 0.570679 Fe
0.000034 0.823860 0.570679 Fe
0.499971 0.994852 0.598815 Fe
0.499971 0.494852 0.598815 Fe
0.999977 0.164339 0.626496 Fe
```

0.999977 0.664339 0.626496 Fe
0.499976 0.328743 0.654032 Fe
0.499976 0.828743 0.654032 Fe
0.000013 0.495850 0.682007 Fe
0.000013 0.995849 0.682007 Fe
0.499934 0.163876 0.709478 Fe
0.499934 0.663876 0.709478 Fe
0.000012 0.331414 0.737716 Fe
0.000012 0.831414 0.737716 Fe
0.499951 0.500704 0.765667 Fe
0.499951 0.000703 0.765667 Fe
-0.000005 0.163737 0.794539 Fe
-0.000005 0.663737 0.794539 Fe
0.499954 0.360342 0.820358 Fe
0.499954 0.860342 0.820358 Fe

5.3. Σ9[110](2̄21)

GB-S9-RA110-S2-21.vasp

```
Fe68
1.0
6.332207 0.000000 0.000000
-1.266441 3.799324 0.000000
0.000000 0.000000 50.973280
Fe
68
direct
0.999045 0.999514 0.189665 Fe
0.231863 0.615976 0.196912 Fe
0.445707 0.222842 0.205355 Fe
0.660958 0.830526 0.215698 Fe
0.884769 0.442348 0.222456 Fe
0.110202 0.055121 0.233555 Fe
0.331535 0.665765 0.242946 Fe
0.555275 0.277631 0.252001 Fe
0.776844 0.888408 0.261475 Fe
0.998191 0.499094 0.270686 Fe
0.221423 0.110718 0.280009 Fe
0.443317 0.721667 0.289373 Fe
0.665796 0.332891 0.298512 Fe
0.887979 0.943983 0.307773 Fe
0.110199 0.555101 0.316974 Fe
0.332363 0.166208 0.326200 Fe
0.554929 0.777426 0.335458 Fe
0.777528 0.388775 0.344735 Fe
0.000206 0.000085 0.353914 Fe
0.222501 0.611241 0.363265 Fe
0.444592 0.222307 0.372454 Fe
0.666790 0.833362 0.381674 Fe
0.888857 0.444427 0.390951 Fe
0.111561 0.055762 0.400131 Fe
0.334512 0.667264 0.409527 Fe
0.556405 0.278198 0.418971 Fe
0.776694 0.888374 0.427891 Fe
0.000841 0.500410 0.437235 Fe
0.223529 0.111799 0.446434 Fe
0.447145 0.723595 0.456952 Fe
0.670530 0.335247 0.465663 Fe
0.881461 0.940748 0.472993 Fe
0.115221 0.557617 0.484620 Fe
```

0.346684 0.173301 0.491119 Fe
0.543305 0.771682 0.513929 Fe
0.772178 0.386089 0.514015 Fe
0.008169 0.004080 0.514027 Fe
0.346789 0.173355 0.536921 Fe
0.115316 0.557683 0.543410 Fe
0.881889 0.940921 0.555063 Fe
0.670859 0.335442 0.562389 Fe
0.447455 0.723782 0.571038 Fe
0.223820 0.111947 0.581603 Fe
0.000901 0.500458 0.590801 Fe
0.776556 0.888269 0.600127 Fe
0.556264 0.278101 0.609023 Fe
0.334510 0.667238 0.618448 Fe
0.111508 0.055710 0.627800 Fe
0.888951 0.444463 0.636977 Fe
0.666704 0.833338 0.646281 Fe
0.444124 0.222092 0.655517 Fe
0.221594 0.610793 0.664713 Fe
0.999074 0.999552 0.674072 Fe
0.776539 0.388265 0.683291 Fe
0.554199 0.777068 0.692483 Fe
0.332013 0.166019 0.701752 Fe
0.109710 0.554847 0.710830 Fe
0.887599 0.943799 0.720219 Fe
0.664344 0.332192 0.729548 Fe
0.442912 0.721471 0.738785 Fe
0.221381 0.110702 0.748245 Fe
0.997457 0.498705 0.757259 Fe
0.776075 0.888023 0.766685 Fe
0.550889 0.275421 0.777811 Fe
0.326843 0.663460 0.784560 Fe
0.111588 0.055764 0.794857 Fe
0.898051 0.449055 0.803355 Fe
0.664982 0.832485 0.810592 Fe

5.4. $\Sigma 11[110](3\bar{3}2)$

GB-S11-RA110-S3-32.vasp

```
Fe42
1.0
4.004839 0.000000 0.000000
0.000000 4.696090 0.000000
0.000000 0.000000 50.973280
Fe
42
direct
0.999991 0.996402 0.257247 Fe
0.499991 0.287613 0.266648 Fe
0.999988 0.535670 0.279054 Fe
0.499992 0.819555 0.288320 Fe
0.999992 0.088682 0.302353 Fe
0.499990 0.364430 0.314026 Fe
0.999986 0.635970 0.326103 Fe
0.499987 0.908944 0.337639 Fe
0.999988 0.181301 0.349768 Fe
0.499989 0.453485 0.361613 Fe
0.999990 0.726869 0.373345 Fe
0.499985 0.999247 0.385282 Fe
0.999984 0.272829 0.396931 Fe
0.499987 0.545193 0.409115 Fe
0.999989 0.819193 0.420656 Fe
0.499986 0.090191 0.433033 Fe
0.999991 0.364313 0.444113 Fe
0.499992 0.636025 0.457310 Fe
0.999987 0.911096 0.467260 Fe
0.499981 0.179510 0.482203 Fe
0.999982 0.463645 0.489470 Fe
0.999979 0.005866 0.511941 Fe
0.499979 0.709611 0.511954 Fe
0.999974 0.464078 0.534358 Fe
0.499975 0.179113 0.541604 Fe
0.999964 0.911575 0.556557 Fe
0.499972 0.636340 0.566458 Fe
0.999973 0.364284 0.579712 Fe
0.499972 0.089837 0.590882 Fe
0.999969 0.818729 0.603272 Fe
0.499969 0.544535 0.614838 Fe
0.999976 0.272244 0.626893 Fe
0.499968 0.998901 0.638550 Fe
```

0.999968	0.726829	0.650513	Fe
0.499968	0.453366	0.662550	Fe
0.999978	0.180895	0.674263	Fe
0.499980	0.909352	0.686263	Fe
0.999978	0.633459	0.697929	Fe
0.499969	0.364764	0.711993	Fe
0.999973	0.080692	0.721253	Fe
0.499967	0.832773	0.733623	Fe
0.999971	0.541577	0.743107	Fe

6. Single solute elemental segregation energies and cohesion effects

The single solute elemental segregation energies and their effects on GB cohesion are tabulated in Tables S17-S24.

6.1. Single atom segregation energies

6.1.1. DFT + other DFT literature comparisons

Element	E _{seg} (eV) - This work				Literature (see caption)
	$\Sigma 3(1\bar{1}1)$	$\Sigma 3(1\bar{1}2)$	$\Sigma 9(2\bar{2}1)$	$\Sigma 11(3\bar{3}2)$	
Co	-0.18	-0.04	-0.14	-0.15	-0.05 ^d [7], -0.09 ^{a,e} [7, 21, 22]
Cr	-0.18	-0.07	-0.21	-0.29	-0.03 ^a [7], -0.09 ^d [7], -0.13 ^a [5], -0.14 ^a [8], -0.18 ^a [23], -0.20 ^{a,e} [4, 21, 22], -0.24 ^f [5]
Cu	-0.51	-0.24	-0.64	-0.74	-0.26 ^e [21, 22], -0.43 ^a [7], -0.57 ^a [4], -0.65 ^d [7]
Mn	-0.50	-0.18	-0.54	-0.62	-0.21 ^e [21, 22], -0.32 ^a [7], -0.33 ^a [24], -0.44 ^{a,d} [7, 8], -0.49 ^a [25], -0.50 ^e [26]
Mo	-0.44	-0.10	-0.43	-0.55	-0.37 ^e [21, 22], -0.44 ^a [8], -0.61 ^a [27]
Nb	-0.77	-0.15	-1.00	-0.91	-0.49 ^e [21, 22], -0.97 ^a [8]
Ni	-0.41	-0.15	-0.43	-0.56	-0.24 ^e [21, 22] -0.31 ^a [7], -0.44 ^d [7]
Ti	-0.48	-0.09	-0.74	-0.65	-0.33 ^e [21, 22], -0.39 ^a [7], -0.49 ^d [7], -0.52 ^a [8], -1.00 ^g [28]
V	-0.11	0.00	-0.12	-0.20	-0.18 ^e [21, 22], -0.17 ^a [8], -0.12 ^a [27], -0.03 ^a [29], -0.04 ^d [7] 0.02 ^a [7],
W	-0.39	-0.08	-0.31	-0.51	-0.41 ^a [8], -0.49 ^a [4]

Table S17: The segregation energies (at the minimum energy position) at the GBs studied (rotation axis [110] omitted for aesthetic purposes).

Superscripts indicate the GB studied for that specific value:

^a - $\Sigma 3[110](1\bar{1}1)$, ^b - $\Sigma 3[110](1\bar{1}2)$, ^c - $\Sigma 9[110](2\bar{2}1)$, ^d - $\Sigma 11[110](3\bar{3}2)$, ^e - $\Sigma 5[100](013)$, ^f - $\Sigma 5[100](012)$, ^g - $\Sigma 5[100](010)$

6.1.2. Our DFT data vs experimental data

Here we present a comparison of our data with available experimental data and theoretically (non-simulation, phenomenological model) predicted data. Do note that comparisons between experiment and DFT data is inherently a comparison between a minimum energy at a site at the interface (DFT) vs an averaged value across some interface (experimental), which is problematic for reasons given in the discussion of the main text. Nevertheless, it is clear here that the qualitative trends in the relative segregation tendencies observed in experiment are in good agreement with our calculations.

Element	E_{seg} (kJ/mol) - This work				Literature (see caption)
	$\Sigma 3(1\bar{1}1)$	$\Sigma 3(1\bar{1}2)$	$\Sigma 9(2\bar{2}1)$	$\Sigma 11(3\bar{3}2)$	
Co	-17	-3	-13	-14	0^a [30, 31], -7^b [30, 31]
Cr	-17	-6	-20	-28	-3^c [32], -8^d [30], 0^a [30, 31], -18^c [30, 31]
Cu	-49	-23	-61	-72	
Mn	-48	-17	-52	-60	-8^a [30, 31], -25^b [30, 31]
Mo	-43	-9	-41	-53	$-9/-12^d$ [33], -17^d [34], -28^e [35], -10^a [30, 31], -27^b [30, 31]
Nb	-74	-15	-97	-88	-38^e [35], -30^a [30, 31], -47^b [30, 31]
Ni	-40	-14	-42	-54	-4^a [30, 31], -20^b [30, 31]
Ti	-46	-9	-71	-60	-28^a [30, 31], -45^b [30, 31]
V	-10	0	-11	-19	-5^f [36], 0^a [30, 31], -14^b [30, 31]
W	-38	-8	-30	-48	

Table S18: The segregation energies (at the minimum energy position) at the GBs studied (rotation axis [110] omitted for aesthetic purposes). This is a comparison of our DFT data to the experimentally available values, and for those predicted by theoretical frameworks.

Superscripts:

^a - theory, special GB

^b - theory, general GB

^c - field ion microscopy, polycrystal

^d - Auger electron spectroscopy, polycrystal

^e - atom probe tomography, 800°C

^f - Auger electron microscopy, $\Sigma 19(111)$ GB, 46.8°

6.2. Single atom cohesion effect - cohesion effect (η)

Here it is important to note that many studies in the literature provide the cohesion changes (aka. embrittling potencies/ strengthening energies) due to the segregated elements only in the units of eV/atom. It is only reasonable and acceptable to provide this where the cell dimensions used to calculate such a quantity are clearly detailed. Since there are many ways of constructing a supercell (orthorhombic/rhombic/cluster etc.) this can cause significant deviations in the areal density of the solute, even when only 1 atom is inserted into the GB. This information is occasionally provided using the term “monolayer”. However, for cells with merged sites, this term becomes unintuitive and hence should be avoided.

In many cases, information regarding the areal density of the solute with respect to interface area present in the cell is omitted. Frustratingly, it is well known that areal density/coverage can significantly affect the cohesive effects of the solute on GB cohesion (e.g. [5]). Thus, any comparisons between quantities given in eV/atom or J/m² without information of the cell dimensions become at best qualitative, and at worst misleading. Therefore, it should be unreasonable to compile eV/atom values for quantitative comparison without also providing cell dimension data. Regrettably, many studies in the literature do not provide sufficient information to reproduce their supercell models, and hence results. This common practice can cause large scatter to appear in compiled literature data, which when accounting for the reasons above, is not surprising to the informed reader. Although information on the cell used can be estimated through graphic depictions of the structure or by means of other inference, this is highly undesirable since it relies on certain assumptions which may or may not be correct. For this reason, the dimensions of the cells should be included in any study on cohesion, and provided in length units (i.e. nm × nm × nm / Å × Å × Å).

Only in recent has the importance of studying different cleavage-planes/fracture-paths to identify the weakest path of fracture been recognised [37]. Many studies in the literature only calculated an η value for a specific chosen cleavage plane (i.e. calculating W_{sep} via computing a segregation energy of the same solute to a free surface), which can provide cohesion effects that are not for the plane of weakest cohesion. Older studies almost exclusively focus on purely the separation at the GB plane. This is insufficient for assessing the true cohesive effect of a segregated solute, which can substantially shift the preferred fracture path. This also contributes to observed scatter of data.

Lastly, it is suggested that all future studies should present their cohesion quantities solely in the units of J/m² such that it is consistent and standardised with the well known quantities of GB

energy and free surface energy. This provides a single, standardised quantity that contains information on a normalised-area basis, which when combined with information on the cell, can back-yield eV/atom values. We suggest that cohesion difference quantities from segregated elements should be termed “cohesion change” or “cohesion effect” (i.e. not “embrittling potency”, “strengthening energy” etc.). This will reduce confusion in the signing of the quantities. The signage should be standardised in the intuitive form: positive values indicate a cohesion enhancement effect, whereas negative values indicate a decohesion effect. The cohesion change is calculated by:

$$\eta = W_{\text{sep}}^{\text{seg}} - W_{\text{sep}}^{\text{pureGB}} \quad (1)$$

Where $W_{\text{sep}}^{\text{seg}}$ is the work of separation of the GB with the segregated solute, and $W_{\text{sep}}^{\text{pureGB}}$ the work of separation of the pure GB. We present the comparison table for change in W_{sep} (η) in J/m² where information on the cell dimensioning (and hence areal density of solute segregation) is available/easily inferred [Table S19], and reluctantly in units of eV/atom including those studies where a conversion may not be reasonably guessed at [Table S20]:

Element	η (J/m ²) - This work				Literature (see caption)
	$\Sigma 3(1\bar{1}1)$	$\Sigma 3(1\bar{1}2)$	$\Sigma 9(2\bar{2}1)$	$\Sigma 11(3\bar{3}2)$	
Co	-0.02	0.03	0.12	0.16	
Cr	0.07	0.09	0.24	0.34	0.09 ^a [8], 0.07 ^b [38]
Cu	-0.27	-0.48	-0.20	-0.16	-0.32 ^a [39], -0.37 ^a [40]
Mn	0.23	0.17	0.28	0.41	0.02 ^a [8]
Mo	0.33	0.40	0.40	0.68	0.34 ^a [8], -0.05 ^b [38]
Nb	0.17	-0.05	0.44	0.57	0.33 ^a [8], -0.09 ^b [38]
Ni	-0.03	-0.25	0.05	0.17	0.02 ^a [8]
Ti	0.03	-0.05	0.30	0.36	0.02 ^a [8]
V	0.12	0.19	0.18	0.35	0.14 ^a [8]
W	0.56	0.41	0.30	0.56	0.57 ^a [8]

Table S19: The cohesion changes (η) in J/m² at the GBs studied. Superscripts indicate the GB studied for that specific value: ^a - $\Sigma 3[110](1\bar{1}1)$, ^b - $\Sigma 5[100](012)$

Element	η (eV/atom*) This work				Literature (see caption)
	$\Sigma 3(1\bar{1}1)$	$\Sigma 3(1\bar{1}2)$	$\Sigma 9(2\bar{2}1)$	$\Sigma 11(3\bar{3}2)$	
Co	-0.04	0.03	0.18	0.19	-0.25 ^a [41] -0.05 ^a [42]
Cr	0.13	0.11	0.36	0.40	0.10 ^a [43], 0.16 ^b [44], 0.16 ^a [8], 0.27 ^a [5], 0.43 ^a [41]
Cu	-0.47	-0.59	-0.30	-0.19	-0.66 ^a [40] -0.56 ^a [39]
Mn	0.39	0.21	0.42	0.48	0.03 ^a [8], -0.20 ^a [24]
Mo	0.57	0.49	0.60	0.79	0.57 ^a [8], 0.59 ^a [45], -0.11 ^b [38], 0.90 ^a [42]
Nb	0.30	-0.06	0.66	0.67	-0.20 ^b [44], 0.33 ^a [8], 0.51 ^a [46]
Ni	-0.05	-0.31	0.07	0.20	
Ti	0.05	-0.07	0.45	0.42	0.37 ^a [47], 0.12 ^a [8], 1.97 ^c [28]
V	0.21	0.23	0.27	0.41	0.25 ^a [8], 0.58 ^a [46]
W	0.96	0.50	0.44	0.66	0.98 ^a [8], 1.31 ^a [45]

Table S20: The cohesion changes (η) in eV/atom at the GBs studied. *Please read the above associated text in this section for an explanation of the scatter, and why this should serve as a qualitative comparison only. Superscripts indicate the GB studied for that specific value: ^a - $\Sigma 3[110](1\bar{1}1)$, ^b - $\Sigma 5[100](012)$, ^c - $\Sigma 5[100](010)$

6.3. Cleavage planes tested

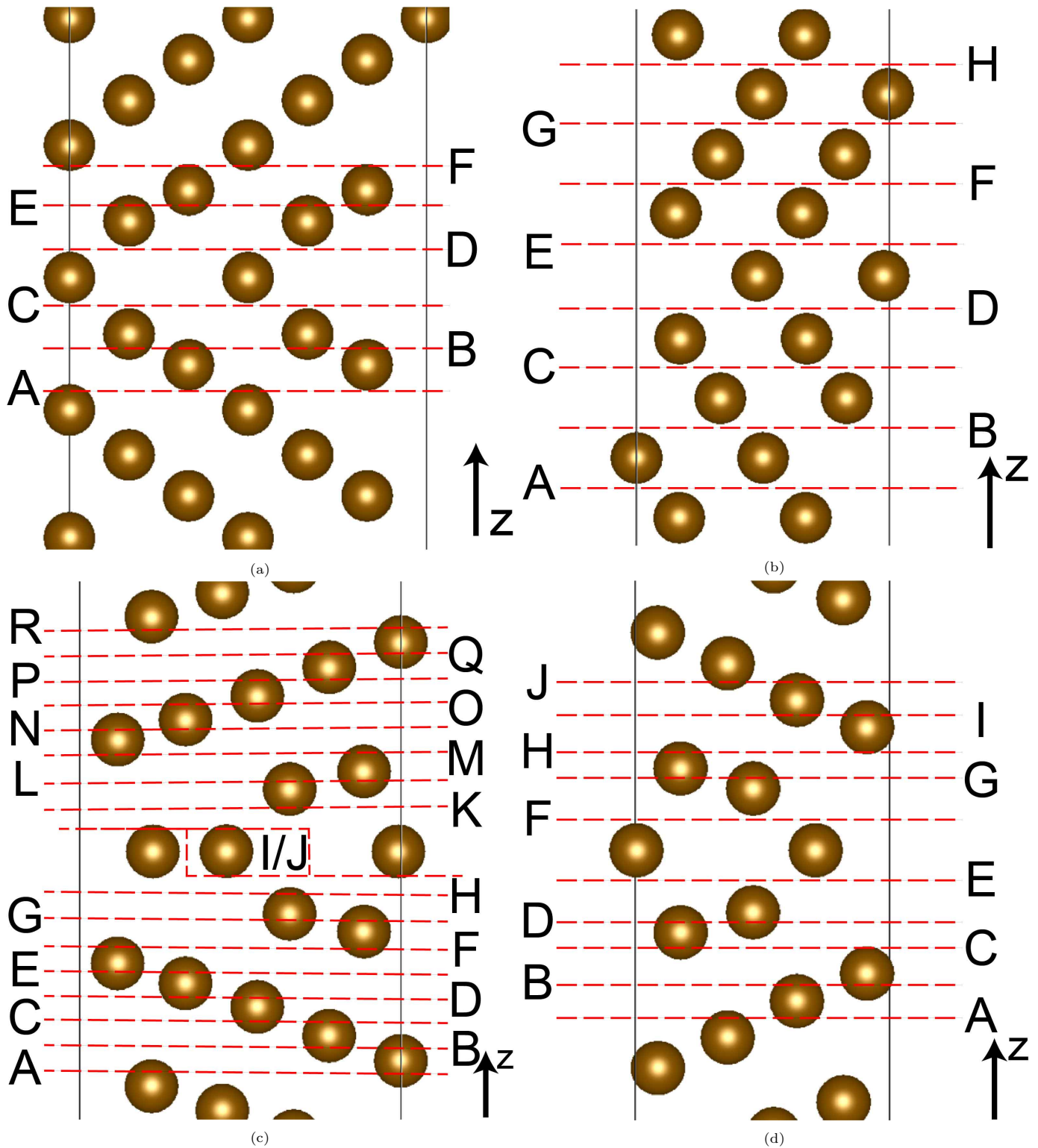


Figure S1: The cleavage planes tested for the S1a $\Sigma_3[110](\bar{1}\bar{1}1)$ S1b $\Sigma_3[110](\bar{1}\bar{1}2)$ S1c $\Sigma_9[110](2\bar{2}1)$ S1d $\Sigma_{11}[110](3\bar{3}2)$ GBs. The positive directions of the cleavage planes are indicated. Sites are indexed from 0-n along the axis indicated, increasing in index as we move towards the positive direction.

6.4. Single atom cohesion effects

6.4.1. $\Sigma 3[110](1\bar{1}\bar{1})$

system	cleavage plane	W_{sep}^{RGS} (J/m ²)	W_{sep} (J/m ²)	η_{RGS} (J/m ²)	η_{rel} (J/m ²)	$\Delta\eta$ (J/m ²)	η_{rel}^{pct} (%)	η_{RGS}^{pct} (%)	E_{seg} (eV)	R_{RGS}	R_{rel}
Co-34-d-1.1	D	4.18	3.78	-0.02	-0.02	0.00	-0.53	-0.48	-0.18	0.84	0.76
Cr-34-d-1.1	C	4.18	3.87	-0.02	0.07	0.09	1.84	-0.48	-0.17	0.84	0.77
Cr-36-d-0.0	D	4.27	3.88	0.07	0.07	0.00	1.84	1.67	-0.18	0.85	0.78
Cu-34-d-1.1	C	3.97	3.53	-0.23	-0.27	-0.04	-7.10	-5.48	-0.51	0.79	0.71
Cu-36-d-0.0	D	3.94	3.52	-0.26	-0.28	-0.02	-7.36	-6.19	-0.49	0.79	0.70
Mn-36-d-0.0	D	4.33	4.03	0.13	0.23	0.10	6.04	3.10	-0.50	0.87	0.81
Mo-36-d-0.0	D	4.68	4.13	0.48	0.33	-0.15	8.67	11.43	-0.44	0.94	0.83
Nb-36-d-0.0	D	4.41	3.98	0.21	0.17	-0.04	4.47	5.00	-0.77	0.88	0.80
Ni-34-d-1.1	C	4.13	3.78	-0.07	-0.03	0.04	-0.79	-1.67	-0.41	0.83	0.76
Ti-36-d-0.0	D	4.19	3.83	-0.01	0.03	0.04	0.79	-0.24	-0.48	0.84	0.77
V-32-d-1.7	D	4.33	3.92	0.13	0.12	-0.01	3.15	3.10	-0.11	0.87	0.78
V-36-d-0.0	D	4.35	3.91	0.15	0.10	-0.05	2.63	3.57	-0.10	0.87	0.78
W-36-d-0.0	D	5.01	4.36	0.81	0.56	-0.25	14.72	19.29	-0.39	1.00	0.87
GB	D	4.20	3.81	N/A	N/A	N/A	N/A	N/A	N/A	0.84	0.76

Table S21: The single element segregation and cohesion data for the $\Sigma 3[110](1\bar{1}\bar{1})$ GB.

6.4.2. $\Sigma 3[110](1\bar{1}2)$

system	cleavage plane	W_{sep}^{RGS} (J/m ²)	W_{sep} (J/m ²)	η_{RGS} (J/m ²)	η_{rel} (J/m ²)	$\Delta\eta$ (J/m ²)	η_{rel}^{pct} (%)	η_{RGS}^{pct} (%)	E_{seg} (eV)	R_{RGS}	R_{rel}
Co-20-d-2.4	E	4.93	4.75	0.05	0.03	-0.02	0.64	1.02	-0.04	0.99	0.95
Co-22-d-1.2	D	4.94	4.72	0.06	0.00	-0.06	0.00	1.23	-0.02	0.99	0.94
Cr-24-d-0.0	E	5.01	4.81	0.12	0.09	-0.03	1.91	2.46	-0.06	1.00	0.96
Cu-20-d-2.4	C	4.43	4.22	-0.46	-0.50	-0.04	-10.59	-9.43	-0.21	0.89	0.84
Cu-22-d-1.2	D	4.47	4.25	-0.41	-0.47	-0.06	-9.96	-8.40	-0.23	0.89	0.85
Cu-24-d-0.0	E	4.43	4.24	-0.45	-0.48	-0.03	-10.17	-9.22	-0.24	0.89	0.85
Mn-22-d-1.2	D	5.09	4.89	0.21	0.17	-0.04	3.60	4.30	-0.18	1.02	0.98
Mn-24-d-0.0	E	4.96	4.85	0.08	0.13	0.05	2.75	1.64	-0.16	0.99	0.97
Mo-24-d-0.0	A	5.28	5.12	0.40	0.40	0.00	8.47	8.20	-0.10	1.06	1.02
Nb-24-d-0.0	E	4.98	4.67	0.10	-0.05	-0.15	-1.06	2.05	-0.15	1.00	0.93
Ni-20-d-2.4	C	4.69	4.45	-0.19	-0.27	-0.08	-5.72	-3.89	-0.14	0.94	0.89
Ni-22-d-1.2	D	4.71	4.48	-0.17	-0.24	-0.07	-5.08	-3.48	-0.14	0.94	0.90
Ni-24-d-0.0	E	4.69	4.47	-0.19	-0.25	-0.06	-5.30	-3.89	-0.15	0.94	0.89
Ti-22-d-1.2	C	4.98	4.67	0.10	-0.05	-0.15	-1.06	2.05	-0.09	1.00	0.93
Ti-24-d-0.0	E	4.87	4.66	-0.01	-0.06	-0.05	-1.27	-0.20	-0.08	0.97	0.93
V-24-d-0.0	E	5.14	4.91	0.26	0.19	-0.07	4.02	5.33	0.01	1.03	0.98
W-24-d-0.0	A	5.29	5.13	0.41	0.41	0.00	8.68	8.40	-0.08	1.06	1.03
GB	E	4.88	4.72	N/A	N/A	N/A	N/A	N/A	N/A	0.98	0.94

Table S22: The single element segregation and cohesion data for the $\Sigma 3[110](1\bar{1}2)$ GB.

6.4.3. $\Sigma 9[110](2\bar{2}1)$

system	cleavage plane	W_{sep}^{RGS} (J/m ²)	W_{sep} (J/m ²)	η_{RGS} (J/m ²)	η_{rel} (J/m ²)	$\Delta\eta$ (J/m ²)	η_{rel}^{pct} (%)	η_{RGS}^{pct} (%)	E_{seg} (eV)	R_{RGS}	R_{rel}
Co-33-d-1.2	K	4.15	3.60	-0.04	0.00	0.04	0.00	-0.95	-0.10	0.83	0.72
Co-36-d-0.0	H	4.29	3.72	0.09	0.12	0.03	3.33	2.15	-0.14	0.86	0.74
Cr-36-d-0.0	K	4.41	3.84	0.21	0.24	0.03	6.67	5.01	-0.21	0.88	0.77
Cu-33-d-1.2	H	3.75	3.40	-0.45	-0.20	0.25	-5.56	-10.73	-0.64	0.75	0.68
Mn-33-d-1.2	H	4.33	3.86	0.14	0.26	0.12	7.22	3.34	-0.51	0.87	0.77
Mn-36-d-0.0	H	4.64	3.88	0.44	0.28	-0.16	7.78	10.49	-0.54	0.93	0.78
Mo-34-d-0.0	H	4.78	4.00	0.59	0.40	-0.19	11.11	14.06	-0.43	0.96	0.80
Nb-34-d-0.0	H	4.59	4.04	0.39	0.44	0.05	12.22	9.30	-1.00	0.92	0.81
Ni-33-d-1.2	H	4.03	3.64	-0.16	0.04	0.20	1.11	-3.81	-0.43	0.81	0.73
Ni-36-d-0.0	H	4.23	3.65	0.04	0.05	0.01	1.39	0.95	-0.43	0.85	0.73
Ti-34-d-0.0	H	4.40	3.90	0.21	0.30	0.09	8.34	5.01	-0.74	0.88	0.78
V-31-d-2.1	H	4.16	3.76	-0.04	0.16	0.20	4.45	-0.95	-0.09	0.83	0.75
V-32-d-1.5	H	4.34	3.87	0.14	0.27	0.13	7.50	3.34	-0.08	0.87	0.77
V-34-d-0.0	H	4.49	3.78	0.30	0.18	-0.12	5.00	7.15	-0.12	0.90	0.76
W-34-d-0.0	F	4.97	3.90	0.77	0.30	-0.47	8.34	18.35	-0.31	0.99	0.78
GB	H	4.20	3.60	N/A	N/A	N/A	N/A	N/A	N/A	0.84	0.72

Table S23: The single element segregation and cohesion data for the $\Sigma 9[110](2\bar{2}1)$ GB.

6.4.4. $\Sigma 11[110](3\bar{3}2)$

system	cleavage plane	W_{sep}^{RGS} (J/m ²)	W_{sep} (J/m ²)	η_{RGS} (J/m ²)	η_{rel} (J/m ²)	$\Delta\eta$ (J/m ²)	η_{rel}^{pct} (%)	η_{RGS}^{pct} (%)	E_{seg} (eV)	R_{RGS}	R_{rel}
Co-21-d-0.0	F	4.43	3.99	0.16	0.16	0.00	4.18	3.74	-0.15	0.89	0.80
Cr-21-d-0.0	F	4.61	4.17	0.33	0.34	0.01	8.88	7.72	-0.29	0.92	0.83
Cu-21-d-0.0	F	4.07	3.67	-0.21	-0.16	0.05	-4.18	-4.91	-0.74	0.81	0.73
Mn-21-d-0.0	F	4.88	4.24	0.61	0.41	-0.20	10.70	14.27	-0.62	0.98	0.85
Mo-19-d-1.5	F	5.06	4.51	0.78	0.68	-0.10	17.75	18.24	-0.54	1.01	0.90
Nb-22-d-0.0	E	4.75	4.40	0.48	0.57	0.09	14.88	11.23	-0.91	0.95	0.88
Ni-21-d-0.0	F	4.38	4.00	0.10	0.17	0.07	4.44	2.34	-0.56	0.88	0.80
Ti-22-d-0.0	E	4.53	4.19	0.25	0.36	0.11	9.40	5.85	-0.62	0.91	0.84
V-22-d-0.0	E	4.72	4.18	0.45	0.35	-0.10	9.14	10.53	-0.20	0.94	0.84
W-22-d-0.0	C	5.30	4.40	1.03	0.56	-0.47	14.62	24.09	-0.50	1.06	0.88
GB	E	4.28	3.83	N/A	N/A	N/A	N/A	N/A	N/A	0.86	0.77

Table S24: The single element segregation and cohesion data for the $\Sigma 11[110](3\bar{3}2)$ GB.

7. Segregation profiles - Elemental segregation (1 atom)

The segregation profiles for a single substitutional atom for all transition metals studied are presented in Figures S2-S5. The tabulated values are presented in Tables S25-S28.

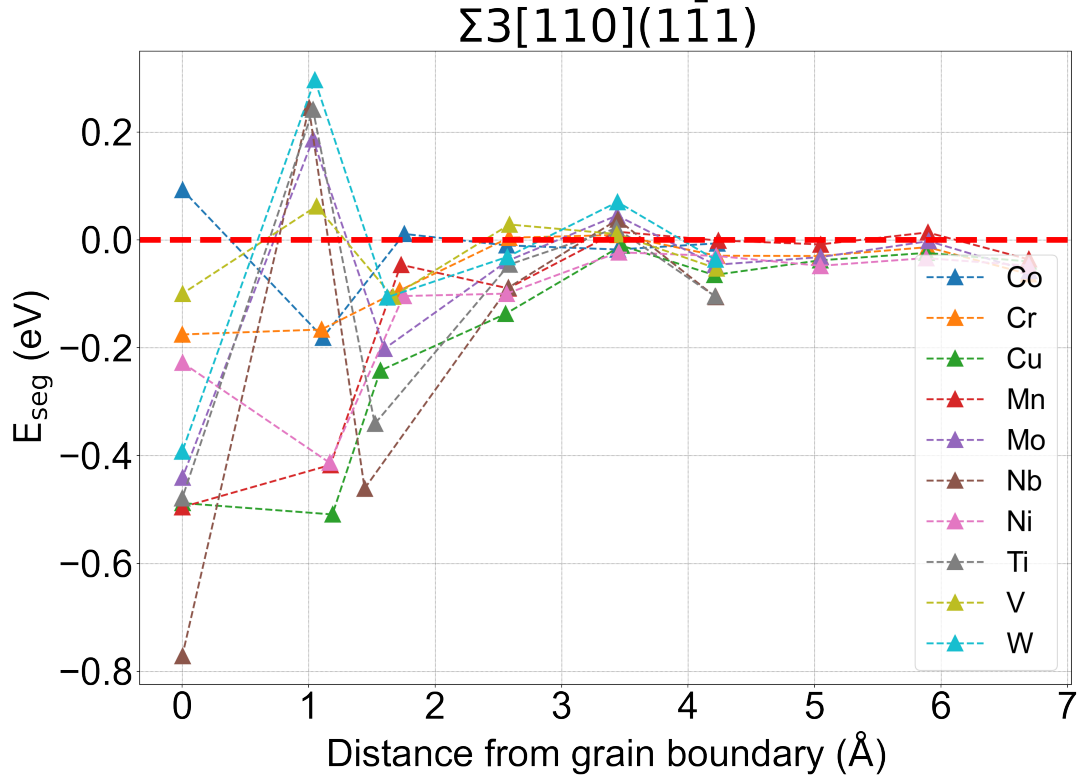


Figure S2: The segregation energy profiles of the tested substitutional solutes as a function of distance from the GB interface for the $\Sigma 3[110](1\bar{1}1)$ GBs.

site	Energies of segregation (substitutional) (eV)												
	distance (Å)	multiplicity	volume (\AA^3)	Ti	V	Cr	Mn	Co	Ni	Cu	Nb	Mo	W
20	6.7	4	11.38			-0.063	-0.036		-0.048	-0.040		-0.058	
22	5.9	4	11.38			-0.014	0.014		-0.034	-0.024		-0.002	
24	5.1	4	11.42			-0.030	-0.008		-0.048	-0.038		-0.032	
26	4.2	4	11.49	-0.105	-0.053	-0.029	-0.001	-0.007	-0.030	-0.065	-0.106	-0.046	-0.037
28	3.4	4	11.32	0.021	0.011	0.009	0.015	-0.018	-0.023	-0.011	0.038	0.045	0.070
30	2.6	4	11.57	-0.046	0.028	0.004	-0.090	-0.010	-0.100	-0.137	-0.089	-0.039	-0.032
32	1.7	4	12.41	-0.341	-0.105	-0.094	-0.046	0.011	-0.104	-0.242	-0.461	-0.202	-0.107
34	1.1	4	11.22	0.241	0.062	-0.166	-0.417	-0.181	-0.413	-0.509	0.245	0.186	0.296
36	0.0	2	13.15	-0.479	-0.100	-0.175	-0.496	0.093	-0.228	-0.488	-0.771	-0.441	-0.392

Table S25: The segregation energies of the substitutional solutes of Ti, V, Cr, Mn, Co, Ni, Cu, Nb, Mo and W are presented for the $\Sigma 3[110](1\bar{1}1)$. The Voronoi volume for the site in the pure GB is presented. Sites are available in the attached poscar files (0 indexed).

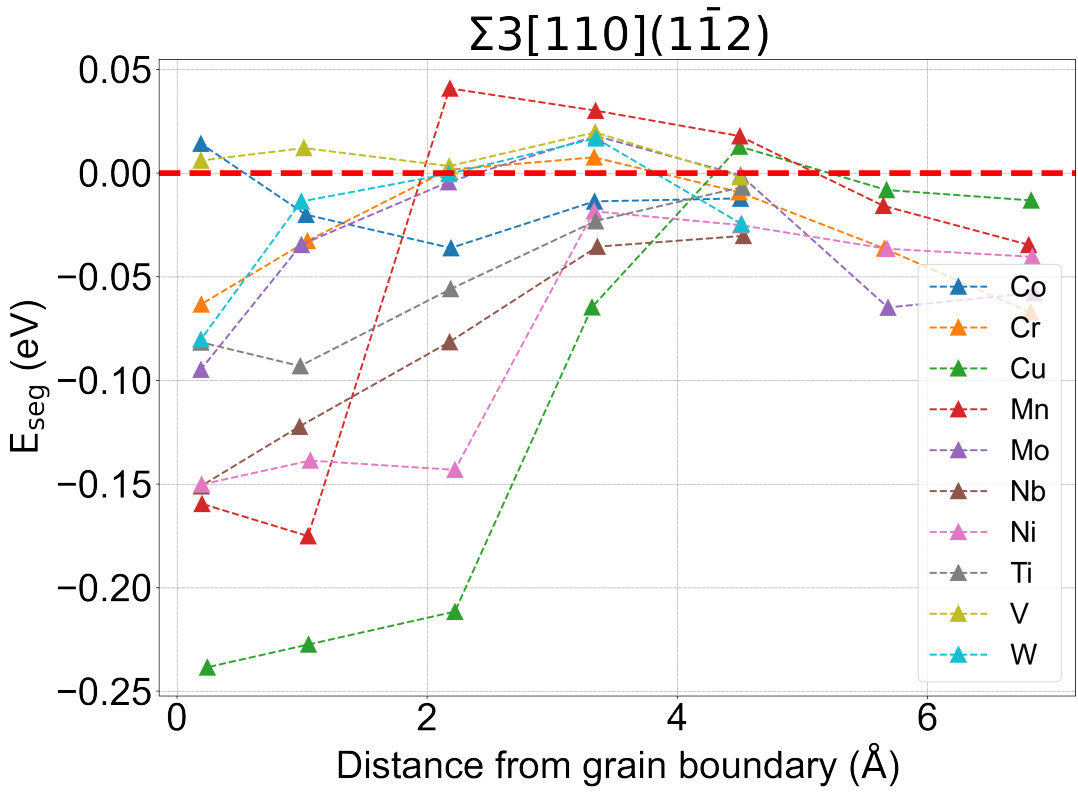


Figure S3: The segregation energy profiles of the tested substitutional solutes as a function of distance from the GB interface for the $\Sigma 3[110](\bar{1}\bar{1}2)$ GBs.

site	distance (Å)	multiplicity	volume (\AA^3)	Energies of segregation (substitutional) (eV)									
				Ti	V	Cr	Mn	Co	Ni	Cu	Nb	Mo	W
12	7.0	4	11.32			-0.07	-0.04		-0.04	-0.01		-0.06	
14	5.9	4	11.34			-0.04	-0.02		-0.04	-0.01		-0.07	
16	4.7	4	11.36	-0.01	0.00	-0.01	0.02	-0.01	-0.03	0.01	-0.03	0.00	-0.03
18	3.5	4	11.39	-0.02	0.02	0.01	0.03	-0.01	-0.02	-0.07	-0.04	0.02	0.02
20	2.4	4	11.45	-0.06	0.00	0.00	0.04	-0.04	-0.14	-0.21	-0.08	0.00	0.00
22	1.2	4	11.64	-0.09	0.01	-0.03	-0.18	-0.02	-0.14	-0.23	-0.12	-0.04	-0.01
24	0.0	2	11.83	-0.08	0.01	-0.06	-0.16	0.01	-0.15	-0.24	-0.15	-0.10	-0.08

Table S26: The segregation energies of the substitutional solutes of Ti, V, Cr, Mn, Co, Ni, Cu, Nb, Mo and W are presented for the $\Sigma 3[110](\bar{1}\bar{1}2)$. The Voronoi volume for the site in the pure GB is presented. Sites are available in the attached poscar files (0 indexed).

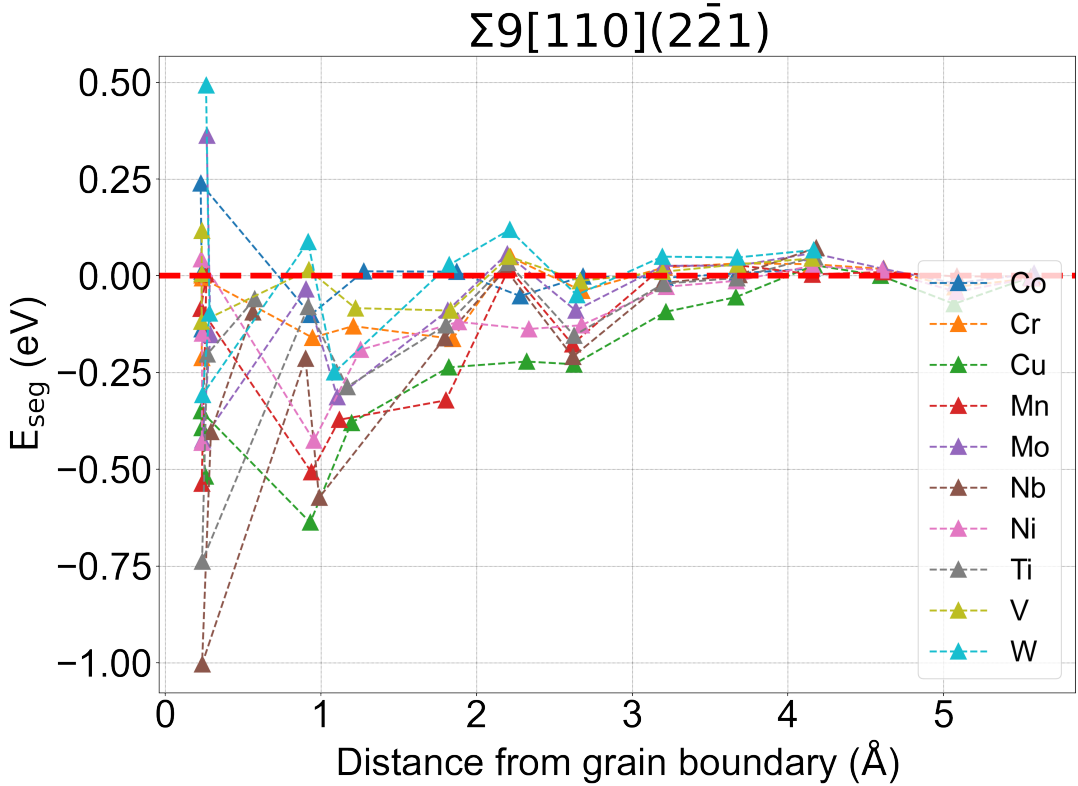


Figure S4: The segregation energy profiles of the tested substitutional solutes as a function of distance from the GB interface for the $\Sigma 9[110](\bar{2}\bar{2}1)$ GB.

site	distance (Å)	multiplicity	volume (\AA^3)	Energies of segregation (substitutional) (eV)									
				Ti	V	Cr	Mn	Co	Ni	Cu	Nb	Mo	W
23	5.8	2	11.37			-0.006	-0.001		-0.005	-0.003		0.006	
24	5.3	2	11.43			-0.029	-0.002		-0.042	-0.073		-0.019	
25	4.8	2	11.41			0.018	0.010		0.014	0.000		0.018	
26	4.4	2	11.30	0.049	0.045	0.030	0.004	0.019	0.026	0.027	0.072	0.059	0.066
27	3.9	2	11.44	-0.006	0.029	0.032	0.027	0.006	-0.013	-0.055	0.003	0.026	0.047
28	3.4	2	11.38	-0.020	0.010	0.021	0.026	-0.005	-0.028	-0.093	-0.019	0.026	0.049
29	2.9	2	11.89	-0.154	-0.013	-0.039	-0.177	-0.001	-0.128	-0.228	-0.209	-0.089	-0.049
30	2.5	2	11.55	0.034	0.050	0.048	0.019	-0.052	-0.137	-0.222	0.017	0.056	0.119
31	2.1	2	11.56	-0.128	-0.090	-0.163	-0.322	0.011	-0.119	-0.236	-0.161	-0.090	0.028
32	1.5	2	12.14	-0.287	-0.084	-0.130	-0.372	0.012	-0.191	-0.379	-0.573	-0.313	-0.249
33	1.2	2	11.43	-0.080	0.015	-0.160	-0.507	-0.101	-0.426	-0.637	-0.214	-0.035	0.088
34	0.0	1	13.86	-0.738	-0.118	-0.006	-0.085	0.239	0.043	-0.349	-1.003	-0.425	-0.308
35	0.0	1	12.11	-0.203	0.005	0.001	0.004	0.011	-0.148	-0.393	-0.403	-0.153	-0.097
36	0.0	1	10.66	-0.060	0.117	-0.212	-0.537	-0.138	-0.431	-0.518	-0.094	0.362	0.493

Table S27: The segregation energies of the substitutional solutes of Ti, V, Cr, Mn, Co, Ni, Cu, Nb, Mo and W are presented for the $\Sigma 9[110](\bar{2}\bar{2}1)$. The Voronoi volume for the site in the pure GB is presented. Sites are available in the attached poscar files (0 indexed).

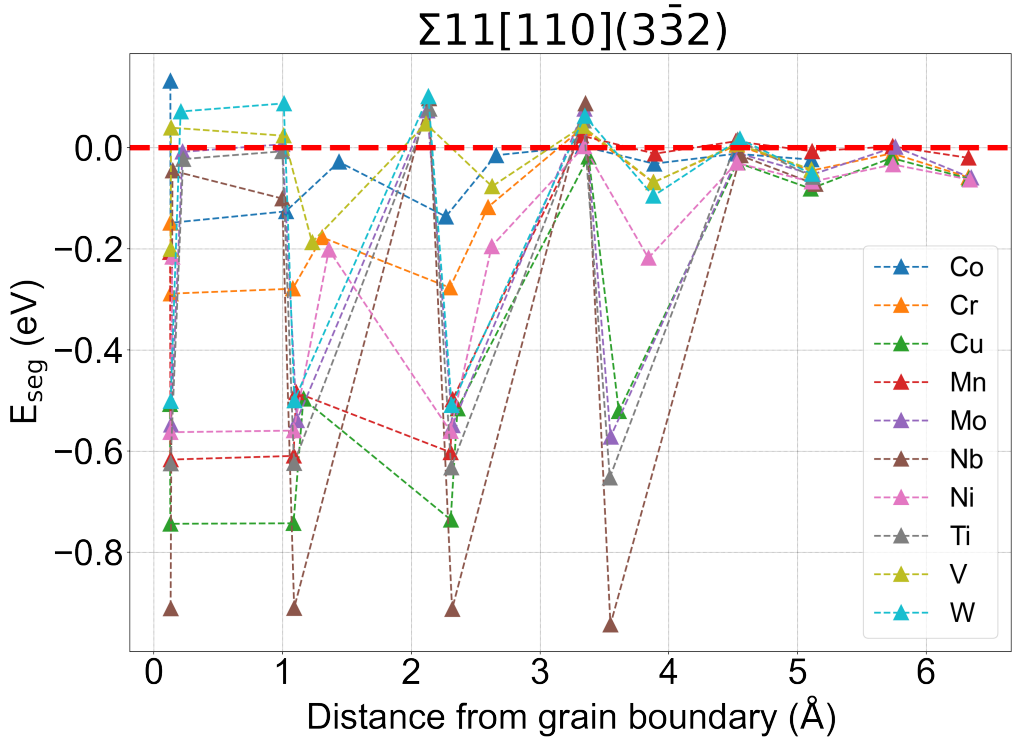


Figure S5: The segregation energy profiles of the tested substitutional solutes as a function of distance from the GB interface for the $\Sigma_{11}[110](\bar{3}\bar{3}2)$ GBs. The peculiarity of the similar energies across the same sites for certain solutes in the $\Sigma_{11}[110](\bar{3}\bar{3}2)$ GB is due to local interface reconstruction via relaxation.

site	distance (Å)	multiplicity	volume (\AA^3)	Energies of segregation (substitutional) (eV)									
				Ti	V	Cr	Mn	Co	Ni	Cu	Nb	Mo	W
11	6.5	2	11.39		-0.058	-0.020			-0.063	-0.061		-0.059	
12	5.9	2	11.34		-0.011	0.003			-0.033	-0.020		0.002	
13	5.2	2	11.43	-0.058	-0.043	-0.045	-0.007	-0.023	-0.067	-0.081	-0.072	-0.052	-0.052
14	4.7	2	11.33	0.015	0.008	0.005	0.013	-0.012	-0.030	-0.029	-0.015	-0.011	0.018
15	4.0	2	11.49	-0.652	-0.068	-0.068	-0.012	-0.031	-0.218	-0.521	-0.943	-0.572	-0.095
16	3.5	2	11.27	0.053	0.043	0.039	0.024	0.003	0.003	-0.018	0.087	0.077	0.063
17	2.8	2	11.80	-0.632	-0.076	-0.117	-0.498	-0.015	-0.195	-0.516	-0.913	-0.549	-0.509
18	2.3	2	11.24	0.077	0.048	-0.277	-0.602	-0.136	-0.561	-0.736	0.098	0.074	0.102
19	1.5	2	12.39	-0.624	-0.187	-0.177	-0.484	-0.028	-0.202	-0.497	-0.910	-0.539	-0.500
20	1.1	2	11.27	-0.007	0.024	-0.279	-0.610	-0.126	-0.559	-0.743	-0.100	0.007	0.088
21	0.0	1	11.31	-0.022	0.040	-0.289	-0.617	-0.148	-0.563	-0.744	-0.045	-0.008	0.072
22	0.0	1	13.05	-0.624	-0.200	-0.149	-0.207	0.133	-0.216	-0.507	-0.911	-0.548	-0.501

Table S28: The segregation energies of the substitutional solutes of Ti, V, Cr, Mn, Co, Ni, Cu, Nb, Mo and W are presented for the $\Sigma_{11}[110](\bar{3}\bar{3}2)$. The Voronoi volume for the site in the pure GB is presented. Sites are available in the attached poscar files (0 indexed).

7.1. Magnetic moment (1 solute)

Data on the magnetic moments of the solutes when segregated in their most favourable positions at each GB is available in Table S29. More detailed data on how the magnetic moment of the solutes vary across different sites at the GB is provided in Tables S30-S33. We find that GBs do not change the magnetic behaviour of solutes segregated to them drastically, aside from the special case of Mn. We find that Ti, V, Cr, Mn, Nb, Mo, W are anti-ferromagnetic, whereas Co, Ni and Cu are ferromagnetic, in agreement with previous works [21, 48, 49].

It is interesting to note that when calculated in a 128 atom bcc-Fe cell, the Mn atom converges to an antiferromagnetic state. However, when placed in the “bulk” of the grain boundary models (i.e. sufficiently far away from the surfaces/interface), the magnetic moment of Mn converges to a ferromagnetic state. Let us note that the only real differentiating factor between these two cases are the distances of the singular Mn atom to its neighbouring images in the supercell model, which are 11.32 Å and 4.00 Å respectively, for the bulk and GB cells respectively. Therefore, we can conclude that the anti-ferromagnetic for Mn only exists in sufficiently dilute limits which allow for consistent large spacing between Mn atoms in the Fe-matrix. These observations are in agreement with Mirzoev et al.’s work [1], and others [25, 26]. However, the segregation of Mn atoms to GBs causes the reappearance of the antiferromagnetic state when occupying sites at the GB interface, even when situated nearby other Mn atoms. The small distance to nearby Mn atoms would induce a ferromagnetic alignment for Mn atoms in the bulk. It is worth noting, however, that some bulk-like sites present at the interface do cause Mn to exhibit bulk-like magnetic behaviour (i.e. ferromagnetically aligned when close to one another) when segregated to those sites. However, segregation of Mn to these sites are less likely to occur due to smaller strength of binding.

	Ti	V	Cr	Mn	Co	Ni	Cu	Nb	Mo	W
Bulk	-0.97	-1.43	-1.86	-2.06	1.68	0.89	0.12	-0.76	-0.83	-0.80
$\Sigma 3(1\bar{1}1)$	-0.88	-1.40	-2.63	-3.12	1.56	0.75	0.12	-0.74	-0.85	-0.77
$\Sigma 3(\bar{1}\bar{1}2)$	-0.95	-1.54	-2.19	-2.81	1.72	0.82	0.12	-0.76	-0.78	-0.76
$\Sigma 9(2\bar{2}1)$	-0.85	-1.57	-1.69	-2.05	1.43	0.70	0.12	-0.64	-0.72	-0.65
$\Sigma 11(3\bar{3}2)$	-0.85	-1.44	-2.13	-2.60	1.47	0.67	0.13	-0.64	-0.66	-0.60

Table S29: The magnetic moments of the solutes in the bulk (128 atom bcc cell) and at their most energetically favourable positions when segregated at the GBs are presented for comparison. The reference magnetic alignment is *positive* for Fe-bulk, so negative values indicate an anti-parallel alignment of the solute.

Magnetic moment (μ_B)											
site	distance (Å)	Ti	V	Cr	Mn	Co	Ni	Cu	Nb	Mo	W
20	6.7			-1.83	0.35		0.90	0.12		-0.81	
22	5.9			-1.84	0.70		0.89	0.12		-0.81	
24	5.1			-1.86	0.32		0.88	0.12		-0.81	
26	4.2	-0.94	-1.42	-1.87	0.66	1.72	0.89	0.12	-0.73	-0.81	-0.76
28	3.4	-0.95	-1.37	-1.73	0.55	1.69	0.87	0.13	-0.73	-0.77	-0.73
30	2.6	-0.95	-1.45	-1.98	-2.45	1.68	0.84	0.11	-0.73	-0.80	-0.76
32	1.7	-0.83	-1.37	-1.93	0.09	1.70	0.85	0.12	-0.62	-0.70	-0.67
34	1.1	-0.96	-1.40	-1.82	-2.32	1.56	0.75	0.12	-0.78	-0.84	-0.80
36	0.0	-0.88	-1.62	-2.63	-3.12	1.74	0.76	0.13	-0.74	-0.85	-0.77

Table S30: The magnetic moments of the substitutional solutes of Ti, V, Cr, Mn, Co, Ni, Cu, Nb, Mo and W are presented for the $\Sigma_3[110](\bar{1}\bar{1}1)$. Sites are available in the attached poscar files (0 indexed). Magnetic moment of bcc-lattice iron is defined as positive.

Magnetic moment (μ_B)											
site	distance (Å)	Ti	V	Cr	Mn	Co	Ni	Cu	Nb	Mo	W
12	7.0			-1.88	1.01		0.90	0.11		-0.79	
14	5.9			-1.87	0.98		0.90	0.11		-0.79	
16	4.7	-0.97	-1.45	-1.88	1.05	1.71	0.89	0.11	-0.75	-0.78	-0.76
18	3.5	-0.96	-1.44	-1.89	1.12	1.71	0.88	0.10	-0.74	-0.78	-0.75
20	2.4	-0.97	-1.46	-1.92	0.95	1.72	0.80	0.12	-0.76	-0.78	-0.76
22	1.2	-0.95	-1.47	-2.10	-2.81	1.71	0.80	0.12	-0.74	-0.78	-0.75
24	0.0	-0.98	-1.54	-2.19	-2.83	1.68	0.82	0.12	-0.76	-0.78	-0.76

Table S31: The magnetic moments of the substitutional solutes of Ti, V, Cr, Mn, Co, Ni, Cu, Nb, Mo and W are presented for the $\Sigma_3[110](\bar{1}\bar{1}2)$. Sites are available in the attached poscar files (0 indexed). Magnetic moment of bcc-lattice iron is defined as positive.

Magnetic moment (μ_B)											
site	distance (Å)	Ti	V	Cr	Mn	Co	Ni	Cu	Nb	Mo	W
23	5.8			-1.79	0.78		0.89	0.11		-0.79	
24	5.3			-1.86	0.59		0.88	0.11		-0.82	
25	4.8			-1.77	0.97		0.89	0.11		-0.77	
26	4.4	-0.93	-1.35	-1.71	0.93	1.68	0.87	0.11	-0.71	-0.77	-0.74
27	3.9	-0.95	-1.41	-1.83	0.90	1.70	0.86	0.10	-0.73	-0.79	-0.75
28	3.4	-0.94	-1.39	-1.78	0.81	1.71	0.86	0.11	-0.73	-0.78	-0.74
29	2.9	-0.93	-1.47	-2.07	-2.72	1.68	0.82	0.11	-0.72	-0.80	-0.76
30	2.5	-0.93	-1.35	-1.71	0.87	1.66	0.82	0.11	-0.70	-0.74	-0.71
31	2.1	-0.82	-1.27	-1.77	-2.45	1.64	0.80	0.13	-0.68	-0.73	-0.70
32	1.5	-0.87	-1.45	-2.21	-2.89	1.69	0.79	0.11	-0.66	-0.72	-0.67
33	1.2	-0.88	-1.39	-2.12	-2.74	1.59	0.70	0.12	-0.76	-0.85	-0.78
34	0.0	-0.85	-1.57	-2.69	3.06	1.88	0.83	0.11	-0.64	-0.72	-0.65
35	0.0	-0.97	-1.46	-2.14	1.92	1.73	0.76	0.11	-0.75	-0.79	-0.74
36	0.0	-0.74	-1.19	-1.69	-2.05	1.43	0.70	0.14	-0.67	-0.78	-0.72

Table S32: The magnetic moments of the substitutional solutes of Ti, V, Cr, Mn, Co, Ni, Cu, Nb, Mo and W are presented for the $\Sigma 9[110](\bar{2}21)$. Sites are available in the attached poscar files (0 indexed). Magnetic moment of bcc-lattice iron is defined as positive.

Magnetic moment (μ_B)											
site	distance (Å)	Ti	V	Cr	Mn	Co	Ni	Cu	Nb	Mo	W
11	6.5			-1.81	0.52		0.89	0.13		-0.80	
12	5.9			-1.74	0.68		0.88	0.13		-0.78	
13	5.2	-0.96	-1.43	-1.83	0.54	1.70	0.87	0.13	-0.75	-0.80	-0.76
14	4.7	-0.96	-1.40	-1.73	0.70	1.70	0.87	0.13	-0.75	-0.79	-0.75
15	4.0	-0.85	-1.45	-1.89	0.46	1.71	0.80	0.12	-0.65	-0.68	-0.76
16	3.5	-0.94	-1.35	-1.65	0.82	1.70	0.86	0.12	-0.72	-0.74	-0.73
17	2.8	-0.85	-1.47	-2.22	-3.22	1.70	0.80	0.11	-0.64	-0.66	-0.60
18	2.3	-0.93	-1.31	-2.11	-2.59	1.52	0.67	0.13	-0.71	-0.74	-0.71
19	1.5	-0.85	-1.46	-2.31	-3.22	1.70	0.79	0.11	-0.65	-0.66	-0.60
20	1.1	-0.86	-1.41	-2.13	-2.60	1.58	0.68	0.13	-0.73	-0.85	-0.78
21	0.0	-0.86	-1.42	-2.13	-2.60	1.47	0.67	0.13	-0.72	-0.86	-0.79
22	0.0	-0.85	-1.44	-2.51	2.60	1.82	0.78	0.11	-0.64	-0.66	-0.60

Table S33: The magnetic moments of the substitutional solutes of Ti, V, Cr, Mn, Co, Ni, Cu, Nb, Mo and W are presented for the $\Sigma 11[110](\bar{3}\bar{3}2)$. Sites are available in the attached poscar files (0 indexed). Magnetic moment of bcc-lattice iron is defined as positive.

7.2. Voronoi volumes (1 solute)

Voronoi site volumes after relaxation (\AA^3)											
site	distance (\AA)	Ti	V	Cr	Mn	Co	Ni	Cu	Nb	Mo	W
20	6.7			11.36	11.20		11.54	11.62		11.84	
22	5.9			11.34	11.19		11.50	11.58		11.82	
24	5.1			11.41	11.25		11.55	11.64		11.87	
26	4.2	11.94	11.53	11.45	11.29	11.46	11.61	11.68	12.36	11.92	11.89
28	3.4	11.75	11.34	11.22	11.13	11.30	11.44	11.52	12.22	11.76	11.75
30	2.6	12.06	11.66	11.59	11.69	11.53	11.68	11.84	12.50	12.03	12.01
32	1.7	13.02	12.42	12.19	12.00	12.24	12.31	12.56	13.52	12.84	12.84
34	1.1	12.10	11.39	11.12	11.04	11.19	11.21	11.33	13.03	12.17	12.17
36	0.0	13.68	13.35	13.27	13.23	13.14	13.16	13.27	14.19	13.62	13.54

Table S34: The Voronoi volumes of the substitutional solutes of Ti, V, Cr, Mn, Co, Ni, Cu, Nb, Mo and W are presented for the $\Sigma 3[110](1\bar{1}\bar{1})$ after relaxation (volumes before relaxation presented in prior section). Sites are available in the attached poscar files (0 indexed).

Voronoi site volumes after relaxation (\AA^3)											
site	distance (\AA)	Ti	V	Cr	Mn	Co	Ni	Cu	Nb	Mo	W
12	7.0			11.40	11.20		11.57	11.60		11.83	
14	5.9			11.39	11.19		11.57	11.60		11.83	
16	4.7	11.80	11.46	11.39	11.20	11.39	11.54	11.58	12.24	11.81	11.84
18	3.5	11.85	11.47	11.40	11.24	11.44	11.58	11.63	12.28	11.83	11.82
20	2.4	11.95	11.52	11.46	11.29	11.51	11.75	11.79	12.40	11.87	11.88
22	1.2	12.14	11.70	11.61	11.68	11.54	11.73	11.82	12.56	12.08	12.09
24	0.0	12.22	11.92	11.82	11.81	11.84	11.90	11.89	12.63	12.21	12.20

Table S35: The Voronoi volumes of the substitutional solutes of Ti, V, Cr, Mn, Co, Ni, Cu, Nb, Mo and W are presented for the $\Sigma 3[110](1\bar{1}2)$ after relaxation (volumes before relaxation presented in prior section). Sites are available in the attached poscar files (0 indexed).

Voronoi site volumes after relaxation (\AA^3)

site	distance (\AA)	Ti	V	Cr	Mn	Co	Ni	Cu	Nb	Mo	W
23	5.8			11.34	11.20		11.54	11.59		11.84	
24	5.3			11.41	11.25		11.59	11.65		11.88	
25	4.8			11.37	11.23		11.55	11.60		11.85	
26	4.4	11.79	11.37	11.27	11.15	11.31	11.46	11.58	12.24	11.79	11.81
27	3.9	11.88	11.50	11.40	11.26	11.42	11.57	11.63	12.33	11.89	11.89
28	3.4	11.90	11.46	11.32	11.20	11.37	11.57	11.67	12.33	11.85	11.84
29	2.9	12.59	12.06	11.90	12.12	11.71	12.05	12.26	12.99	12.41	12.34
30	2.5	12.01	11.58	11.48	11.37	11.51	11.62	11.77	12.56	12.06	12.03
31	2.1	12.36	11.77	11.66	11.83	11.60	11.90	12.14	13.14	12.37	12.34
32	1.5	12.79	12.33	12.27	12.32	12.15	12.33	12.48	13.53	12.82	12.83
33	1.2	13.13	11.97	11.71	11.78	11.30	11.71	12.14	14.06	12.87	12.76
34	0.0	14.13	13.85	13.88	13.96	13.78	13.79	13.99	14.35	13.96	13.91
35	0.0	13.01	12.19	12.06	12.09	12.06	12.11	12.39	13.65	12.86	12.80
36	0.0	12.56	10.80	10.57	10.54	10.66	10.74	11.19	13.71	11.72	11.73

Table S36: The Voronoi volumes of the substitutional solutes of Ti, V, Cr, Mn, Co, Ni, Cu, Nb, Mo and W are presented for the $\Sigma 9[110](2\bar{2}1)$ after relaxation (volumes before relaxation presented in prior section). Sites are available in the attached poscar files (0 indexed).Voronoi site volumes after relaxation (\AA^3)

site	distance (\AA)	Ti	V	Cr	Mn	Co	Ni	Cu	Nb	Mo	W
11	6.5			11.40	11.22		11.57	11.70		11.87	
12	5.9			11.33	11.19		11.52	11.63		11.85	
13	5.2	11.94	11.52	11.43	11.26	11.44	11.60	11.72	12.41	11.92	11.91
14	4.7	11.83	11.43	11.30	11.16	11.34	11.49	11.60	12.35	11.87	11.84
15	4.0	13.59	11.61	11.52	11.31	11.48	12.12	13.13	13.83	13.22	12.02
16	3.5	11.79	11.33	11.20	11.11	11.27	11.42	11.57	12.28	11.77	11.83
17	2.8	13.56	12.04	12.08	13.06	11.76	12.08	13.11	13.81	13.21	13.15
18	2.3	11.83	11.31	11.22	11.29	11.27	11.32	11.62	12.31	11.80	11.81
19	1.5	13.57	12.88	12.53	13.04	11.80	12.38	13.06	13.83	13.21	13.15
20	1.1	12.69	11.58	11.23	11.28	11.23	11.32	11.64	13.77	12.37	12.32
21	0.0	12.74	11.39	11.23	11.28	11.18	11.32	11.63	14.61	12.38	12.33
22	0.0	13.56	13.03	13.02	12.92	12.92	12.35	13.07	13.80	13.21	13.14

Table S37: The Voronoi volumes of the substitutional solutes of Ti, V, Cr, Mn, Co, Ni, Cu, Nb, Mo and W are presented for the $\Sigma 11[110](3\bar{3}2)$ after relaxation (volumes before relaxation presented in prior section). Sites are available in the attached poscar files (0 indexed).

7.3. E_{seg} vs Voronoi volumes

To demonstrate the relationship between site volume and segregation tendency for large solutes, we plot the final Voronoi volume calculated for a solute against their segregation energy at that site, in the single solute case in Figs S6-S15. The site preferencing of differing sized solutes here is evident, with smaller solutes generally preferring smaller sites to larger sites [e.g. Co], and inverse is true for larger solutes [e.g. Ti, V, Nb, Mo, W].

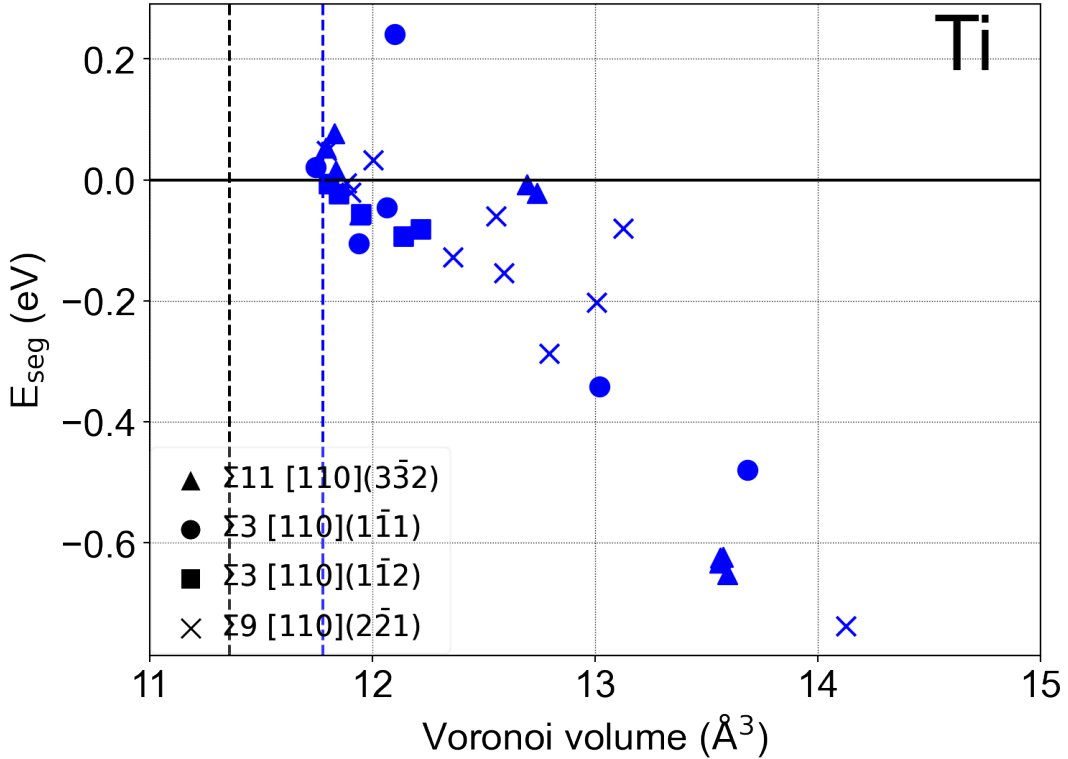


Figure S6: The segregation energy (E_{seg}) is plotted against the relaxed Voronoi volume occupied by the solute at that site, for Ti. The black/coloured dashed lines indicate Voronoi volume occupied in the bulk by a Fe/X atom, respectively.

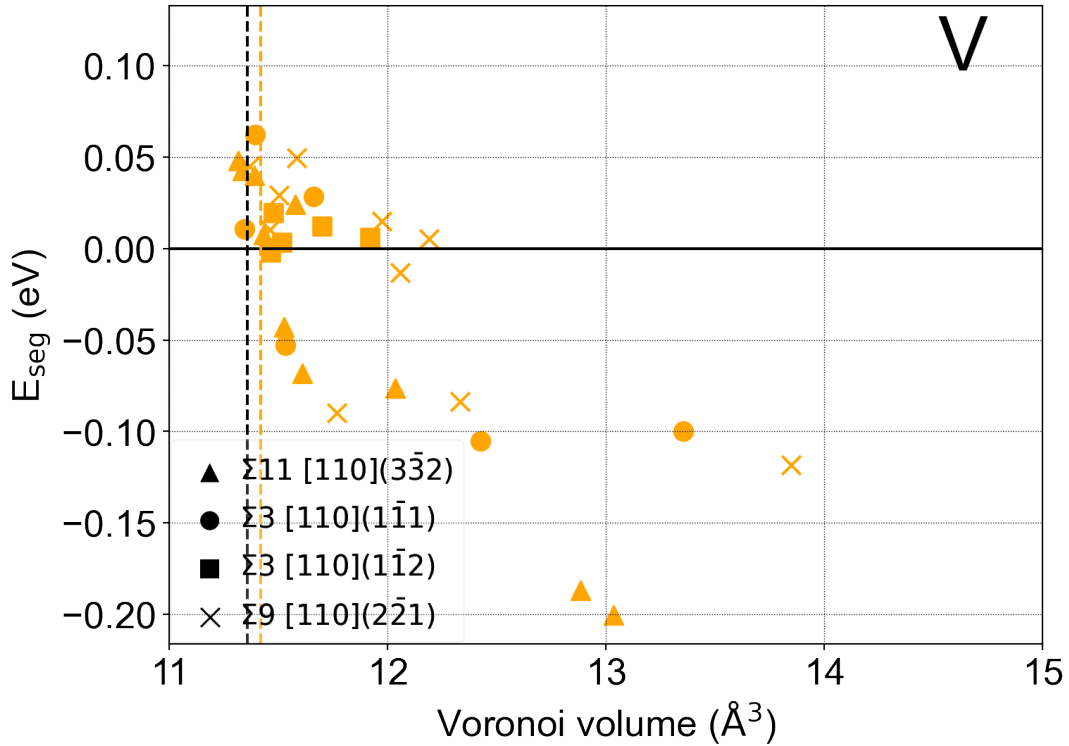


Figure S7: The segregation energy (E_{seg}) is plotted against the relaxed Voronoi volume occupied by the solute at that site, for V. The black/coloured dashed lines indicate Voronoi volume occupied in the bulk by a Fe/X atom, respectively.

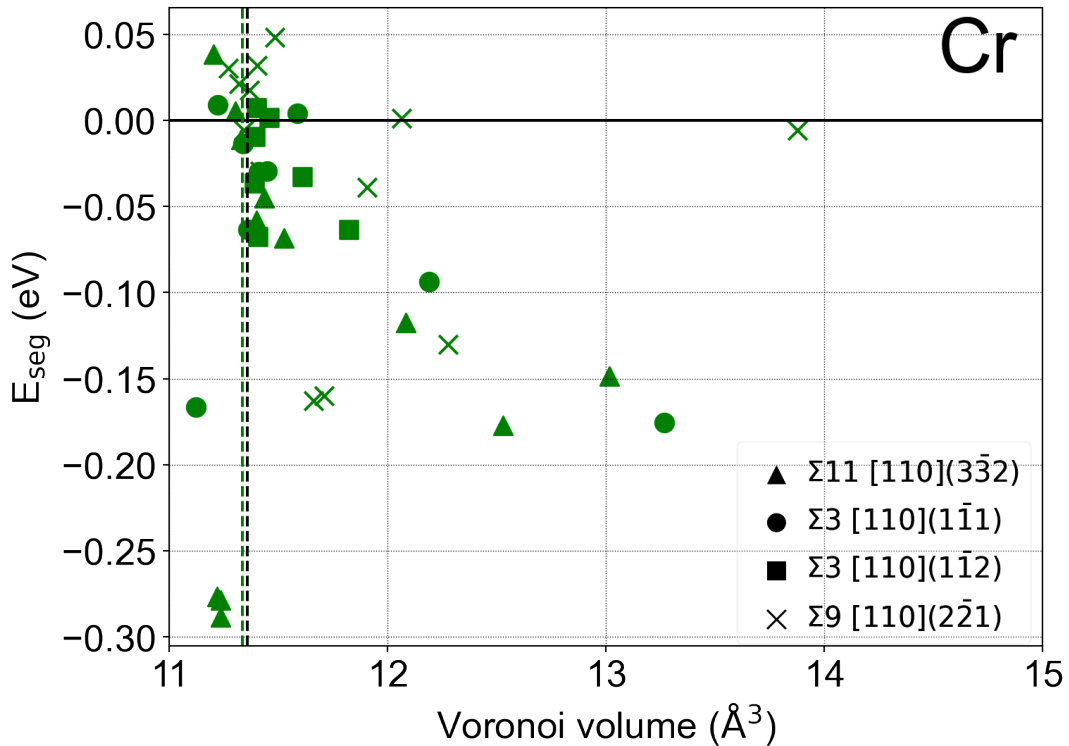


Figure S8: The segregation energy (E_{seg}) is plotted against the relaxed Voronoi volume occupied by the solute at that site, for Cr. The black/coloured dashed lines indicate Voronoi volume occupied in the bulk by a Fe/X atom, respectively.

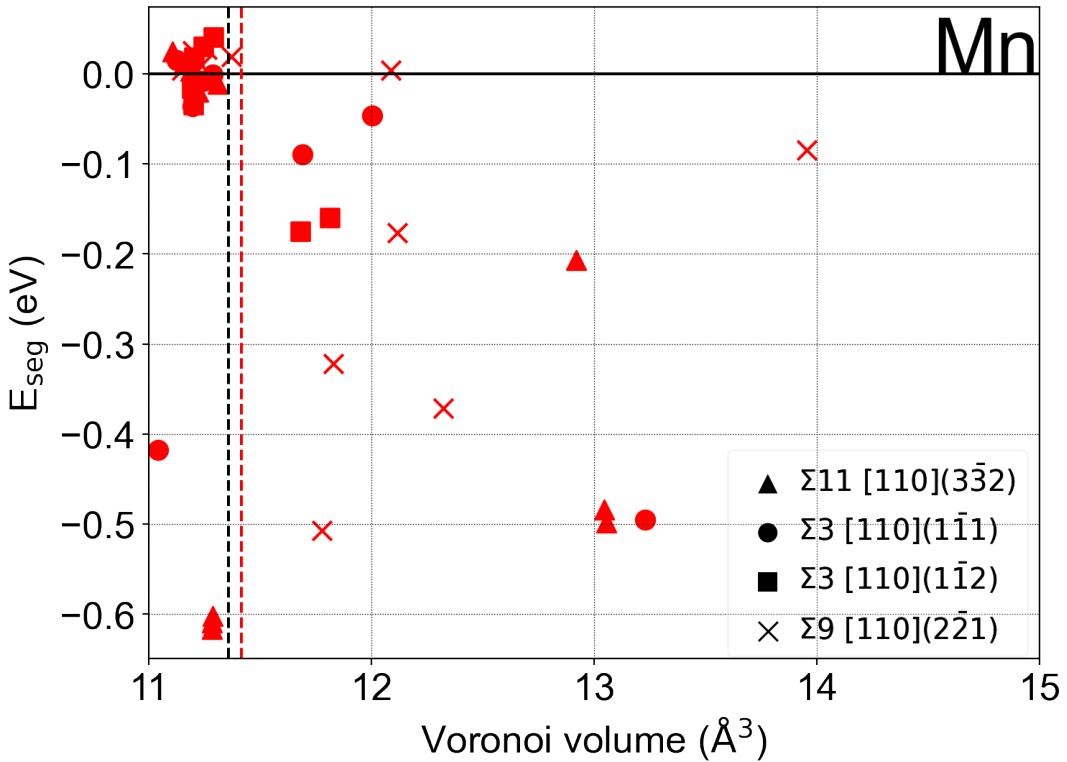


Figure S9: The segregation energy (E_{seg}) is plotted against the relaxed Voronoi volume occupied by the solute at that site, for Mn. The black/coloured dashed lines indicate Voronoi volume occupied in the bulk by a Fe/X atom, respectively.

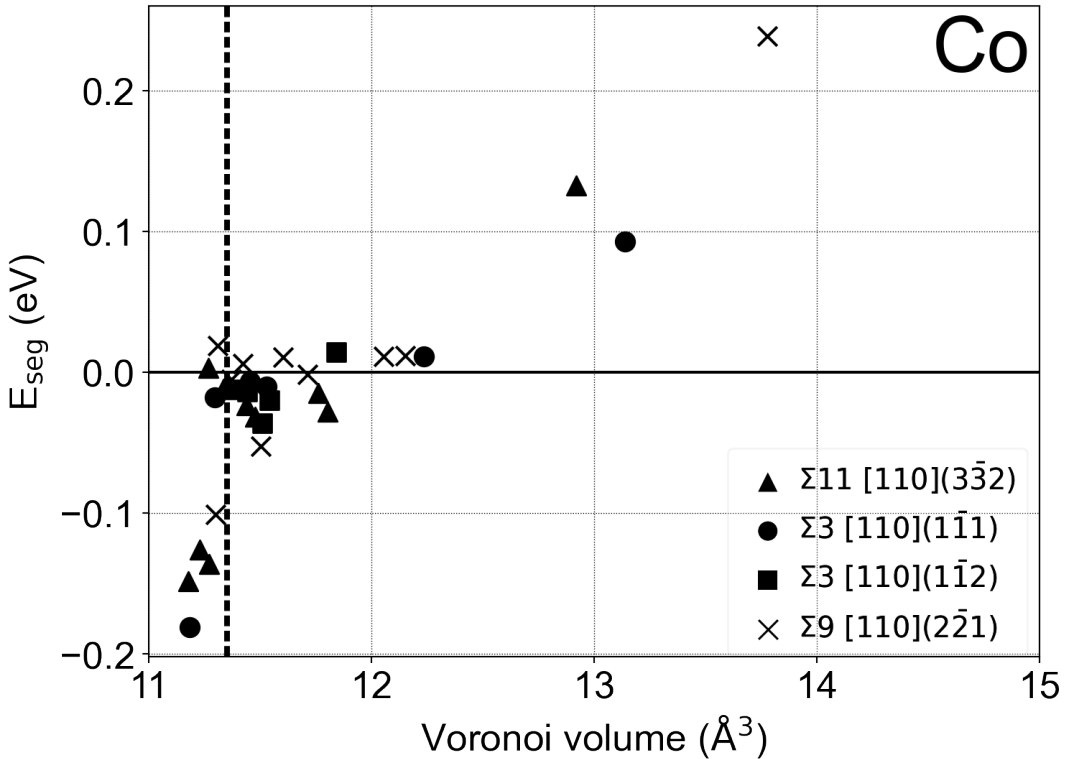


Figure S10: The segregation energy (E_{seg}) is plotted against the relaxed Voronoi volume occupied by the solute at that site, for Co. The black/coloured dashed lines indicate Voronoi volume occupied in the bulk by a Fe/X atom, respectively.

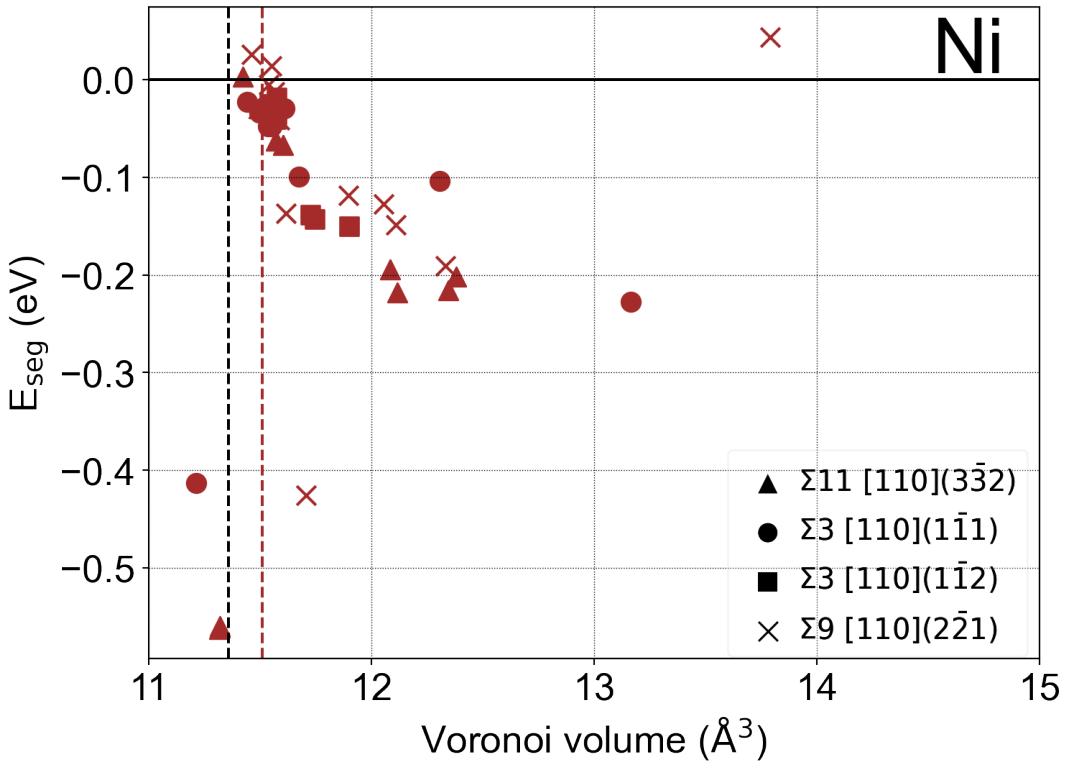


Figure S11: The segregation energy (E_{seg}) is plotted against the relaxed Voronoi volume occupied by the solute at that site, for Ni. The black/coloured dashed lines indicate Voronoi volume occupied in the bulk by a Fe/X atom, respectively.

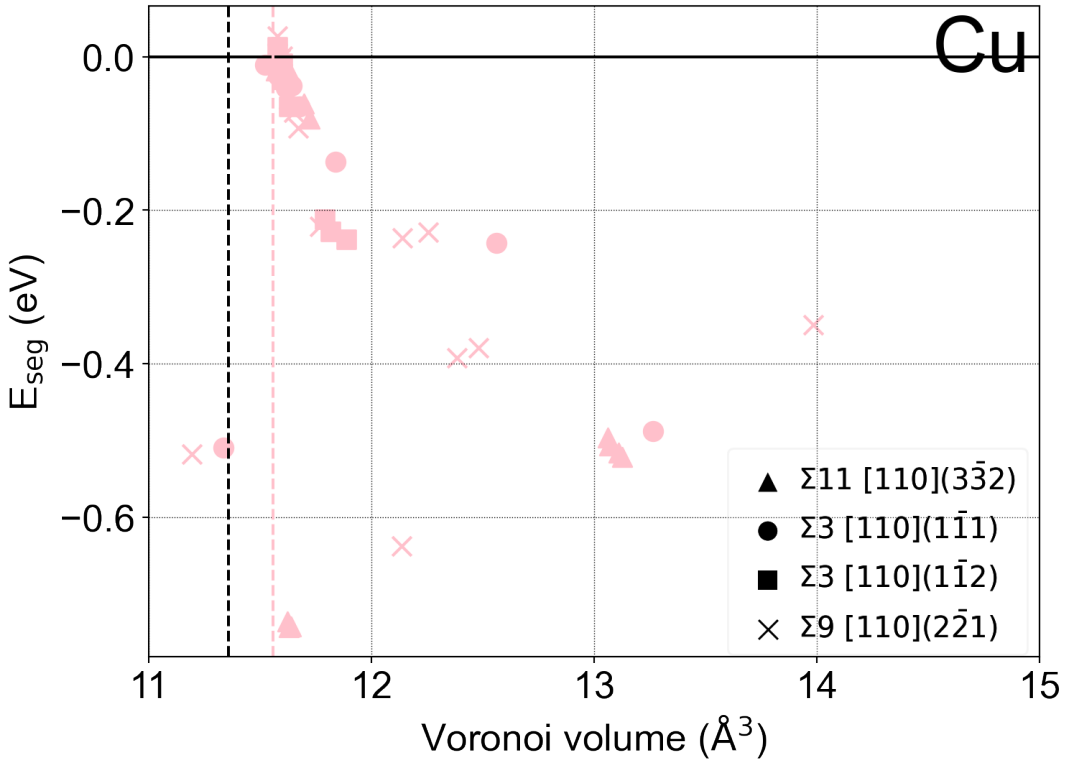


Figure S12: The segregation energy (E_{seg}) is plotted against the relaxed Voronoi volume occupied by the solute at that site, for Cu. The black/coloured dashed lines indicate Voronoi volume occupied in the bulk by a Fe/X atom, respectively.

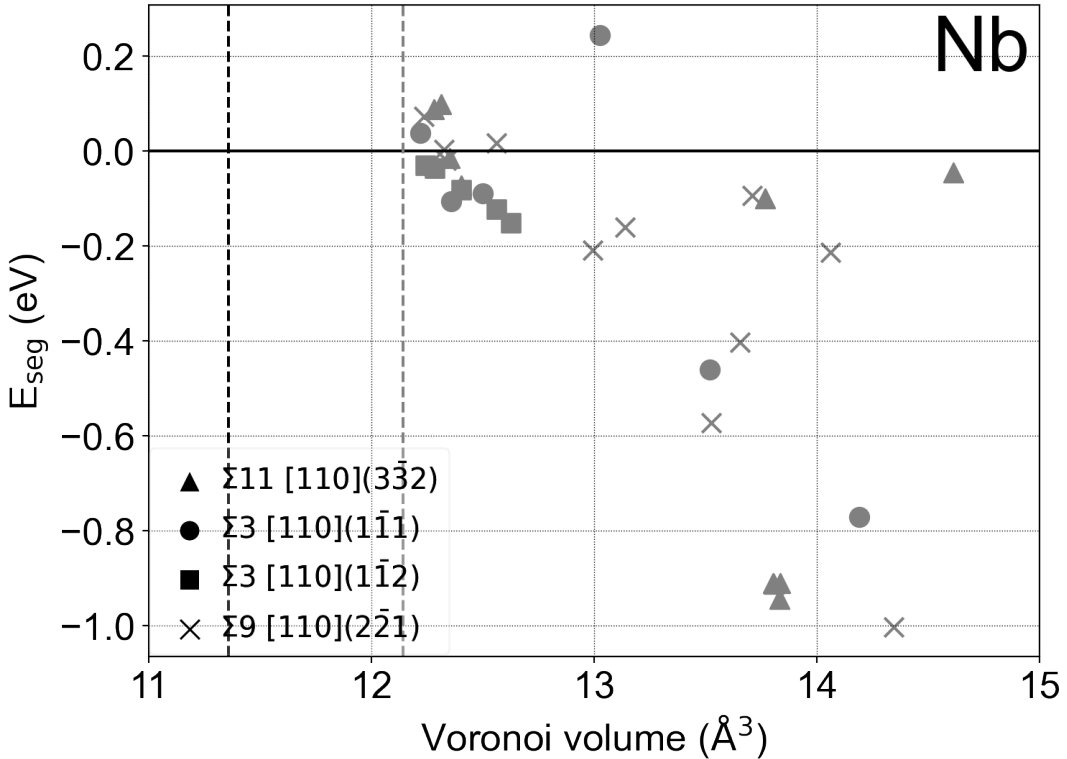


Figure S13: The segregation energy (E_{seg}) is plotted against the relaxed Voronoi volume occupied by the solute at that site, for Nb. The black/coloured dashed lines indicate Voronoi volume occupied in the bulk by a Fe/X atom, respectively.

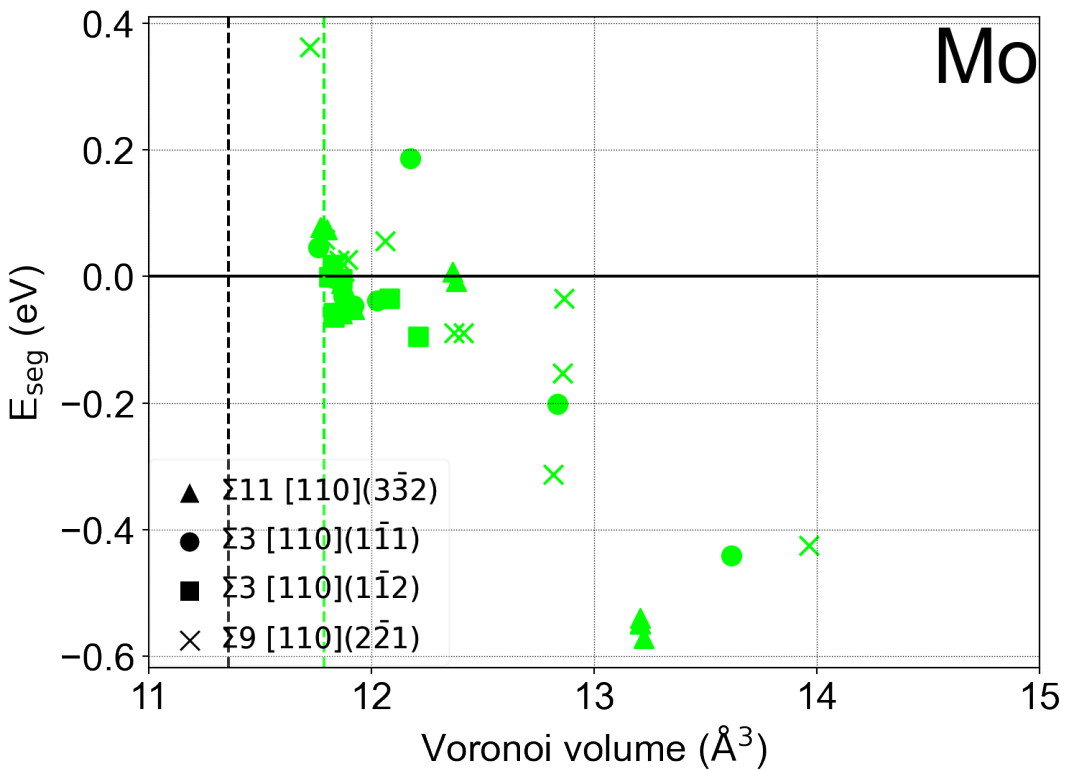


Figure S14: The segregation energy (E_{seg}) is plotted against the relaxed Voronoi volume occupied by the solute at that site, for Mo. The black/coloured dashed lines indicate Voronoi volume occupied in the bulk by a Fe/X atom, respectively.

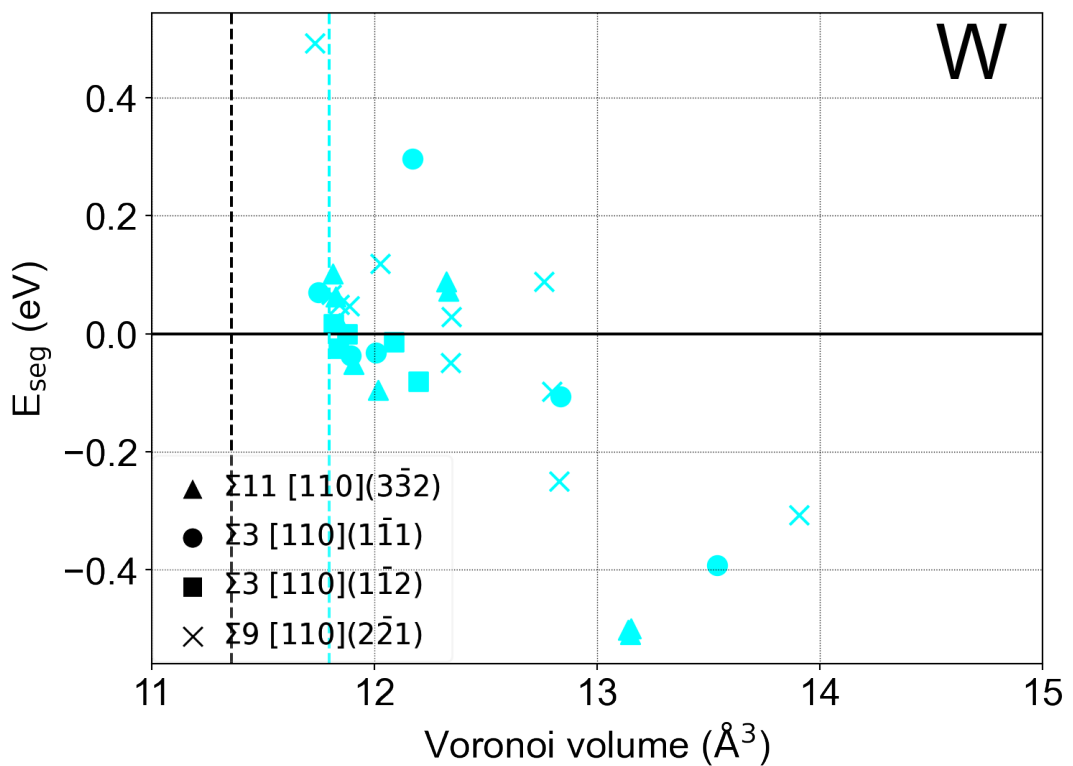


Figure S15: The segregation energy (E_{seg}) is plotted against the relaxed Voronoi volume occupied by the solute at that site, for W. The black/coloured dashed lines indicate Voronoi volume occupied in the bulk by a Fe/X atom, respectively.

7.4. E_{seg} vs Magnetic moment

To investigate if there was any relationship between the magnetic state of a solute and its segregation energy at a GB, we plot the final magnetic moment calculated for a solute against their segregation energy at that site, in the single solute case in Figs S16-S25.

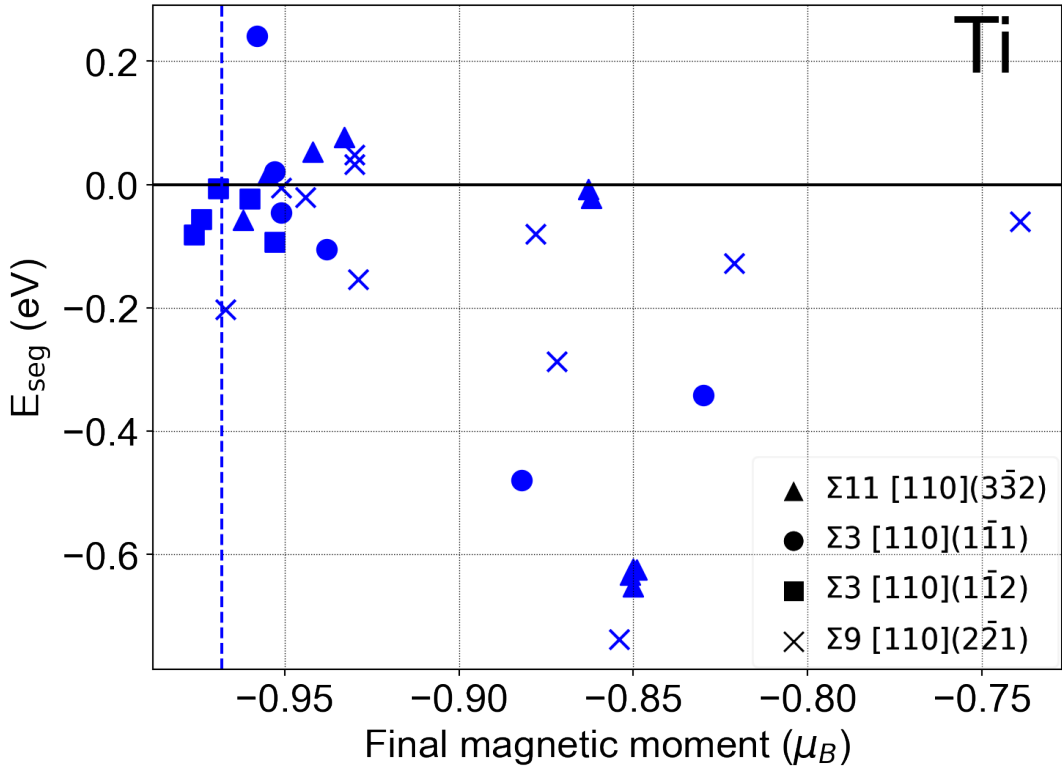


Figure S16: The segregation energy (E_{seg}) for Ti is plotted against the magnetic moment (μ_B) of the site. The black/coloured dashed lines indicate magnetic moments of the Fe/solute atom when located in the bulk, respectively.

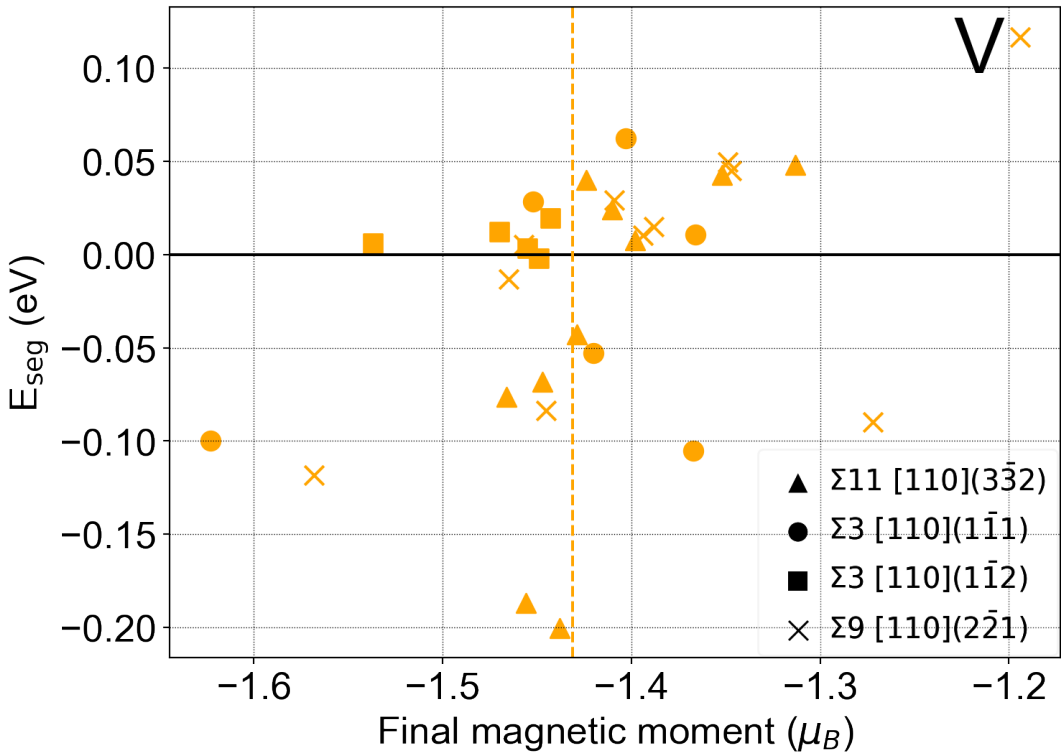


Figure S17: The segregation energy (E_{seg}) for V is plotted against the magnetic moment (μ_B) of the site. The black/coloured dashed lines indicate magnetic moments of the Fe/solute atom when located in the bulk, respectively.

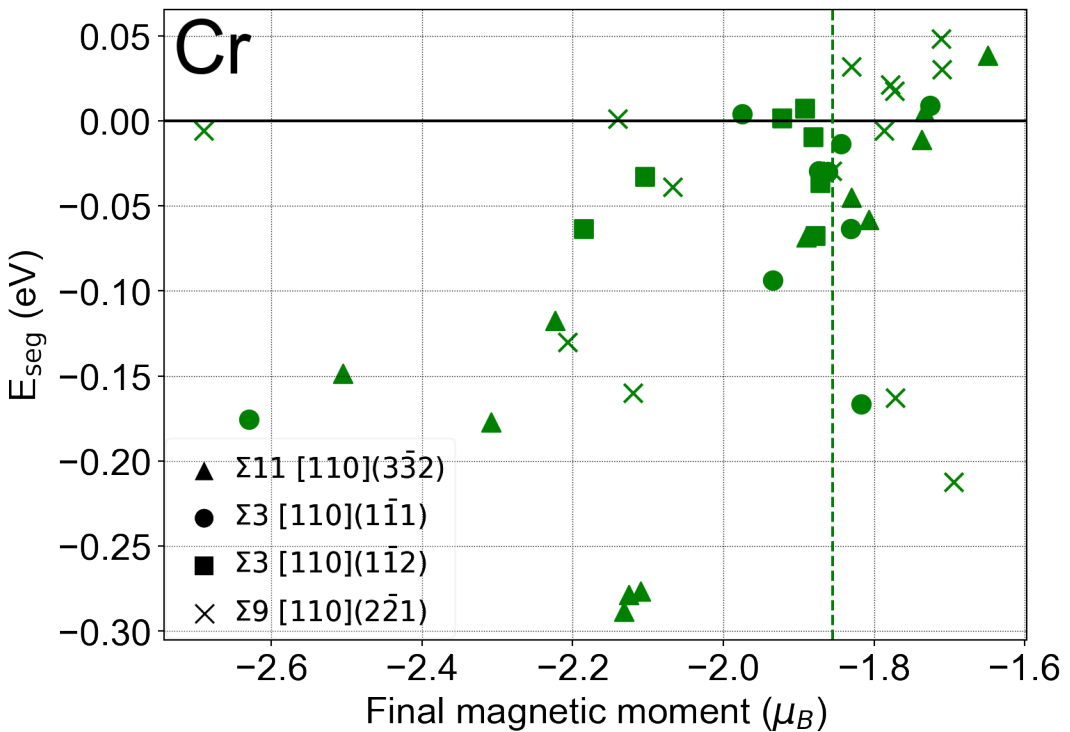


Figure S18: The segregation energy (E_{seg}) for Cr is plotted against the magnetic moment (μ_B) of the site. The black/coloured dashed lines indicate magnetic moments of the Fe/solute atom when located in the bulk, respectively.

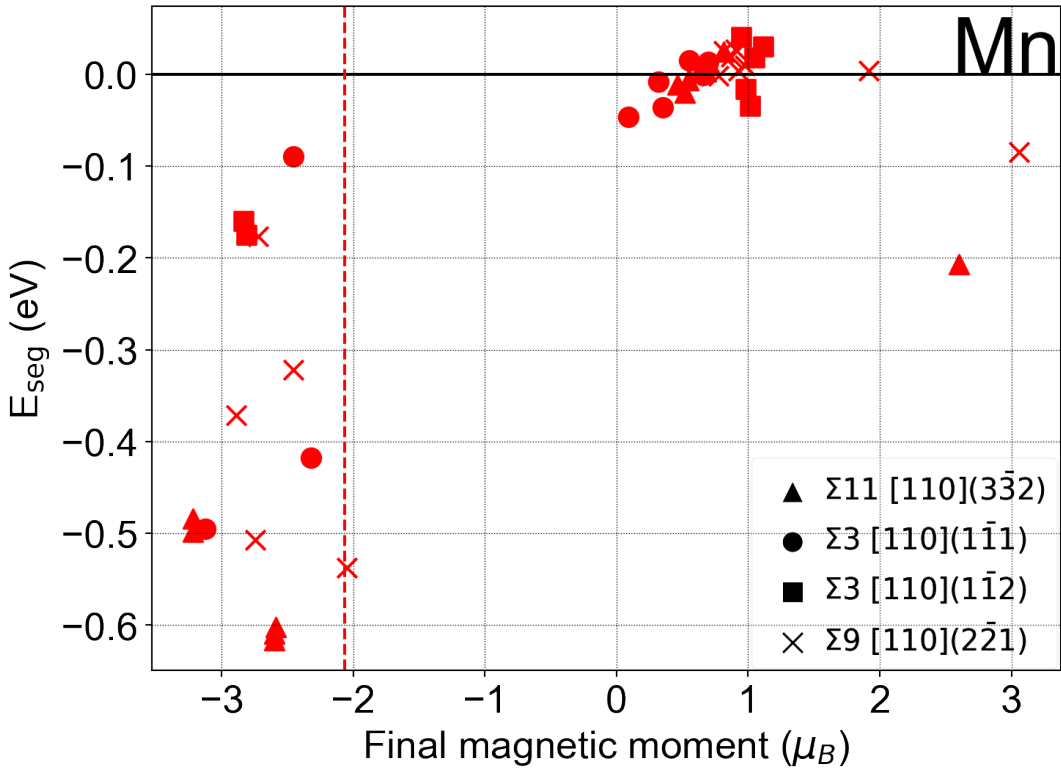


Figure S19: The segregation energy (E_{seg}) for Mn is plotted against the magnetic moment (μ_B) of the site. The black/coloured dashed lines indicate magnetic moments of the Fe/solute atom when located in the bulk, respectively.

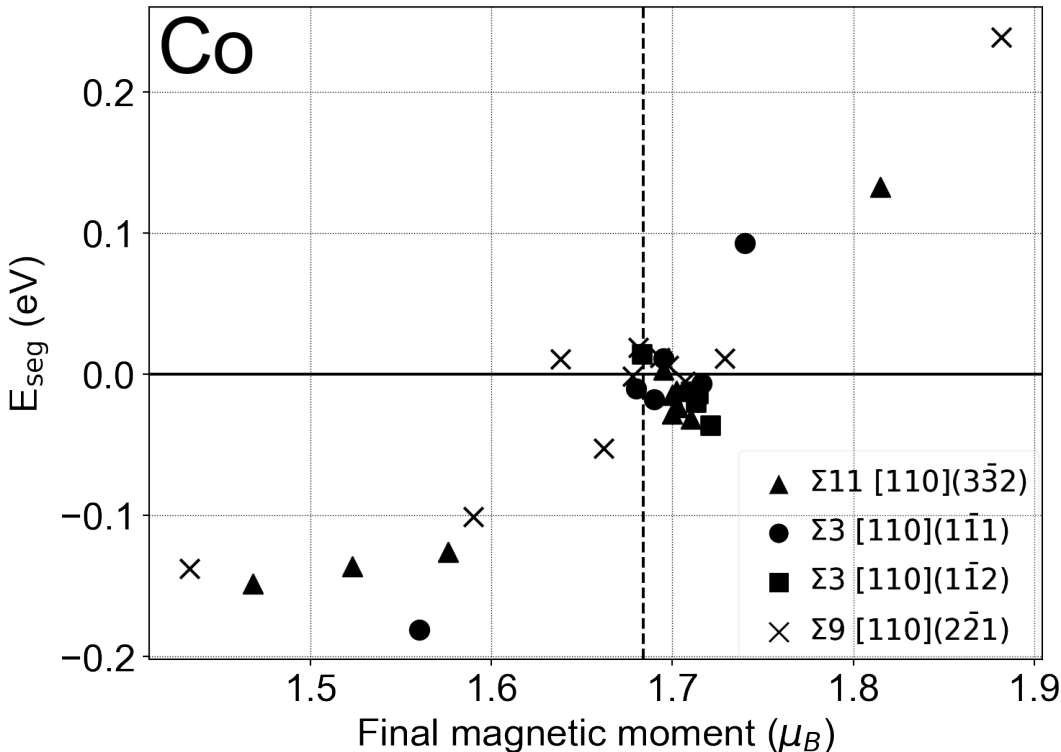


Figure S20: The segregation energy (E_{seg}) for Co is plotted against the magnetic moment (μ_B) of the site. The black/coloured dashed lines indicate magnetic moments of the Fe/solute atom when located in the bulk, respectively.

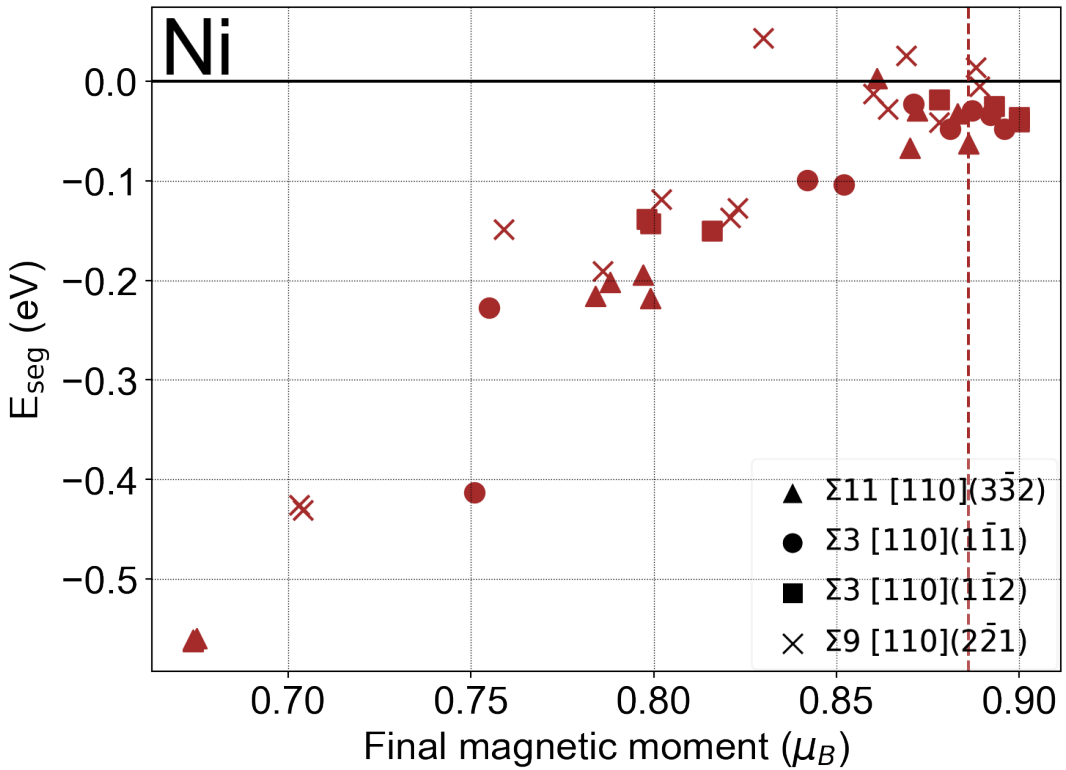


Figure S21: The segregation energy (E_{seg}) for Ni is plotted against the magnetic moment (μ_B) of the site. The black/coloured dashed lines indicate magnetic moments of the Fe/solute atom when located in the bulk, respectively.

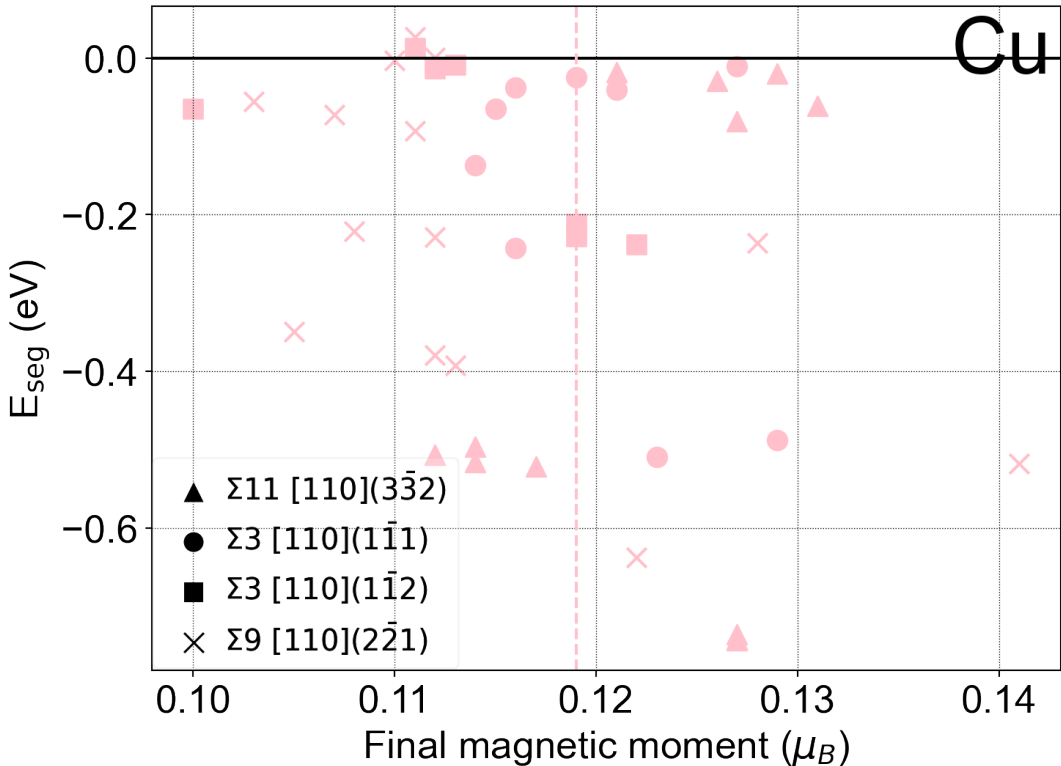


Figure S22: The segregation energy (E_{seg}) for Cu is plotted against the magnetic moment (μ_B) of the site. The black/coloured dashed lines indicate magnetic moments of the Fe/solute atom when located in the bulk, respectively.

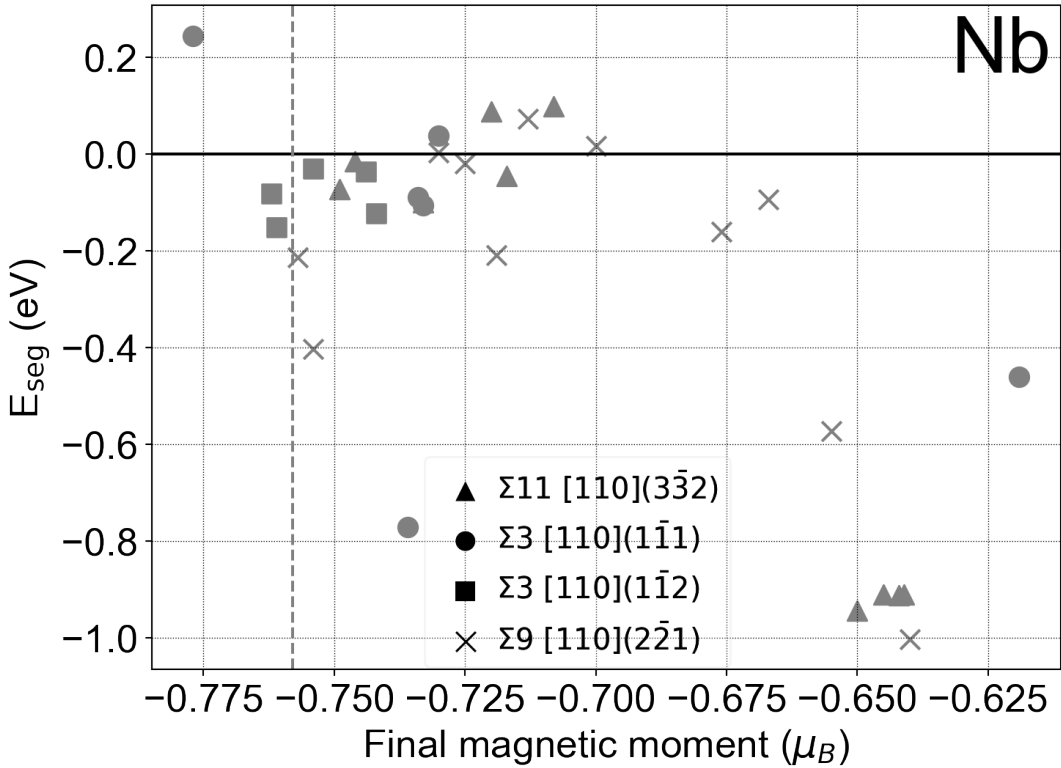


Figure S23: The segregation energy (E_{seg}) for Nb is plotted against the magnetic moment (μ_B) of the site. The black/coloured dashed lines indicate magnetic moments of the Fe/solute atom when located in the bulk, respectively.

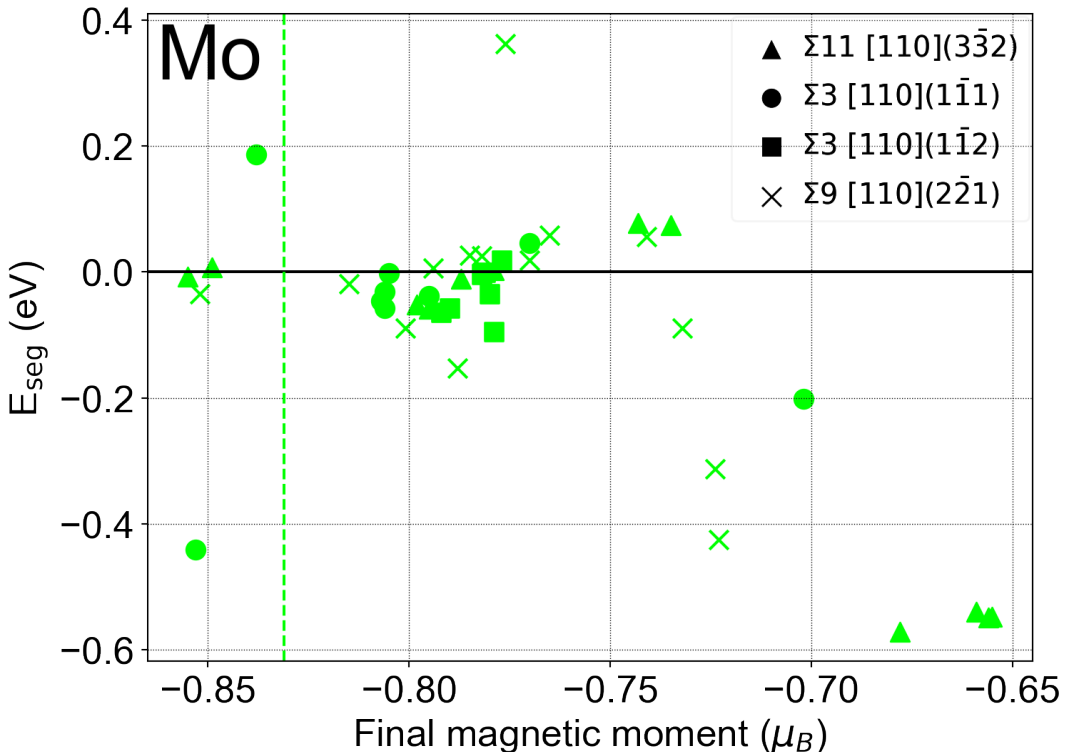


Figure S24: The segregation energy (E_{seg}) for Mo is plotted against the magnetic moment (μ_B) of the site. The black/coloured dashed lines indicate magnetic moments of the Fe/solute atom when located in the bulk, respectively.

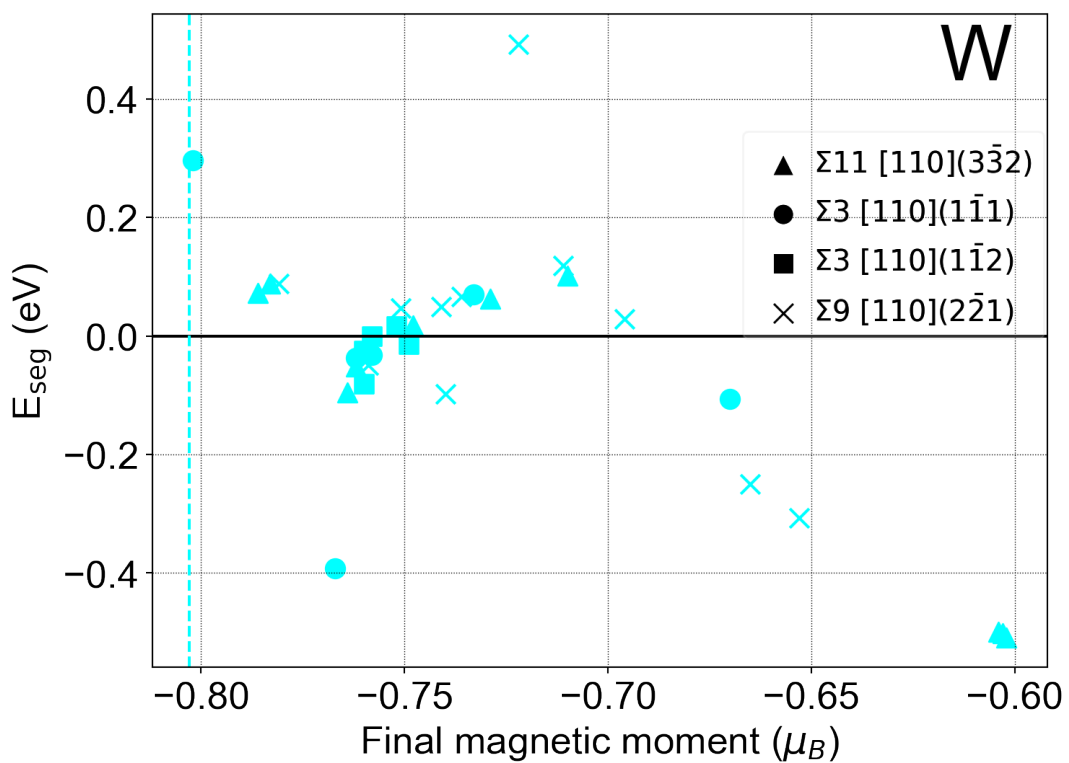


Figure S25: The segregation energy (E_{seg}) for W is plotted against the magnetic moment (μ_B) of the site. The black/coloured dashed lines indicate magnetic moments of the Fe/solute atom when located in the bulk, respectively.

7.5. Magnetic moment vs Voronoi volume at a site

To investigate any possible relationship between the magnetic state of a solute and the volume of a site, we plot the final magnetic moment of a solute against the calculated Voronoi volume in the final relaxed GB, in the single solute segregation case [Figs S26-S35]. From these plots, it is evident that the magnetic moment of V, Cr become more deeply negative (i.e. antiparallel to the Fe matrix) at sites with greater volumes, and that Co's ferromagnetic magnetic moment becomes stronger with increasing site volume.

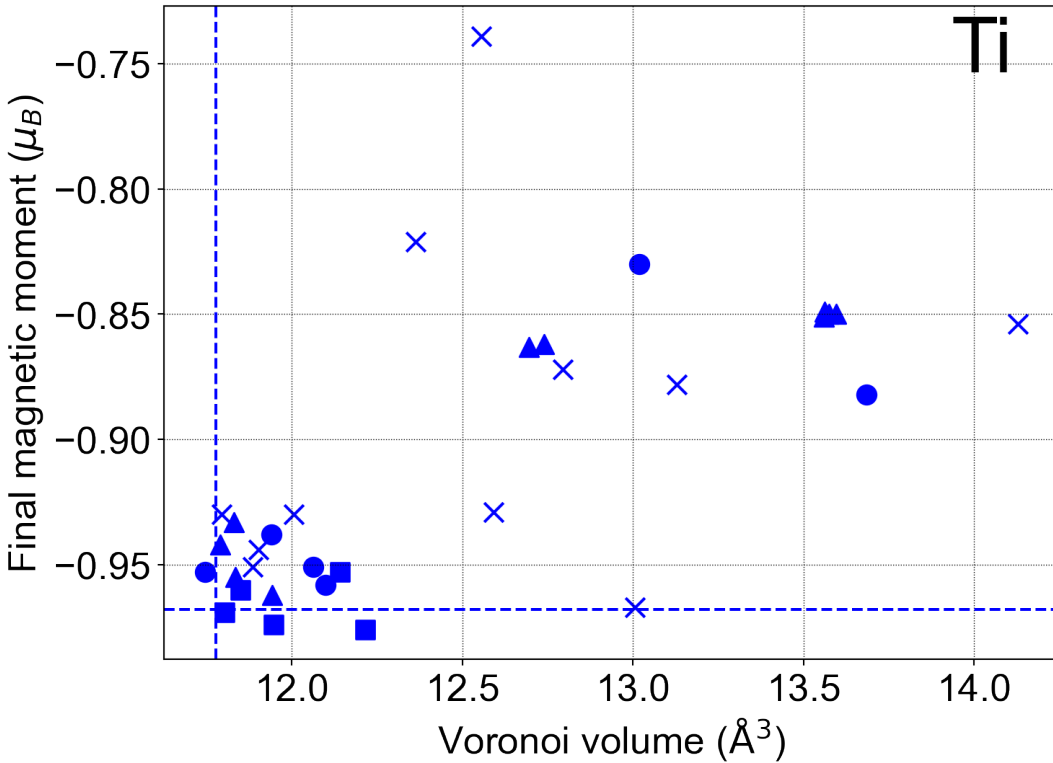


Figure S26: The magnetic moment (μ_B) for Ti is plotted against the relaxed Voronoi volume occupied by the solute at that site. The black/coloured dashed lines indicate the respective bulk values for the Fe/solute atom, respectively.

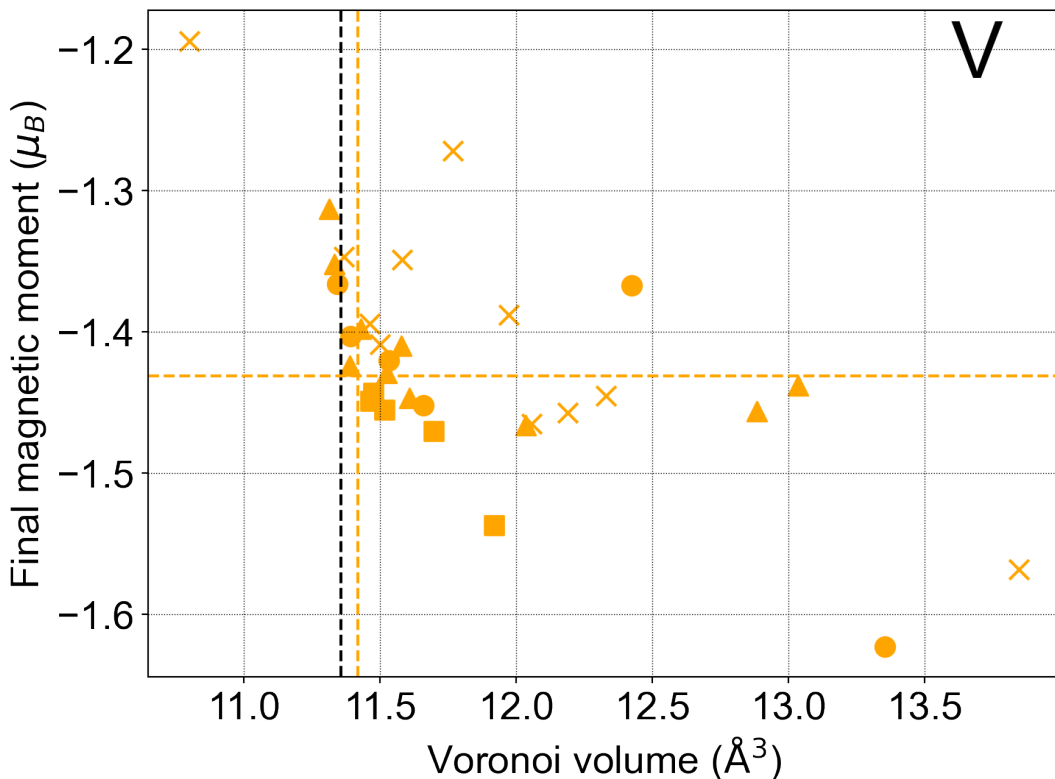


Figure S27: The magnetic moment (μ_B) for V is plotted against the relaxed Voronoi volume occupied by the solute at that site. The black/coloured dashed lines indicate the respective bulk values for the Fe/solute atom, respectively

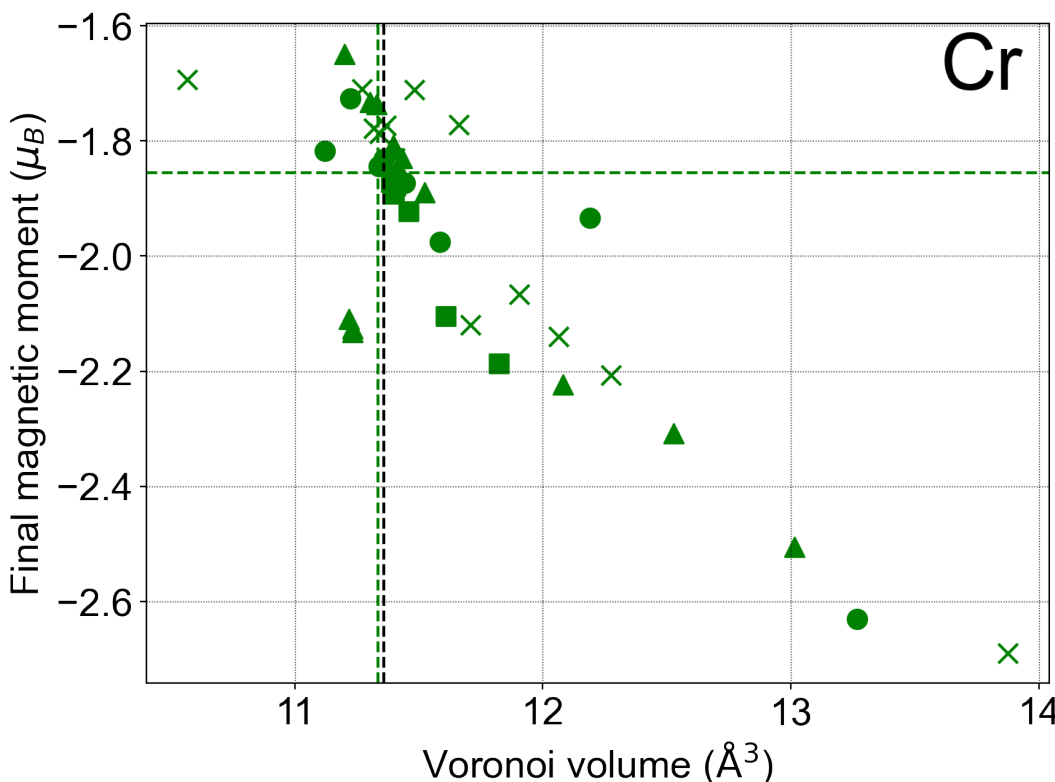


Figure S28: The magnetic moment (μ_B) for Cr is plotted against the relaxed Voronoi volume occupied by the solute at that site. The black/coloured dashed lines indicate the respective bulk values for the Fe/solute atom, respectively

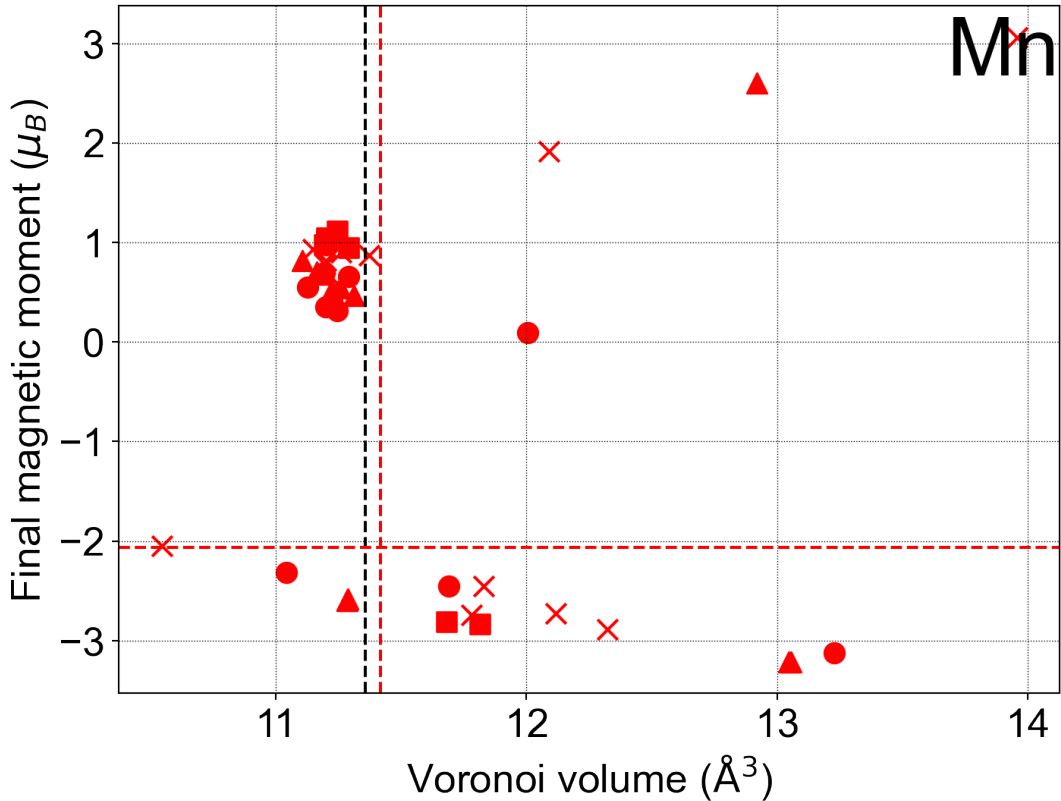


Figure S29: The magnetic moment (μ_B) for Mn is plotted against the relaxed Voronoi volume occupied by the solute at that site. The black/coloured dashed lines indicate the respective bulk values for the Fe/solute atom, respectively

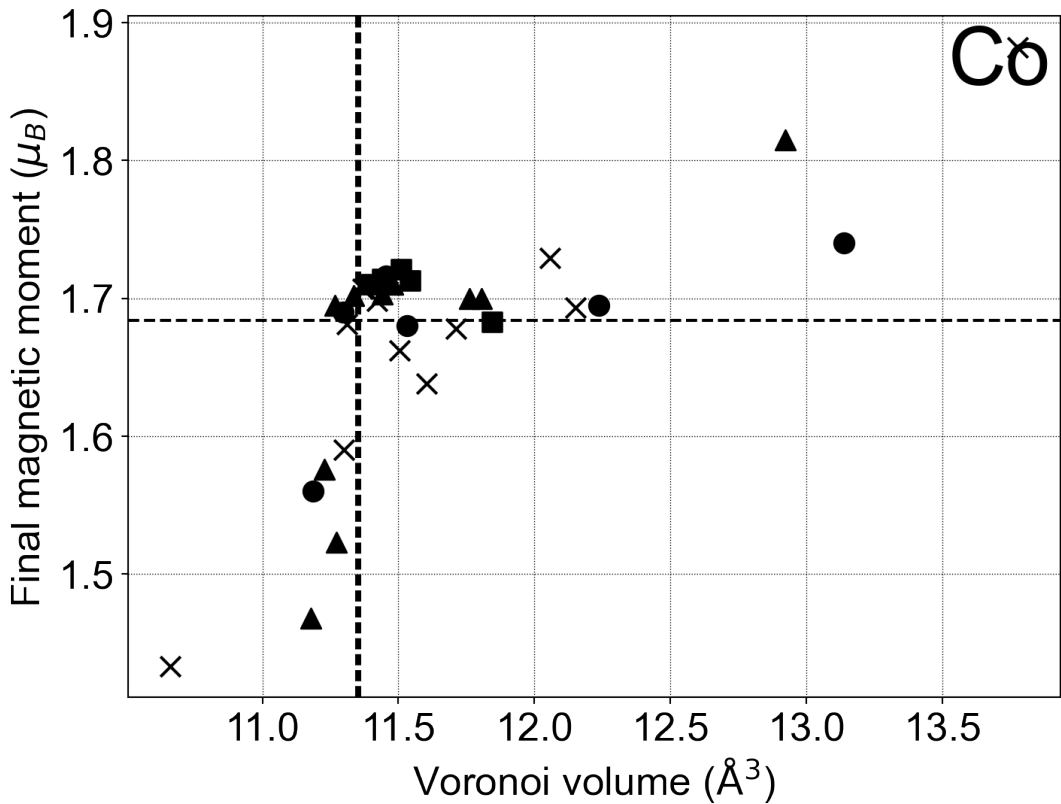


Figure S30: The magnetic moment (μ_B) for Co is plotted against the relaxed Voronoi volume occupied by the solute at that site. The black/coloured dashed lines indicate the respective bulk values for the Fe/solute atom, respectively

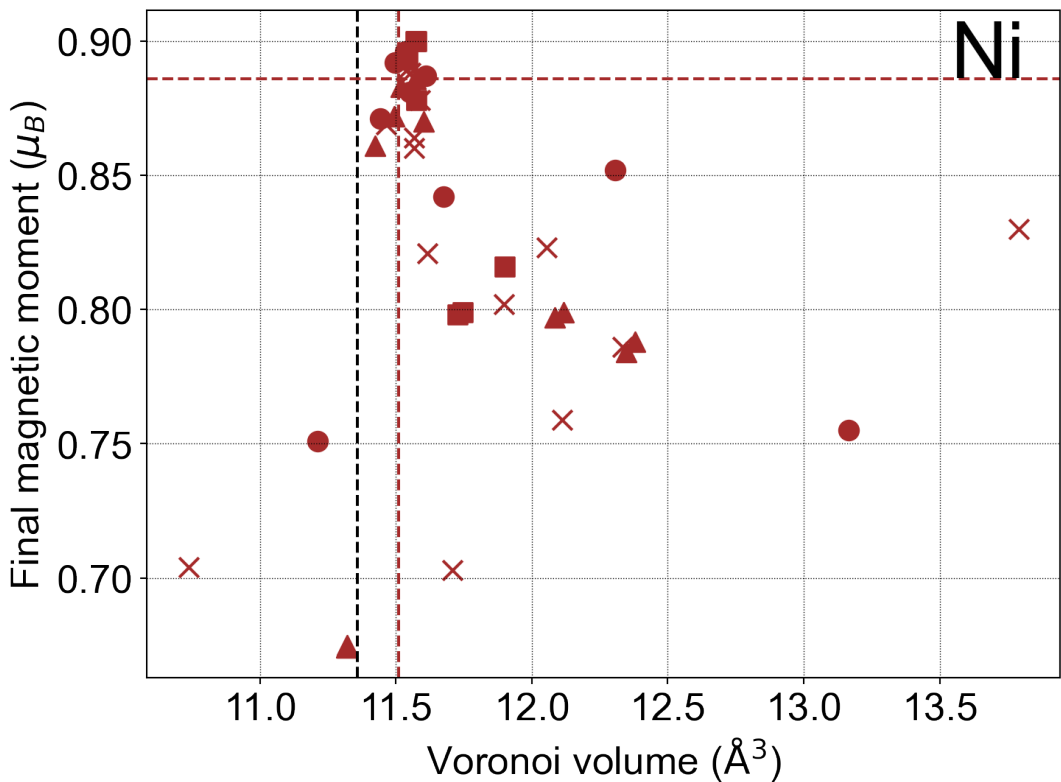


Figure S31: The magnetic moment (μ_B) for Ni is plotted against the relaxed Voronoi volume occupied by the solute at that site. The black/coloured dashed lines indicate the respective bulk values for the Fe/solute atom, respectively

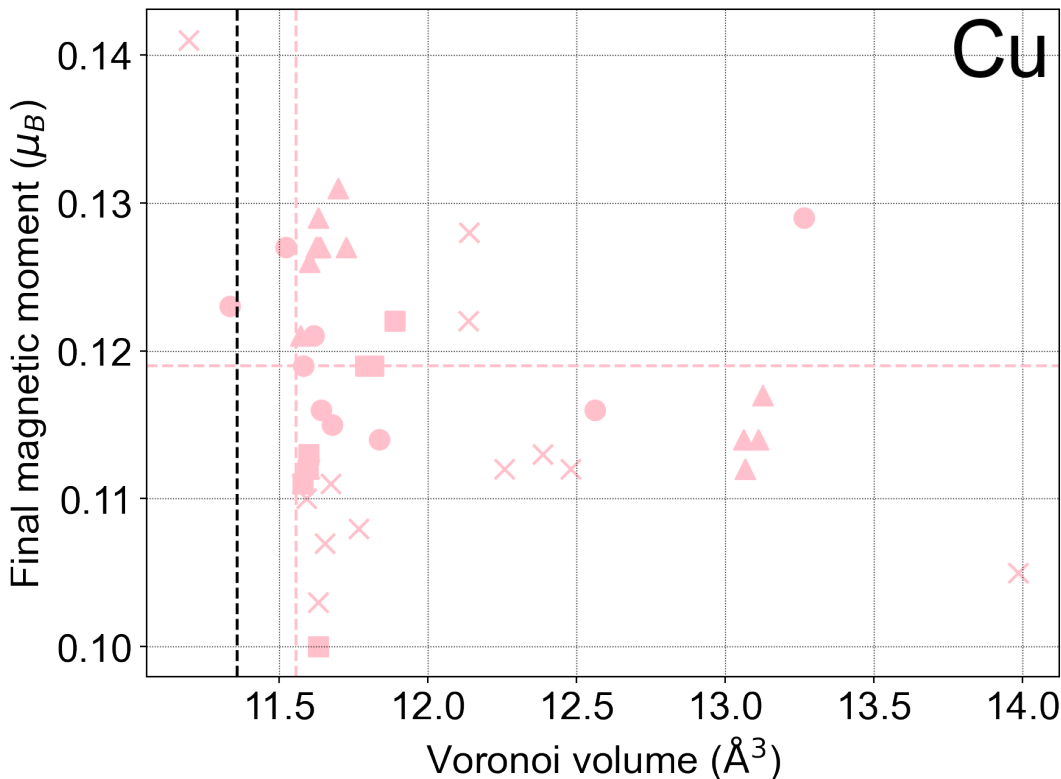


Figure S32: The magnetic moment (μ_B) for Cu is plotted against the relaxed Voronoi volume occupied by the solute at that site. The black/coloured dashed lines indicate the respective bulk values for the Fe/solute atom, respectively

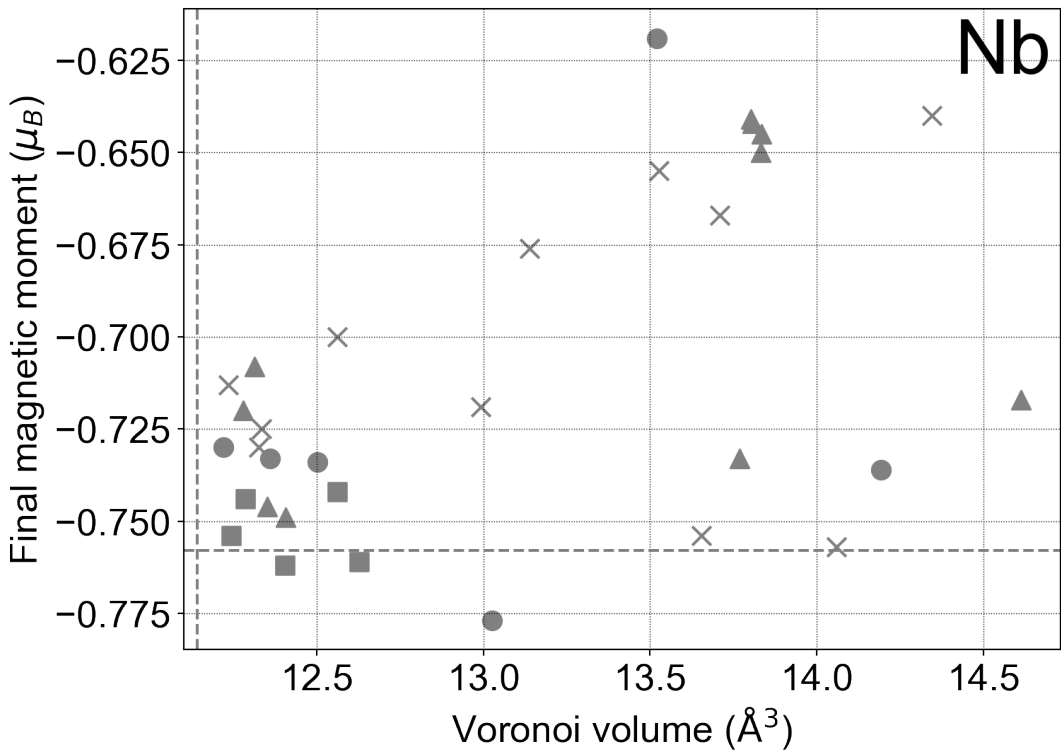


Figure S33: The magnetic moment (μ_B) for Nb is plotted against the relaxed Voronoi volume occupied by the solute at that site. The black/coloured dashed lines indicate the respective bulk values for the Fe/solute atom, respectively

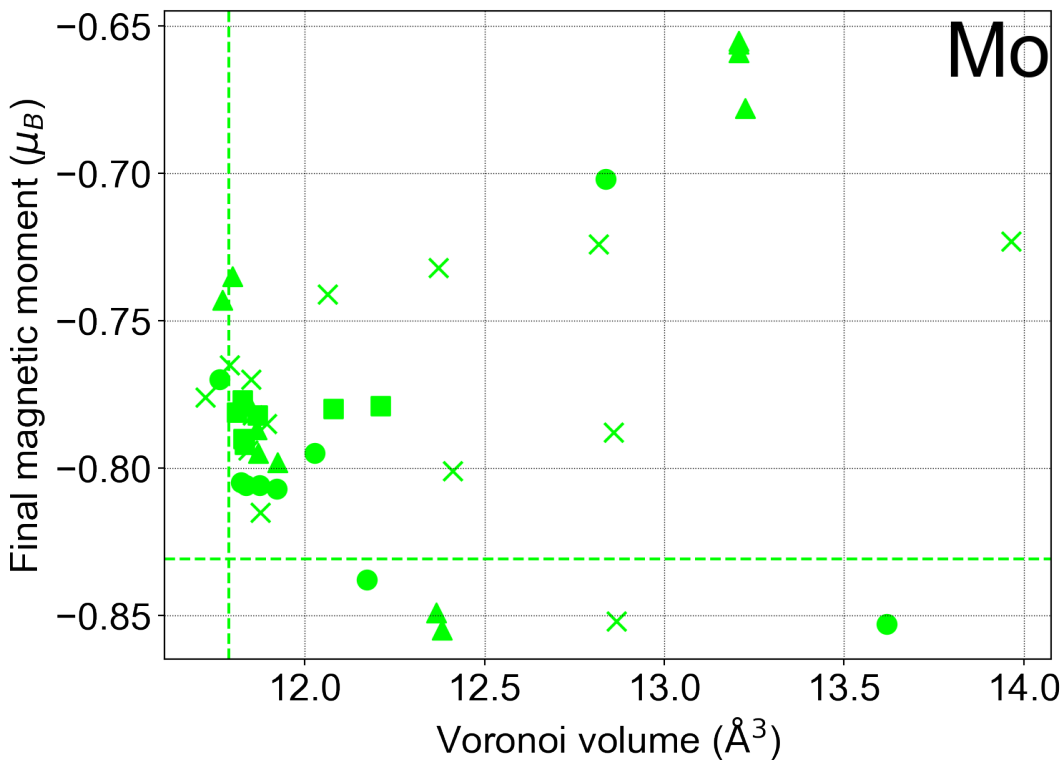


Figure S34: The magnetic moment (μ_B) for Mo is plotted against the relaxed Voronoi volume occupied by the solute at that site. The black/coloured dashed lines indicate the respective bulk values for the Fe/solute atom, respectively

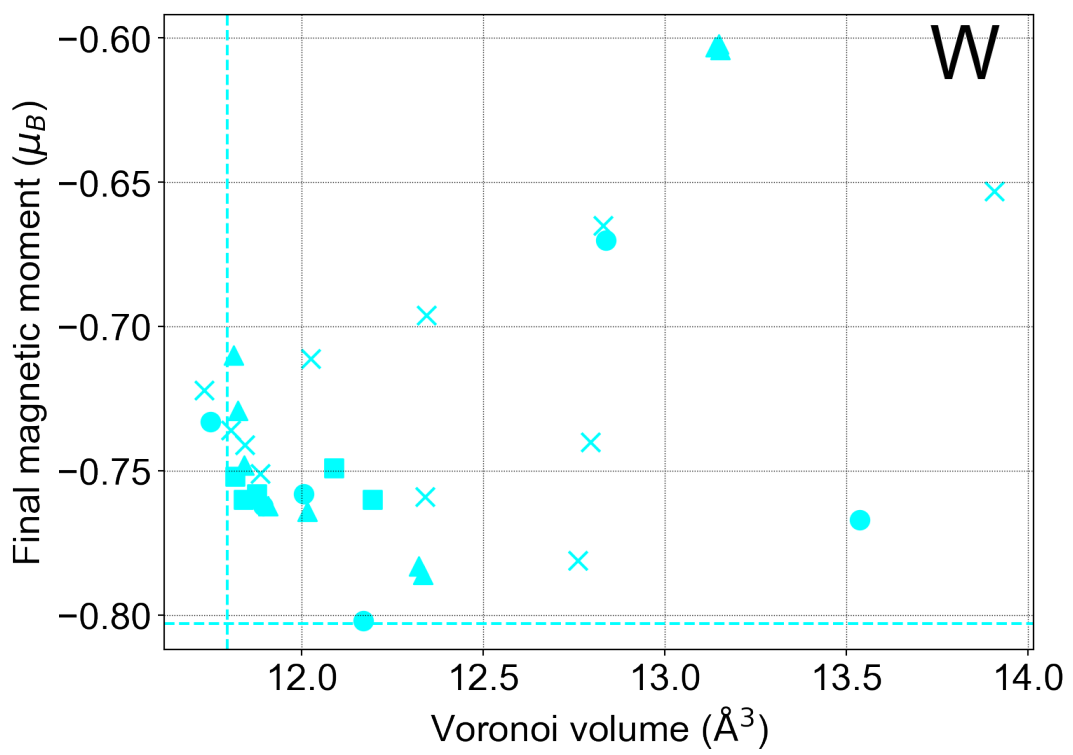


Figure S35: The magnetic moment (μ_B) for W is plotted against the relaxed Voronoi volume occupied by the solute at that site. The black/coloured dashed lines indicate the respective bulk values for the Fe/solute atom, respectively

7.6. Single solute segregation vs cohesion

We plot the cohesion (work of separation - W_{sep} and cohesion effects - η) against the segregation tendencies (segregation energy - E_{seg}) of each element to the GB [Fig. S36]. In the main text, the effect is presented for results calculated in the *relaxed* framework. Here, we present the cohesion effects and cohesion calculated in the *rigid* framework. In effect, this represents the likelihood of a segregating element against their effect on cohesion, and hence the vulnerability/strengthening of the segregated GB with respect to the pure GB.

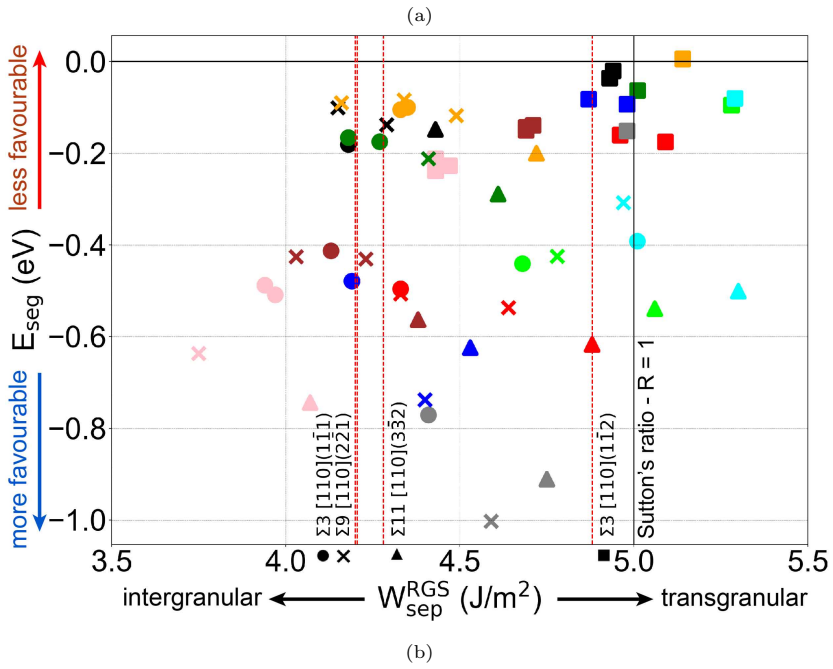
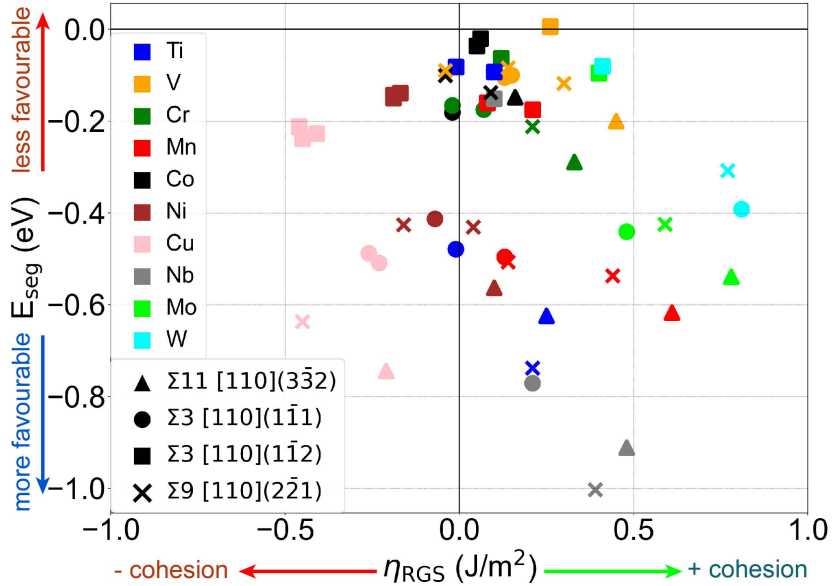


Figure S36: The segregation energy, representative of tendency for a particular element to segregate to a GB, is plotted against the effect that the solute has on GB cohesion. S36a The cohesion effect in the *rigid* framework (η_{RGS}) is plotted against their individual elemental segregation energies. S36b The work of separation calculated in the *rigid* framework (W_{sep}^{RGS}) is plotted against their individual elemental segregation energies. The ratio R describes the likelihood of intergranular fracture ($R \ll 1$ = intergranular fracture, $R \approx 1$ transgranular fracture).

8. A demonstration of occupation probability

In Figure S37 we plot the Langmuir-McLean isotherm across the temperature range of 300-800 K and bulk solute concentrations ranging $1 \text{ appm} < X < 1\text{at\%}$. In the text, we had stated that a $E_{\text{seg}}^{\text{inc}} > -0.1 \text{ eV}$ can be considered a very weak segregation binding tendency. Obviously, this threshold is subjective and can be arbitrarily determined, according to the heat treatments that are being applied in any specific case. However, we demonstrate that at any slightly elevated temperature ($>300 \text{ K}$) the probability of any GB site occupation at 0.1 eV reduces down to almost 0, and thus it is a reasonable threshold to qualify “weak” segregation tendency.

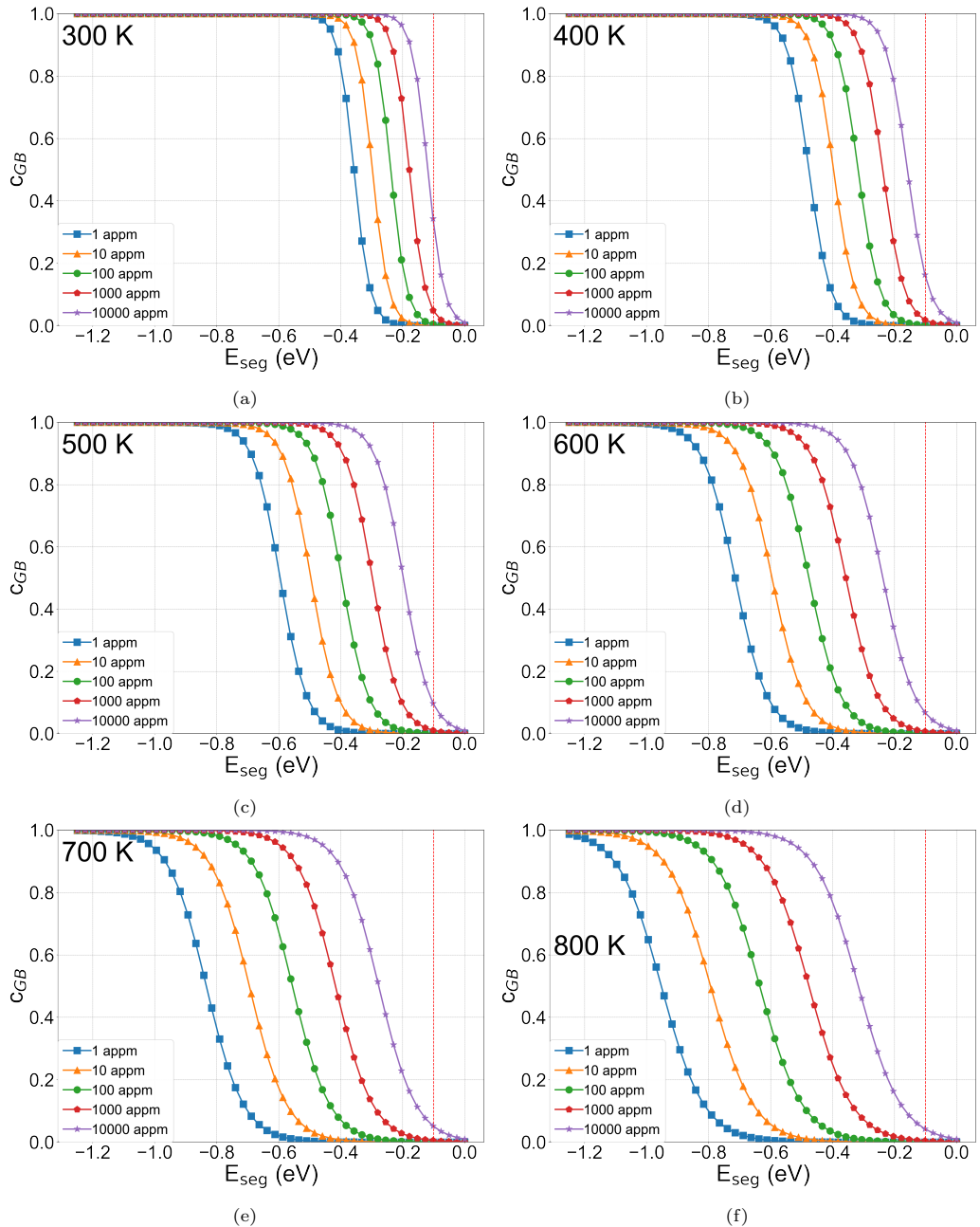


Figure S37: The segregation energies of the solutes may be input into to various isotherm theories calculate the probability that these sites at the GB are occupied across a range of specified temperatures (300-600K). The -0.1 eV “non-cosegregating” threshold is indicated by the vertical red line.

9. Co-segregation interaction classification threshold justification

The criterion that we set in the main text for interaction classifications were: *negligible* where $|E_{int}| \leq 0.05$ eV and *significant* where $|E_{int}| > 0.05$ eV, which we further classify into *moderate* where $0.05 < |E_{int}| < 0.2$ eV, and *major* in the case where $|E_{int}| \geq 0.2$ eV.

Recall that the criterion to qualify as a non-segregating permutation is $E_{seg}^{inc} > -0.1$ eV. Therefore, the cases which contain repulsive interactions (0 eV $< E_{int} < 0.05$ eV) that meet the “negligible” criterion would bind solutes in the pure GB at the site with strength $E_{seg}^{inc} > -0.15$ eV. In these cases, the very weak/non-existent segregation in these permutations may be attributed to a lack of available segregation sites that bind the specific segregant strongly even in the pure GB, not the repulsive interaction. Such values of E_{seg}^{inc} imply that binding is not strong enough to result in non-negligible segregation, even when excluding the prior-segregated solute’s repulsive influence. For majorly repulsive interactions in non-segregating permutations - in these cases, the sites would bind at least with a minimum strength of $E_{seg}^{inc} < -0.30$ eV in the pure case. This would be sufficient to cause a substantial probability of segregation coverage in the pure GB case [see Fig S37]. In this case, we may understand that the solute-solute interactions play a significant role in determining the non-cosegregating nature of a specific permutation.

We mainly focus on the repulsive interaction side when classifying their size, since they make up the bulk of the interactions. Afterwards, we simply preserve the symmetry with respect to the attractive interactions, so that the moderate/major thresholds refer to the same magnitude of interaction when referring to either the attractive or repulsive interactions.

10. Incremental energy of segregation: $E_{\text{seg}}^{\text{inc}}$ (eV)

	Ti	V	Cr	Mn	Co	Ni	Cu	Nb	Mo	W
Ti	-0.53	-0.11	-0.17	-0.48	-0.15	-0.39	-0.47	-0.93	-0.57	-0.50
	-0.05	-0.01	0.00	-0.01	-0.02	-0.17	-0.23	-0.15	-0.06	-0.05
	-0.10	0.00	-0.05	-0.35	-0.09	-0.33	-0.43	-0.14	-0.03	0.00
	-0.12	-0.04	-0.02	-0.10	-0.13	-0.51	-0.56	-0.31	-0.12	-0.04
V	-0.39	-0.08	-0.06	-0.38	-0.16	-0.38	-0.50	-0.62	-0.29	-0.23
	-0.13	0.00	-0.10	-0.37	-0.10	-0.38	-0.49	-0.29	-0.13	-0.05
	-0.34	-0.04	-0.04	-0.37	-0.10	-0.45	-0.54	-0.58	-0.24	-0.18
Cr	-0.47	-0.07	-0.14	-0.46	-0.09	-0.41	-0.49	-0.79	-0.43	-0.37
	0.00	0.00	0.00	-0.21	0.00	-0.12	-0.24	0.00	0.00	0.00
	-0.57	0.00	0.00	-0.32	-0.09	-0.43	-0.59	-0.79	-0.21	-0.08
	-0.26	0.00	0.00	-0.18	-0.07	-0.33	-0.44	-0.51	-0.25	-0.19
Mn	-0.46	-0.08	-0.13	-0.45	-0.13	-0.48	-0.56	-0.79	-0.45	-0.39
	-0.06	0.00	-0.09	-0.29	-0.02	-0.23	-0.34	-0.04	-0.08	-0.06
	-0.55	0.00	0.00	-0.34	-0.07	-0.39	-0.56	-0.76	-0.22	-0.09
	-0.12	0.00	0.00	-0.27	0.00	-0.24	-0.45	-0.40	-0.24	-0.13
Co	-0.45	-0.09	-0.13	-0.44	-0.18	-0.41	-0.53	-0.71	-0.34	-0.29
	-0.08	-0.02	-0.02	-0.14	-0.03	-0.14	-0.26	-0.09	-0.01	-0.02
	-0.69	-0.08	-0.15	-0.48	-0.09	-0.44	-0.66	-0.93	-0.34	-0.21
	-0.60	-0.15	-0.20	-0.47	-0.17	-0.54	-0.68	-0.84	-0.42	-0.39
Ni	-0.45	-0.09	-0.17	-0.56	-0.18	-0.40	-0.73	-0.71	-0.33	-0.26
	-0.11	0.00	-0.03	-0.26	-0.02	-0.23	-0.39	-0.12	-0.01	0.00
	-0.64	-0.07	-0.14	-0.49	-0.13	-0.45	-0.68	-0.87	-0.30	-0.18
	-0.58	-0.09	-0.07	-0.29	-0.12	-0.38	-0.53	-0.76	-0.32	-0.26
Cu	-0.44	-0.09	-0.16	-0.55	-0.18	-0.46	-0.74	-0.70	-0.32	-0.24
	-0.09	0.00	-0.06	-0.28	-0.06	-0.28	-0.52	-0.17	-0.07	-0.03
	-0.54	-0.08	-0.19	-0.47	-0.16	-0.48	-0.63	-0.75	-0.16	-0.03
	-0.44	-0.04	-0.04	-0.26	-0.09	-0.35	-0.64	-0.58	-0.18	-0.07
Nb	-0.62	-0.17	-0.20	-0.51	-0.12	-0.36	-0.45	-1.03	-0.65	-0.57
	-0.05	0.00	0.00	-0.07	0.00	-0.13	-0.25	-0.17	-0.02	-0.01
	-0.03	0.00	0.00	-0.30	-0.07	-0.30	-0.38	-0.03	0.00	0.00
	-0.07	-0.02	0.00	-0.11	-0.08	-0.41	-0.41	-0.12	-0.01	0.00
Mo	-0.61	-0.14	-0.17	-0.50	-0.08	-0.30	-0.44	-0.97	-0.58	-0.50
	0.00	0.00	0.00	-0.19	0.00	-0.06	-0.22	0.00	0.00	0.00
	-0.09	0.00	-0.05	-0.33	-0.05	-0.31	-0.37	-0.23	-0.10	-0.03
	-0.21	-0.02	0.00	-0.32	-0.03	-0.34	-0.38	-0.35	-0.18	-0.11
W	-0.59	-0.11	-0.15	-0.50	-0.07	-0.28	-0.46	-0.95	-0.55	-0.46
	-0.02	0.00	0.00	-0.16	0.00	-0.04	-0.18	-0.09	0.00	0.00
	-0.08	0.00	-0.06	-0.32	-0.04	-0.30	-0.34	-0.22	-0.09	-0.02
	-0.16	-0.01	0.00	-0.24	-0.04	-0.33	-0.31	-0.30	-0.14	-0.07

Table S38: The incremental energy of segregation ($E_{\text{seg}}^{\text{inc}}$) (eV) of the second solute (indicated in the column) when the first solute (in the row) is present. This is a copyable version of Table 2 in the main text.

11. Interaction energies: E_{int} (eV)

	Ti	V	Cr	Mn	Co	Ni	Cu	Nb	Mo	W
Ti	-0.05	-0.01	0.01	0.01	0.03	0.02	0.04	-0.15	-0.13	-0.11
	0.04	-0.03	0.07	0.17	0.02	-0.03	0.01	-0.03	-0.02	-0.04
	0.19	0.09	0.12	0.19	0.04	0.10	0.21	0.43	0.28	0.25
	0.51	0.03	0.05	0.51	0.02	0.05	0.19	0.61	0.42	0.46
V	0.09	0.03	0.11	0.12	0.02	0.03	-0.01	0.15	0.15	0.16
	0.16	0.09	0.06	0.17	0.04	0.05	0.15	0.29	0.19	0.20
	0.30	0.03	0.24	0.23	0.03	0.12	0.20	0.33	0.31	0.33
Cr	0.01	0.03	0.03	0.04	0.09	0.01	0.02	-0.02	0.01	0.02
	0.09	0.00	0.07	-0.05	0.04	0.02	-0.01	0.12	0.07	0.03
	0.17	0.12	0.16	0.19	0.01	0.00	0.05	0.22	0.21	0.23
	0.37	0.20	0.28	0.02	0.06	0.23	0.31	0.40	0.30	0.32
Mn	0.02	0.02	0.04	0.05	0.05	-0.07	-0.05	-0.02	0.00	0.00
	0.00	0.00	-0.06	-0.12	-0.01	-0.07	-0.12	0.04	-0.05	-0.04
	0.19	0.12	0.16	0.17	0.03	0.03	0.08	0.24	0.21	0.22
	0.51	0.20	0.28	-0.06	0.14	0.32	0.06	0.51	0.31	0.37
Co	0.03	0.01	0.04	0.05	0.00	0.00	-0.04	0.06	0.10	0.11
	0.02		-0.03	0.02		0.00	-0.02	0.07	-0.03	-0.03
	0.04	0.04	0.01	0.03	0.01	-0.01	-0.02	0.07	0.09	0.10
	0.02	0.04	0.08	0.14	-0.04	0.02	0.06	0.07	0.13	0.11
Ni	0.03	0.02	0.01	-0.07	0.00	0.01	-0.59	0.06	0.11	0.13
	-0.03	0.00	0.00	-0.10	0.00	-0.09	-0.16	0.00	0.03	0.03
	0.10	0.05	0.02	0.02	-0.08	-0.03	-0.04	0.13	0.13	0.07
	0.05	0.10	0.21	0.32	0.00	0.18	0.22	0.15	0.23	0.24
Cu	0.04	0.01	0.02	-0.05	0.00	-0.05	-0.60	0.08	0.12	0.16
	0.00	-0.02	-0.03	-0.12	-0.02	-0.14	-0.28	-0.05	-0.04	-0.04
	0.20	0.01	-0.03	0.07	-0.02	-0.05	-0.25	0.25	0.27	0.22
	0.19	0.03	0.11	0.35	0.04	0.21	-0.13	0.33	0.37	0.43
Nb	-0.14	-0.07	-0.02	-0.02	0.06	0.05	0.06	-0.26	-0.21	-0.18
	0.01	0.00	0.07	0.09	0.04	0.01	-0.02	-0.09	-0.02	-0.01
	0.26	0.09	0.21	0.24	0.07	0.13	0.26	0.54	0.31	0.25
	0.59	0.05	0.29	0.51	0.07	0.15	0.33	0.79	0.56	0.09
Mo	-0.13	-0.04	0.01	-0.01	0.11	0.11	0.04	-0.20	-0.14	-0.10
	0.02	0.00	0.07	-0.03	0.04	0.08	0.01	0.12	0.07	0.03
	0.20	0.09	0.11	0.21	0.09	0.13	0.27	0.35	0.21	0.22
	0.42	0.06	0.07	0.30	0.00	0.22	0.36	0.56	0.37	0.39
W	-0.11	-0.01	0.02	0.00	0.11	0.13	0.03	-0.18	-0.11	-0.07
	0.03	0.00	0.07	0.00	0.04	0.10	0.05	-0.01	0.07	0.03
	0.20	0.09	0.10	0.22	0.10	0.14	0.18	0.35	0.23	0.23
	0.46	0.06	0.29	0.37	0.11	0.24	0.43	0.62	0.40	0.43

Table S39: The interaction energy (E_{int}) (eV) of the second solute (indicated in the column) when the first solute (in the row) is present. This is a copyable version of Table 3 in the main text.

12. Cohesion effect at favoured configuration ($\eta_{X,Y}$) (J/m²) vs total energy of segregation ($E_{\text{seg}}^{\text{tot}}$) (eV)

	Ti	V	Cr	Mn	Co	Ni	Cu	Nb	Mo	W
Ti		-0.49	-0.64	-0.96	-0.63	-0.87	-0.95	-1.39	-1.05	-0.98
				-0.23	-0.11	-0.26	-0.33	-0.20	-0.10	-0.11
			-0.78	-1.09	-0.83	-1.07	-1.18	-1.03	-0.51	
		-0.54	-0.55	-0.74	-0.75	-1.14	-1.18	-0.98	-0.75	-0.67
V		0.17		-0.24	-0.57	-0.27	-0.50	-0.60	-0.94	-0.58
		-0.03			-0.06		-0.24			-0.51
		0.38		-0.21		-0.22	-0.50	-0.72		
Cr		0.15	0.26		-0.63	-0.31	-0.58	-0.67	-0.97	-0.61
		0.41	0.33		-0.27		-0.18	-0.30		-0.55
		0.41				-0.28	-0.57	-0.83		-0.37
Mn		0.22	0.26	0.21		-0.63	-0.98	-1.06	-1.29	-0.94
		0.20		0.06		-0.18	-0.41	-0.52	-0.22	-0.28
		0.45				-0.62	-0.92	-1.10	-1.30	-0.76
		0.48				-0.85	-1.00	-1.02	-0.85	-0.75
Co		0.01	0.18	0.01	0.12		-0.59	-0.69	-0.89	-0.52
		-0.09	0.02		0.16		-0.17	-0.30		-0.46
		0.43	0.32	0.31	0.37		-0.56	-0.80	-1.07	-0.48
		0.50	0.47	0.44			-0.69	-0.83	-0.99	-0.57
Ni		-0.02	0.06	0.04	0.08	-0.06		-0.97	-1.13	-0.75
		-0.27		-0.17	-0.20	-0.23		-0.52	-0.28	-0.16
		0.35	0.25	0.26	0.31	0.17		-1.11	-1.31	-0.73
		0.43	0.43	0.34	0.32	0.21		-1.09	-1.32	-0.88
Cu		-0.27	-0.12	-0.21	-0.02	-0.20	-0.18		-1.22	-0.89
		-0.52	-0.46	-0.37	-0.46	-0.44	-0.60		-0.40	-0.31
		-0.03	0.00	0.05	0.28	-0.07	-0.12		-1.38	-0.79
		0.04	-0.15	0.00	0.05	-0.19	-0.15		-1.32	-0.92
Nb		0.29	0.38	0.37	0.36	0.19	0.11	-0.14		-1.41
		0.06			-0.09		-0.30	-0.49		-0.10
		0.44			0.54	0.59	0.51	0.07		-0.17
		0.58	0.58		0.45	0.72	0.59	0.20		-0.89
Mo		0.42	0.54	0.52	0.47	0.35	0.23	0.12	0.66	
		0.11			0.29		-0.04	-0.28	0.09	
		0.60		0.51	0.49	0.56	0.47	0.02		
		0.68	0.68		0.68	0.86	0.71	0.30	0.61	
W		0.63	0.74	0.74	0.70	0.57	0.44	0.36	0.86	1.68
		0.18			0.43			-0.42	0.13	
				0.41	0.50	0.39	0.63	-0.09		0.88
		0.85	0.65		0.64	0.70	0.79	0.11	0.61	1.39

Table S40: The cohesion effect at the favoured configuration at the specified energy of segregation (E_{int}) (eV) of the second solute (indicated in the column) when the first solute (in the row) is present. This is a copyable version of Table 4 in the main text.

13. Total energy of segregation $E_{\text{seg}}^{\text{tot}}$ (eV)

	Ti	V	Cr	Mn	Co	Ni	Cu	Nb	Mo	W
Ti	-1.009	-0.593	-0.645	-0.960	-0.633	-0.869	-0.951	-1.404	-1.049	-0.983
	-0.147	-0.106	-0.093	-0.098	-0.108	-0.260	-0.326	-0.244	-0.148	-0.142
	-0.833	-0.738	-0.786	-1.089	-0.832	-1.072	-1.169	-0.881	-0.768	-0.738
	-0.739	-0.664	-0.646	-0.729	-0.752	-1.139	-1.181	-0.929	-0.744	-0.665
V	-0.490	-0.182	-0.166	-0.482	-0.262	-0.485	-0.603	-0.723	-0.398	-0.339
	-0.249	-0.121	-0.217	-0.491	-0.216	-0.502	-0.611	-0.407	-0.244	-0.171
	-0.538	-0.242	-0.242	-0.571	-0.295	-0.645	-0.737	-0.781	-0.439	-0.384
Cr	-0.644	-0.242	-0.320	-0.631	-0.265	-0.584	-0.669	-0.965	-0.610	-0.546
	-0.063	-0.063	-0.063	-0.275	-0.063	-0.186	-0.302	-0.063	-0.063	-0.063
	-0.783	-0.212	-0.212	-0.535	-0.305	-0.638	-0.800	-0.999	-0.426	-0.293
	-0.551	-0.289	-0.289	-0.471	-0.357	-0.617	-0.726	-0.802	-0.536	-0.480
Mn	-0.956	-0.573	-0.629	-0.943	-0.625	-0.977	-1.055	-1.288	-0.940	-0.888
	-0.234	-0.175	-0.266	-0.467	-0.195	-0.400	-0.519	-0.218	-0.259	-0.231
	-1.089	-0.537	-0.537	-0.880	-0.605	-0.931	-1.095	-1.301	-0.756	-0.624
	-0.735	-0.617	-0.617	-0.887	-0.617	-0.853	-1.062	-1.019	-0.854	-0.745
Co	-0.632	-0.272	-0.307	-0.625	-0.362	-0.593	-0.713	-0.891	-0.520	-0.466
	-0.111	-0.056	-0.060	-0.178	-0.066	-0.172	-0.296	-0.122	-0.049	-0.053
	-0.832	-0.216	-0.283	-0.619	-0.232	-0.575	-0.795	-1.069	-0.475	-0.350
	-0.752	-0.298	-0.349	-0.615	-0.316	-0.684	-0.830	-0.988	-0.568	-0.540
Ni	-0.868	-0.499	-0.584	-0.977	-0.593	-0.817	-1.138	-1.127	-0.744	-0.674
	-0.259	-0.150	-0.180	-0.414	-0.167	-0.376	-0.537	-0.270	-0.160	-0.150
	-1.070	-0.502	-0.572	-0.916	-0.558	-0.884	-1.111	-1.302	-0.730	-0.609
	-1.138	-0.650	-0.631	-0.853	-0.685	-0.940	-1.088	-1.323	-0.883	-0.827
Cu	-0.945	-0.602	-0.669	-1.055	-0.691	-0.970	-1.249	-1.206	-0.826	-0.746
	-0.329	-0.239	-0.300	-0.522	-0.299	-0.521	-0.755	-0.409	-0.309	-0.266
	-1.179	-0.717	-0.827	-1.102	-0.796	-1.114	-1.264	-1.389	-0.797	-0.669
	-1.181	-0.782	-0.782	-1.000	-0.831	-1.090	-1.380	-1.324	-0.923	-0.813
Nb	-1.393	-0.942	-0.969	-1.285	-0.892	-1.133	-1.220	-1.805	-1.424	-1.341
	-0.200	-0.151	-0.151	-0.224	-0.151	-0.279	-0.402	-0.319	-0.174	-0.165
	-1.031	-1.003	-1.003	-1.303	-1.070	-1.307	-1.381	-1.035	-1.003	-1.003
	-0.977	-0.931	-0.911	-1.020	-0.989	-1.322	-1.323	-1.030	-0.922	-0.915
Mo	-1.050	-0.576	-0.611	-0.941	-0.517	-0.745	-0.885	-1.410	-1.018	-0.938
	-0.097	-0.095	-0.095	-0.283	-0.095	-0.158	-0.312	-0.095	-0.095	-0.095
	-0.512	-0.425	-0.473	-0.755	-0.475	-0.730	-0.791	-0.650	-0.529	-0.457
	-0.745	-0.559	-0.540	-0.854	-0.568	-0.881	-0.920	-0.886	-0.717	-0.646
W	-0.983	-0.506	-0.545	-0.890	-0.462	-0.674	-0.851	-1.343	-0.938	-0.855
	-0.105	-0.080	-0.080	-0.243	-0.080	-0.123	-0.261	-0.168	-0.080	-0.080
	-0.391	-0.308	-0.372	-0.624	-0.351	-0.604	-0.647	-0.529	-0.395	-0.324
	-0.665	-0.514	-0.501	-0.745	-0.540	-0.826	-0.815	-0.796	-0.644	-0.573

Table S41: The total energies of segregation $E_{\text{seg}}^{\text{tot}}$ (eV) in all calculated permutations.

14. Co-segregation sites

	Ti	V	Cr	Mn	Co	Ni	Cu	Nb	Mo	W
Ti	36-37	36-37	36-37	36-37	36-35	36-34	36-34	36-37	36-37	36-37
	22-27	22-30	N/A	22-23	22-20	22-23	22-25	22-27	22-27	22-27
	34-32	N/A	34-31	34-36	34-36	34-36	34-33	34-32	34-32	N/A
	22-19	22-15	22-15	22-21	22-21	22-21	22-21	22-19	22-19	22-19
V	32-37	32-40	32-38	32-36	32-38	32-38	32-37	32-37	32-36	32-36
	N/A									
	N/A	34-31	34-31	N/A	34-36	34-36	34-33	N/A	N/A	N/A
	22-17	22-15	N/A	N/A	22-20	22-20	22-18	22-17	22-17	22-17
Cr	36-37	36-37	36-37	36-37	36-34	36-35	36-35	36-37	36-37	36-37
	N/A	N/A	N/A	24-25	N/A	24-23	24-23	N/A	N/A	N/A
	36-34	36-28	N/A	N/A	36-33	36-33	36-33	N/A	36-34	36-34
	21-17	N/A	N/A	N/A	21-20	21-20	21-20	N/A	N/A	N/A
Mn	36-37	36-37	36-37	36-37	36-35	36-35	36-35	36-37	36-37	36-37
	22-28	N/A	22-23	22-23	22-31	22-25	22-23	22-28	22-23	22-23
	36-34	N/A	N/A	36-33	36-33	36-33	36-33	36-34	36-34	36-34
	21-17	N/A	N/A	21-22	N/A	21-20	21-22	21-22	21-22	21-22
Co	34-37	34-40	34-38	34-37	34-35	34-35	34-37	34-36	34-36	34-36
	20-22	20-14	N/A	20-25	20-14	20-23	20-25	N/A	N/A	N/A
	36-34	36-34	36-33	36-33	36-33	36-33	36-33	36-34	36-34	36-34
	21-22	21-19	21-20	N/A	21-20	21-20	21-20	21-22	21-22	21-22
Ni	34-36	34-40	34-37	34-37	34-35	34-39	34-31	34-36	34-36	34-36
	24-25	N/A	24-22	24-25	24-22	24-23	24-23	24-23	24-23	N/A
	36-34	36-34	36-33	36-33	36-30	36-33	36-33	36-34	36-34	36-32
	21-22	21-19	21-20	21-20	21-20	21-20	21-20	21-22	21-22	21-22
Cu	34-36	34-40	34-37	34-37	34-39	34-39	34-31	34-36	34-36	34-36
	24-23	24-19	24-23	24-25	24-21	24-23	24-25	24-23	24-23	24-19
	33-34	33-31	33-31	33-36	33-36	33-36	33-32	33-34	33-34	33-38
	21-22	21-15	21-22	21-20	21-20	21-20	21-22	21-22	21-22	21-19
Nb	36-37	36-37	36-37	36-37	36-34	36-34	36-34	36-37	36-37	36-37
	24-21	N/A	N/A	24-25	N/A	24-22	24-22	24-21	24-21	24-21
	34-32	N/A	N/A	34-36	34-36	34-36	34-33	34-32	N/A	N/A
	22-15	22-15	N/A	22-21	22-21	22-21	22-21	22-19	22-15	22-15
Mo	36-37	36-37	36-37	36-37	36-34	36-34	36-37	36-37	36-37	36-37
	24-19	N/A	N/A	24-25	N/A	24-22	24-22	24-19	N/A	N/A
	34-32	N/A	34-31	34-36	34-36	34-36	34-33	N/A	34-32	34-32
	19-22	19-26	N/A	19-20	19-28	19-20	19-20	19-22	19-22	19-22
W	36-37	36-37	36-37	36-37	36-34	36-34	36-37	36-37	36-37	36-37
	24-21	N/A	N/A	24-25	N/A	N/A	24-22	24-21	N/A	N/A
	N/A	N/A	34-31	34-36	34-36	34-36	34-36	N/A	34-32	34-32
	22-19	22-15	N/A	22-21	22-21	22-21	22-20	22-17	22-19	22-19

Table S42: The sites occupied in each co-segregating permutations with the minimal total energies are presented. The sites are displayed corresponding to the elements present in the ROW-COLUMN, respectively. The rows indicate the first segregant, the columns indicate the second segregant. Greyed values indicate that the segregation of the second atom (column) is unfavourable.

15. Co-segregation table - η (ΔW_{sep}) (J/m²)

	Ti	V	Cr	Mn	Co	Ni	Cu	Nb	Mo	W
Ti	0.09	0.17	0.15	0.22	0.01	-0.02	-0.27	0.29	0.42	0.63
	0.02	-0.03	-0.02	-0.08	-0.09	-0.27	-0.52	0.06	0.11	0.18
	0.35	0.38	0.41	0.45	0.43	0.35	-0.04	0.38	0.60	0.56
	0.29	0.38	0.41	0.27	0.50	0.43	0.04	0.42	0.68	0.85
V	0.16	0.31	0.12	0.25	0.18	0.07	-0.12	0.30	0.46	0.68
	N/A									
	0.25	0.28	0.33	0.32	0.32	0.25	-0.12	0.35	0.54	0.67
	0.43	0.37	0.44	0.51	0.46	0.43	-0.02	0.61	0.75	0.64
Cr	0.15	0.26	0.28	0.21	0.10	0.04	-0.21	0.36	0.52	0.74
	0.08	0.07	0.14	0.06	0.09	-0.17	-0.37	0.07	0.10	0.10
	0.53	0.25	0.28	0.36	0.31	0.26	-0.01	0.67	0.63	0.61
	0.44	0.33	0.35	0.39	0.44	0.32	-0.07	0.63	0.66	0.65
Mn	0.22	0.26	0.20	0.41	0.12	0.08	-0.02	0.36	0.47	0.70
	0.20	0.13	0.05	0.44	0.16	-0.03	-0.47	0.13	0.18	0.25
	0.45	0.32	0.34	0.44	0.36	0.31	0.03	0.52	0.49	0.50
	0.48	0.35	0.42	0.58	0.21	0.32	0.05	0.45	0.68	0.64
Co	0.01	0.18	0.01	0.12	-0.04	-0.06	-0.20	0.19	0.35	0.57
	-0.09	0.02	-0.04	0.12	0.03	-0.23	-0.44	-0.08	-0.04	-0.04
	0.43	0.32	0.29	0.37	0.16	0.17	-0.07	0.59	0.56	0.39
	0.50	0.47	0.43	0.46	0.35	0.21	-0.19	0.72	0.86	0.70
Ni	-0.02	0.06	0.04	0.08	-0.06	-0.09	-0.18	0.11	0.23	0.44
	-0.30	-0.26	-0.17	-0.20	-0.25	-0.44	-0.60	-0.30	-0.04	-0.17
	0.35	0.25	0.22	0.30	0.04	0.11	-0.12	0.51	0.47	0.63
	0.42	0.43	0.34	0.32	0.21	0.20	-0.15	0.59	0.71	0.79
Cu	-0.27	-0.18	-0.21	-0.02	-0.30	-0.30	-0.41	-0.15	-0.02	0.19
	-0.52	-0.46	-0.37	-0.46	-0.44	-0.61	-0.81	-0.49	-0.28	-0.42
	-0.03	0.00	0.05	0.03	-0.07	-0.12	-0.41	0.07	0.02	-0.09
	0.04	-0.15	0.00	-0.04	-0.19	-0.15	-0.41	0.20	0.30	0.11
Nb	0.28	0.38	0.37	0.36	0.19	0.11	-0.14	0.51	0.66	0.86
	0.07	-0.01	0.00	-0.09	-0.05	-0.30	-0.49	0.08	0.09	0.16
	0.44	0.49	0.67	0.54	0.59	0.51	0.07	0.44	0.67	0.45
	0.58	0.58	0.59	0.45	0.72	0.59	0.20	0.47	0.61	0.61
Mo	0.42	0.54	0.52	0.47	0.34	0.23	0.12	0.66	0.81	1.68
	0.32	0.42	0.42	0.29	0.12	-0.04	-0.28	0.28	0.16	0.16
	0.44	0.48	0.51	0.49	0.56	0.47	0.02	0.53	0.74	0.88
	0.68	0.68	0.64	0.68	0.66	0.71	0.29	0.77	1.05	1.39
W	0.63	0.74	0.74	0.70	0.56	0.44	0.36	0.86	1.68	1.74
	0.12	0.42	0.43	0.43	0.42	0.02	-0.20	0.13	0.43	0.43
	0.56	0.56	0.41	0.50	0.39	0.40	0.18	0.60	0.82	0.94
	0.85	0.65	0.65	0.64	0.70	0.79	0.11	0.63	1.38	1.38

Table S43: The cohesion change (η) occupied in each co-segregating permutations with the minimal total energies are presented. Negative (red) values indicate an embrittling effect (reduction in GB cohesion), whereas positive (green) values represent an increase in GB cohesion. Greyed values indicate that the segregation of the second atom (column) is unfavourable.

16. Co-segregation cohesion table - W_{sep}^{RGS} (J/m^2)

	Ti	V	Cr	Mn	Co	Ni	Cu	Nb	Mo	W
Ti	3.90	3.98	3.96	4.03	3.82	3.80	3.54	4.10	4.23	4.44
	4.74	4.69	4.70	4.64	4.63	4.45	4.20	4.78	4.83	4.90
	3.95	3.98	4.01	4.05	4.03	3.95	3.57	3.98	4.20	4.16
	4.12	4.21	4.24	4.10	4.33	4.26	3.87	4.25	4.51	4.68
V	3.97	4.12	3.93	4.06	3.99	3.88	3.69	4.11	4.27	4.49
	3.85	3.88	3.93	3.92	3.92	3.85	3.48	3.95	4.14	4.27
	4.26	4.20	4.27	4.34	4.29	4.26	3.81	4.44	4.58	4.47
Cr	3.96	4.07	4.09	4.02	3.91	3.85	3.60	4.17	4.33	4.55
	4.80	4.79	4.86	4.78	4.81	4.55	4.35	4.79	4.82	4.82
	4.13	3.85	3.88	3.96	3.91	3.86	3.59	4.27	4.23	4.21
	4.27	4.16	4.18	4.22	4.27	4.15	3.76	4.46	4.49	4.48
Mn	4.03	4.07	4.01	4.22	3.93	3.89	3.79	4.17	4.28	4.51
	4.92	4.85	4.77	5.16	4.88	4.69	4.25	4.85	4.90	4.97
	4.05	3.92	3.94	4.04	3.96	3.91	3.63	4.12	4.09	4.10
	4.31	4.18	4.25	4.41	4.04	4.15	3.88	4.28	4.51	4.47
Co	3.82	3.99	3.82	3.93	3.77	3.75	3.61	4.00	4.16	4.38
	4.64	4.74	4.68	4.84	4.75	4.50	4.28	4.65	4.68	4.68
	4.03	3.92	3.89	3.97	3.76	3.77	3.53	4.19	4.16	3.99
	4.33	4.30	4.26	4.29	4.18	4.04	3.64	4.55	4.69	4.53
Ni	3.79	3.87	3.85	3.89	3.75	3.72	3.63	3.92	4.04	4.25
	4.42	4.47	4.55	4.52	4.47	4.29	4.12	4.42	4.68	4.55
	3.95	3.85	3.82	3.90	3.64	3.71	3.48	4.11	4.07	4.23
	4.25	4.26	4.17	4.15	4.04	4.03	3.68	4.42	4.54	4.62
Cu	3.54	3.63	3.60	3.79	3.51	3.51	3.40	3.66	3.79	4.00
	4.21	4.26	4.35	4.26	4.28	4.11	3.91	4.23	4.44	4.30
	3.57	3.60	3.65	3.88	3.53	3.48	3.19	3.67	3.62	3.51
	3.87	3.68	3.83	3.79	3.64	3.68	3.42	4.03	4.13	3.94
Nb	4.09	4.19	4.18	4.17	4.00	3.92	3.67	4.32	4.47	4.67
	4.79	4.71	4.72	4.63	4.67	4.42	4.23	4.80	4.81	4.88
	4.04	4.09	4.27	4.14	4.19	4.11	3.67	4.04	4.27	4.05
	4.41	4.41	4.42	4.28	4.55	4.42	4.03	4.30	4.44	4.44
Mo	4.23	4.35	4.33	4.28	4.15	4.04	3.93	4.47	4.62	5.49
	5.04	5.14	5.14	5.01	4.84	4.68	4.44	5.00	4.88	4.88
	4.04	4.08	4.11	4.09	4.16	4.07	3.62	4.13	4.34	4.48
	4.51	4.51	4.47	4.51	4.49	4.54	4.12	4.60	4.88	5.22
W	4.44	4.55	4.55	4.51	4.37	4.25	4.17	4.67	5.49	5.55
	4.84	5.14	5.15	5.15	5.14	4.74	4.52	4.85	5.15	5.15
	4.16	4.16	4.01	4.10	3.99	4.00	3.78	4.20	4.42	4.54
	4.68	4.48	4.48	4.47	4.53	4.62	3.94	4.46	5.21	5.21

Table S44: The co-segregation cohesion table for the work of separation values calculated in the relaxed separation scheme in J/m^2 (W_{sep})- in each co-segregating permutation with the minimal total energies are presented.

17. Co-segregation table - η_{RGS} ($\Delta W_{\text{sep}}^{\text{RGS}}$) (J/m²)

	Ti	V	Cr	Mn	Co	Ni	Cu	Nb	Mo	W
Ti	0.07	0.23	0.12	0.11	0.01	-0.08	-0.31	0.35	0.60	0.92
	0.07	0.11	0.14	-0.07	0.10	-0.18	-0.41	0.16	0.17	0.23
	0.21	0.16	0.16	0.47	0.30	0.24	-0.30	0.15	0.41	0.51
	0.08	0.26	0.29	0.25	0.37	0.24	-0.05	0.22	0.52	0.73
V	0.15	0.30	0.07	0.18	0.17	0.03	-0.08	0.32	0.58	0.91
	0.10	0.11	0.23	0.45	0.40	0.36	-0.30	0.16	0.44	0.65
	0.23	0.36	0.32	0.57	0.37	0.30	-0.13	0.43	0.70	0.93
Cr	0.12	0.28	0.18	0.14	0.08	0.01	-0.20	0.37	0.64	0.98
	0.11	0.14	0.18	0.03	0.13	-0.11	-0.31	0.11	0.14	0.14
	0.40	0.05	0.08	0.24	0.10	0.03	-0.24	0.55	0.74	0.87
	0.35	0.32	0.34	0.24	0.31	0.16	-0.21	0.52	0.86	0.88
Mn	0.11	0.24	0.14	0.27	0.07	0.03	-0.11	0.30	0.56	0.90
	0.25	0.18	0.02	0.39	0.19	-0.01	-0.47	0.24	0.24	0.35
	0.47	-0.01	0.42	0.17	0.31	0.22	-0.05	0.58	0.69	0.88
	0.54	0.54	0.65	0.82	0.57	0.33	-0.01	0.42	0.87	1.07
Co	0.01	0.17	-0.06	0.07	-0.03	-0.02	-0.20	0.24	0.49	0.81
	0.09	0.05	0.07	0.16	0.05	-0.16	-0.40	0.08	0.06	0.05
	0.29	0.40	0.03	0.19	-0.03	-0.07	-0.34	0.47	0.68	0.79
	0.36	0.38	0.29	0.57	0.23	0.18	-0.19	0.56	0.89	1.03
Ni	-0.09	0.04	0.01	0.03	-0.02	-0.11	-0.21	0.10	0.32	0.64
	-0.20	-0.18	-0.10	-0.16	-0.19	-0.36	-0.54	-0.13	0.06	-0.09
	0.24	0.37	-0.04	0.12	-0.25	-0.12	-0.38	0.42	0.64	0.50
	0.23	0.30	0.15	0.30	0.17	0.04	-0.30	0.43	0.84	1.00
Cu	-0.31	-0.13	-0.20	-0.11	-0.28	-0.31	-0.41	-0.14	0.10	0.41
	-0.42	-0.41	-0.31	-0.47	-0.39	-0.55	-0.87	-0.36	-0.23	-0.39
	-0.30	-0.23	-0.18	0.04	-0.33	-0.38	-0.69	-0.18	-0.12	-0.31
	-0.06	-0.21	-0.07	-0.05	-0.25	-0.30	-0.60	0.18	0.56	0.17
Nb	0.33	0.50	0.37	0.30	0.24	0.11	-0.13	0.61	0.88	1.19
	0.19	0.14	0.17	-0.06	0.10	-0.12	-0.35	0.21	0.19	0.24
	0.32	0.32	0.55	0.49	0.47	0.42	-0.18	0.21	0.49	0.28
	0.46	0.47	0.48	0.43	0.56	0.42	0.18	0.25	0.47	0.48
Mo	0.59	0.76	0.64	0.56	0.48	0.33	0.24	0.87	1.16	1.47
	0.37	0.41	0.42	0.34	0.38	0.11	-0.19	0.37	0.41	0.41
	0.44	0.48	0.47	0.69	0.68	0.63	-0.12	0.41	0.78	0.97
	0.54	0.76	0.69	0.87	0.76	0.83	0.52	0.57	1.04	1.19
W	0.91	1.08	0.97	0.90	0.81	0.64	0.60	1.19	1.47	1.53
	0.37	0.42	0.42	0.42	0.42	0.15	-0.09	0.23	0.42	0.42
	0.54	0.63	0.52	0.87	0.79	0.79	0.61	0.50	0.80	1.07
	0.75	1.07	0.91	1.08	1.03	0.99	0.21	0.44	1.19	1.19

Table S45: The cohesion changes η_{RGS} for the rigid separation scheme in each co-segregating permutation with the minimal total energies are presented. Negative (red) values indicate an embrittling effect (reduction in GB cohesion), whereas positive (green) values represent an increase in GB cohesion. Greyed values indicate that the segregation of the second atom (column) is unfavourable.

18. Co-segregation cohesion table - W_{sep}^{RGS} (J/m^2)

	Ti	V	Cr	Mn	Co	Ni	Cu	Nb	Mo	W
Ti	4.27	4.43	4.32	4.31	4.21	4.12	3.89	4.55	4.80	5.12
	4.95	4.99	5.02	4.81	4.98	4.70	4.47	5.04	5.05	5.11
	4.41	4.36	4.36	4.67	4.50	4.44	3.90	4.35	4.61	4.71
	4.36	4.54	4.57	4.53	4.65	4.52	4.23	4.50	4.80	5.01
V	4.35	4.50	4.27	4.38	4.37	4.23	4.12	4.52	4.78	5.11
	4.30	4.31	4.43	4.65	4.60	4.56	3.90	4.36	4.64	4.85
	4.51	4.64	4.60	4.85	4.65	4.58	4.15	4.71	4.98	5.21
Cr	4.32	4.48	4.38	4.34	4.28	4.21	4.00	4.57	4.84	5.18
	4.99	5.02	5.06	4.91	5.01	4.77	4.57	4.99	5.02	5.02
	4.60	4.25	4.28	4.44	4.30	4.23	3.96	4.75	4.94	5.07
	4.63	4.60	4.62	4.52	4.59	4.44	4.07	4.80	5.14	5.16
Mn	4.31	4.44	4.34	4.47	4.27	4.23	4.09	4.50	4.76	5.10
	5.13	5.06	4.90	5.27	5.07	4.87	4.41	5.12	5.12	5.23
	4.67	4.19	4.62	4.37	4.51	4.42	4.15	4.78	4.89	5.08
	4.82	4.82	4.93	5.10	4.85	4.61	4.27	4.70	5.15	5.35
Co	4.21	4.37	4.14	4.27	4.17	4.18	4.01	4.44	4.69	5.01
	4.97	4.93	4.95	5.04	4.93	4.73	4.48	4.96	4.94	4.93
	4.49	4.60	4.23	4.39	4.17	4.13	3.87	4.67	4.88	4.99
	4.64	4.66	4.57	4.85	4.51	4.46	4.09	4.84	5.17	5.31
Ni	4.11	4.24	4.21	4.23	4.19	4.09	3.99	4.30	4.52	4.84
	4.68	4.70	4.79	4.73	4.70	4.52	4.34	4.75	4.94	4.79
	4.44	4.57	4.16	4.32	3.95	4.08	3.82	4.62	4.84	4.70
	4.51	4.58	4.43	4.58	4.45	4.32	3.98	4.71	5.12	5.28
Cu	3.89	4.07	4.00	4.09	3.92	3.89	3.79	4.06	4.30	4.61
	4.47	4.47	4.57	4.41	4.49	4.34	4.01	4.53	4.65	4.49
	3.90	3.97	4.02	4.24	3.87	3.82	3.51	4.02	4.08	3.89
	4.22	4.07	4.21	4.23	4.03	3.98	3.69	4.46	4.84	4.45
Nb	4.53	4.70	4.57	4.50	4.44	4.31	4.07	4.81	5.08	5.39
	5.07	5.02	5.05	4.83	4.98	4.76	4.53	5.09	5.07	5.12
	4.52	4.52	4.75	4.69	4.67	4.62	4.03	4.41	4.69	4.48
	4.74	4.75	4.76	4.71	4.84	4.70	4.46	4.53	4.75	4.76
Mo	4.79	4.96	4.84	4.76	4.68	4.53	4.44	5.07	5.36	5.67
	5.25	5.29	5.30	5.22	5.26	4.99	4.70	5.25	5.29	5.29
	4.64	4.68	4.67	4.89	4.88	4.83	4.08	4.61	4.98	5.17
	4.82	5.04	4.97	5.15	5.04	5.11	4.80	4.85	5.32	5.47
W	5.11	5.28	5.17	5.10	5.01	4.84	4.80	5.39	5.67	5.73
	5.25	5.30	5.30	5.30	5.30	5.03	4.79	5.11	5.30	5.30
	4.74	4.83	4.72	5.07	4.99	4.99	4.81	4.70	5.00	5.27
	5.03	5.35	5.19	5.36	5.31	5.27	4.49	4.72	5.47	5.47

Table S46: The co-segregation cohesion table for the work of separation values calculated in the rigid separation scheme (W_{sep}^{RGS})- in each co-segregating permutation with the minimal total energies are presented.

19. Co-segregation table - Heuristic errors ($\eta_{(X,Y)} - (\eta_X + \eta_Y)$) (J/m²)

	Ti	V	Cr	Mn	Co	Ni	Cu	Nb	Mo	W
Ti	0.03	0.02	0.05	-0.04	0.00	-0.02	-0.03	0.09	0.06	0.04
	0.12	-0.17	-0.06	-0.20	-0.07	0.03	0.01	0.16	-0.25	-0.19
	-0.25	-0.10	-0.13	-0.13	0.01	0.00	-0.14	-0.36	-0.10	-0.04
	-0.43	-0.33	-0.29	-0.50	-0.03	-0.11	-0.16	-0.51	-0.36	-0.07
V	0.01	0.07	-0.07	-0.10	0.08	-0.02	0.03	0.01	0.01	-0.01
	N/A									
	-0.23	-0.08	-0.10	-0.14	0.02	0.02	-0.10	-0.27	-0.04	0.19
	-0.28	-0.33	-0.25	-0.25	-0.05	-0.10	-0.21	-0.31	-0.28	-0.27
Cr	0.05	0.07	0.14	-0.10	0.05	0.00	-0.01	0.12	0.12	0.11
	0.04	-0.21	-0.04	-0.21	-0.03	-0.01	0.02	0.03	-0.39	-0.40
	-0.01	-0.17	-0.20	-0.16	-0.05	-0.03	-0.05	-0.01	-0.01	0.07
	-0.26	-0.36	-0.33	-0.36	-0.06	-0.19	-0.25	-0.28	-0.36	-0.25
Mn	-0.04	-0.09	-0.10	-0.05	-0.09	-0.12	0.02	-0.04	-0.09	-0.09
	0.08	-0.23	-0.21	0.10	-0.04	0.05	-0.16	0.01	-0.39	-0.33
	-0.13	-0.14	-0.18	-0.12	-0.04	-0.03	-0.05	-0.20	-0.19	-0.08
	-0.29	-0.41	-0.33	-0.25	-0.36	-0.26	-0.20	-0.53	-0.41	-0.33
Co	0.00	0.08	-0.04	-0.09	0.00	-0.01	0.09	0.04	0.04	0.03
	-0.07	-0.20	-0.16	-0.08	-0.03	-0.01	0.01	-0.06	-0.47	-0.48
	0.01	0.02	-0.07	-0.04	-0.09	0.00	0.01	0.03	0.04	-0.03
	-0.03	-0.04	-0.07	-0.11	0.03	-0.12	-0.19	-0.01	0.02	-0.02
Ni	-0.02	-0.03	0.00	-0.12	-0.01	-0.03	0.12	-0.03	-0.07	-0.09
	0.00	-0.20	-0.01	-0.12	-0.03	0.07	0.13	0.00	-0.19	-0.33
	0.00	0.02	-0.07	-0.04	-0.13	0.01	0.03	0.02	0.02	0.28
	-0.11	-0.09	-0.17	-0.26	-0.12	-0.14	-0.16	-0.15	-0.14	0.06
Cu	-0.03	-0.03	-0.01	0.02	-0.01	0.00	0.13	-0.05	-0.08	-0.11
	0.02	-0.17	0.02	-0.15	0.01	0.12	0.15	0.04	-0.20	-0.35
	-0.13	0.02	0.01	-0.05	0.01	0.03	-0.01	-0.17	-0.18	-0.19
	-0.16	-0.34	-0.18	-0.29	-0.19	-0.16	-0.09	-0.21	-0.23	-0.30
Nb	0.08	0.09	0.13	-0.04	0.04	-0.03	-0.04	0.17	0.16	0.13
	0.17	-0.15	-0.04	-0.21	-0.03	0.00	0.04	0.18	-0.26	-0.20
	-0.30	-0.13	-0.01	-0.18	0.03	0.02	-0.17	-0.44	-0.17	-0.29
	-0.35	-0.34	-0.32	-0.53	-0.01	-0.15	-0.21	-0.67	-0.64	-0.52
Mo	0.06	0.09	0.12	-0.09	0.03	-0.07	0.06	0.16	0.15	0.79
	-0.03	-0.17	-0.07	-0.28	-0.31	-0.19	-0.20	-0.08	-0.64	-0.65
	-0.26	-0.10	-0.13	-0.19	0.04	0.02	-0.18	-0.31	-0.06	0.18
	-0.36	-0.35	-0.38	-0.41	-0.18	-0.14	-0.23	-0.48	-0.31	0.15
W	0.04	0.06	0.11	-0.09	0.02	-0.09	0.07	0.13	0.79	0.62
	-0.24	-0.18	-0.08	-0.15	-0.02	-0.14	-0.13	-0.23	-0.38	-0.39
	-0.04	0.08	-0.13	-0.08	-0.03	0.05	0.08	-0.14	0.12	0.34
	-0.07	-0.26	-0.25	-0.33	-0.02	0.06	-0.29	-0.50	0.14	0.26

Table S47: The errors associated with predicting the errors in each co-segregating permutation through summing the individual cohesion effects of either element in isolation are presented. Positive (green) values indicate that the true value is *larger* than predicted, i.e. cohesion is better than predicted, and negative (red) values indicate that the cohesion values are worse than predicted. Greyed values indicate that the segregation of the second atom (column) is unfavourable

20. Co-segregation table - Heuristic errors (rigid) ($\eta_{(X,Y)}^{\text{RGS}} - (\eta_X^{\text{RGS}} + \eta_Y^{\text{RGS}})$) (J/m²)

	Ti	V	Cr	Mn	Co	Ni	Cu	Nb	Mo	W
Ti	0.09	0.11	0.06	-0.01	0.04	0.00	-0.07	0.15	0.13	0.12
	-0.13	-0.25	-0.08	-0.38	-0.05	-0.09	-0.06	-0.04	-0.33	-0.28
	-0.22	-0.35	-0.26	-0.18	-0.01	-0.01	-0.06	-0.45	-0.39	-0.47
	-0.42	-0.44	-0.29	-0.61	-0.05	-0.11	-0.09	-0.51	-0.51	-0.55
V	0.03	0.04	-0.13	-0.08	0.06	-0.03	0.02	-0.02	-0.03	-0.03
	-0.41	-0.49	-0.28	-0.29	0.01	0.02	-0.15	-0.53	-0.45	-0.42
	-0.47	-0.54	-0.46	-0.49	-0.24	-0.25	-0.37	-0.50	-0.53	-0.55
Cr	0.06	0.08	0.04	-0.06	0.03	0.01	-0.04	0.09	0.09	0.10
	-0.11	-0.25	-0.06	-0.30	-0.04	-0.04	0.02	-0.11	-0.38	-0.39
	-0.02	-0.46	-0.34	-0.41	-0.20	-0.22	0.00	-0.05	-0.06	-0.11
	-0.23	-0.46	-0.33	-0.71	-0.18	-0.28	-0.33	-0.29	-0.25	-0.48
Mn	-0.01	-0.02	-0.06	0.01	-0.04	-0.04	-0.01	-0.04	-0.05	-0.04
	-0.06	-0.30	-0.31	-0.03	-0.07	-0.03	-0.23	-0.08	-0.37	-0.27
	-0.18	-0.75	-0.23	-0.72	-0.22	-0.26	-0.04	-0.25	-0.34	-0.34
	-0.32	-0.52	-0.30	-0.40	-0.20	-0.38	-0.41	-0.67	-0.52	-0.57
Co	0.04	0.06	-0.11	-0.04	0.01	0.07	0.06	0.05	0.03	0.02
	-0.06	-0.26	-0.10	-0.10	-0.05	-0.02	0.00	-0.07	-0.39	-0.41
	-0.01	0.01	-0.28	-0.34	-0.21	-0.20	0.03	-0.01	-0.01	-0.07
	-0.05	-0.23	-0.20	-0.20	-0.09	-0.08	-0.14	-0.08	-0.05	-0.16
Ni	-0.01	-0.02	0.01	-0.03	0.08	0.03	0.09	-0.04	-0.09	-0.10
	-0.11	-0.25	-0.03	-0.18	-0.05	0.02	0.10	-0.04	-0.15	-0.31
	-0.01	0.03	-0.29	-0.36	-0.38	-0.20	0.03	-0.01	0.01	-0.31
	-0.12	-0.25	-0.29	-0.41	-0.10	-0.16	-0.19	-0.15	-0.04	-0.13
Cu	-0.07	-0.03	-0.04	-0.01	-0.03	-0.01	0.05	-0.12	-0.15	-0.17
	-0.07	-0.22	0.02	-0.23	0.01	0.10	0.03	-0.01	-0.18	-0.35
	-0.06	-0.08	0.06	0.05	0.03	0.03	0.21	-0.12	-0.26	-0.63
	-0.10	-0.45	-0.19	-0.45	-0.20	-0.19	-0.18	-0.09	-0.02	-0.65
Nb	0.13	0.16	0.09	-0.04	0.05	-0.03	-0.11	0.19	0.19	0.17
	-0.01	-0.22	-0.05	-0.37	-0.05	-0.03	0.00	0.01	-0.32	-0.27
	-0.28	-0.38	-0.05	-0.34	-0.01	-0.01	-0.12	-0.57	-0.49	-0.88
	-0.27	-0.46	-0.33	-0.66	-0.08	-0.16	-0.10	-0.71	-0.79	-1.03
Mo	0.12	0.15	0.09	-0.05	0.02	-0.08	-0.01	0.18	0.20	0.18
	-0.13	-0.25	-0.11	-0.27	-0.07	-0.10	-0.14	-0.13	-0.39	-0.40
	-0.36	-0.41	-0.33	-0.34	-0.01	0.00	-0.26	-0.57	-0.40	-0.39
	-0.50	-0.47	-0.42	-0.52	-0.18	-0.05	-0.05	-0.69	-0.52	-0.62
W	0.11	0.14	0.09	-0.04	0.02	-0.10	0.02	0.17	0.18	-0.09
	-0.14	-0.25	-0.11	-0.20	-0.04	-0.07	-0.05	-0.28	-0.39	-0.40
	-0.44	-0.44	-0.46	-0.34	-0.07	-0.02	0.29	-0.66	-0.56	-0.47
	-0.53	-0.41	-0.45	-0.57	-0.16	-0.14	-0.61	-1.08	-0.62	-0.87

Table S48: The errors associated with predicting the cohesion change in each co-segregating permutation through summing the individual cohesion effects of either element in isolation are presented. Positive (green) values indicate that the true value is *larger* than predicted, i.e. cohesion is better than predicted, and negative (red) values indicate that the cohesion values are worse than predicted. Greyed values indicate that the segregation of the second atom (column) is unfavourable

21. Minimum energy configuration vs configurational energy difference (eV)

	Ti	V	Cr	Mn	Co	Ni	Cu	Nb	Mo	W
Ti	Ti-Ti	0.103	0.001	0.004	0.001	0.001	0.006	0.011	0.001	0.000
	Ti-Ti			0.136	0.003	0.001	0.003	0.044	0.051	0.037
	Ti-Ti		0.003	0.000	0.000	0.002	0.010	0.150	0.256	
	Ti-Ti	0.126	0.095	0.006	0.000	0.001	0.000	0.048	0.001	0.000
V	V-Ti	V-V	0.076	0.091	0.010	0.014	0.001	0.219	0.178	0.167
	Ti-V	V-V				0.000	0.000	0.106		
	Ti	V-V	0.005			0.003	0.005	0.045	0.150	0.120
	V-Ti	V-V								0.130
Cr	Cr-Ti	V-Cr	Cr-Cr	0.002	0.042	0.000	0.000	0.004	0.001	0.001
	Ti	Cr	Cr	0.009		0.006	0.002			
	Cr-Ti	Cr-V	Cr		0.022	0.066	0.027		0.047	0.079
	Cr-Ti	Cr	Cr	0.008	0.014	0.056				
Mn	Mn-Ti	V-Mn	Mn-Cr	Mn-Mn	0.000	0.000	0.000	0.003	0.001	0.002
	Ti-Mn	Mn	Mn-Cr	Mn-Mn	0.017	0.014	0.003	0.006	0.024	0.012
	Mn-Ti	Mn	Mn	Mn-Mn	0.014	0.015	0.007	0.002	0.001	0.000
	Ti-Mn	Mn	Mn	Mn-Mn		0.000	0.062	0.001	0.000	0.000
Co	Co-Ti	V-Co	Cr-Co	Co-Mn	Co-Co	0.000	0.022	0.001	0.003	0.004
	Ti-Co	V-Co	Cr	Co-Mn	Co-Co	0.005	0.003			
	Co-Ti	Co-V	Co-Cr	Mn-Co	Co-Co	0.017	0.001	0.001	0.000	0.001
	Co-Ti	V-Co	Co-Cr	Mn	Co-Co	0.001	0.001	0.001	0.000	0.000
Ni	Ni-Ti	V-Ni	Ni-Cr	Ni-Mn	Ni-Co	Ni-Ni	0.168	0.006	0.001	0.000
	Ni-Ti	Ni	Ni-Cr	Mn-Ni	Ni-Co	Ni-Ni	0.016	0.009	0.002	
	Ni-Ti	Ni-V	Ni-Cr	Ni-Mn	Ni-Co	Ni-Ni	0.003	0.005	0.000	0.005
	Ni-Ti	V-Ni	Cr-Ni	Ni-Mn	Co-Ni	Ni-Ni	0.002	0.001	0.002	0.001
Cu	Cu-Ti	Cu-V	Cu-Cr	Cu-Mn	Cu-Co	Cu-Ni	Cu-Cu	0.014	0.059	0.105
	Ti-Cu	V-Cu	Cu-Cr	Mn-Cu	Co-Cu	Cu-Ni	Cu-Cu	0.007	0.003	0.005
	Ti-Cu	V-Cu	Cr-Cu	Mn-Cu	Co-Cu	Ni-Cu	Cu-Cu	0.008	0.006	0.022
	Cu-Ti	V-Cu	Cr-Cu	Cu-Mn	Co-Cu	Ni-Cu	Cu-Cu	0.001	0.003	0.002
Nb	Nb-Ti	V-Nb	Cr-Nb	Nb-Mn	Co-Nb	Ni-Nb	Cu-Nb	Nb-Nb	0.014	0.002
	Nb-Ti	Nb	Nb	Mn-Nb	Nb	Ni-Nb	Nb-Cu	Nb-Nb	0.079	0.003
	Ti-Nb	Nb	Nb	Mn-Nb	Co-Nb	Ni-Nb	Nb-Cu	Nb-Nb		
	Ti-Nb	V-Nb	Nb	Mn-Nb	Co-Nb	Nb-Ni	Nb-Cu	Nb-Nb	0.036	0.119
Mo	Ti-Mo	V-Mo	Cr-Mo	Mn-Mo	Mo-Co	Ni-Mo	Cu-Mo	Mo-Nb	Mo-Mo	0.000
	Mo-Ti	Mo	Mo	Mn-Mo	Mo	Mo-Ni	Cu-Mo	Mo-Nb	Mo	
	Mo-Ti	Mo	Cr-Mo	Mo-Mn	Mo-Co	Mo-Ni	Mo-Cu	Nb	Mo-Mo	0.062
	Ti-Mo	V-Mo	Mo	Mo-Mn	Mo-Co	Mo-Ni	Mo-Cu	Mo-Nb	Mo-Mo	0.002
W	W-Ti	V-W	W-Cr	Mn-W	W-Co	W-Ni	Cu-W	Nb-W	W-Mo	W-W
	W-Ti	W	W	Mn-W	W	Ni	W-Cu	Nb-W	Mo	W
	Ti	W	Cr-W	W-Mn	Co-W	W-Ni	W-Cu	Nb	W-Mo	W-W
	W-Ti	V-W	W	W-Mn	W-Co	W-Ni	Cu-W	W-Nb	W-Mo	W-W

Table S49: The minimum configuration (in order of segregation, i.e. X-Y indicates X first, Y second) and the corresponding configurational energy differences between the two permutations studied. Cells with no values indicate that the segregation of the second atom is unfavourable.

22. Cohesion: heuristic errors (ϵ_{heur}) (J/m²) and configurational variation (ϵ_{config}) (J/m²)
each elemental combination

	Ti	V	Cr	Mn	Co	Ni	Cu	Nb	Mo	W
Ti	0.03	0.01	0.00	0.00	0.00	0.00	0.00	0.01	0.00	0.00
	0.12	N/A	N/A	0.28	0.00	0.03	0.00	-0.01	-0.22	0.06
	-0.25	N/A	-0.11	0.00	0.00	0.00	0.01	0.06	0.16	N/A
	-0.43	-0.04	-0.04	0.21	0.00	0.00	0.00	0.16	0.00	0.00
V	0.02	0.07	0.15	0.01	0.00	0.00	0.06	0.08	0.08	0.07
	N/A									
	N/A	-0.08	N/A	N/A	0.00	0.00	0.12	N/A	N/A	N/A
	-0.33	-0.33	N/A	N/A	0.00	0.00	-0.13	-0.03	-0.07	0.00
Cr	0.05	0.07	0.14	0.00	-0.08	0.00	0.00	0.00	0.00	0.00
	N/A	N/A	N/A	0.01	N/A	0.00	0.00	N/A	N/A	N/A
	-0.13	-0.10	N/A	N/A	0.02	0.05	0.06	N/A	-0.11	-0.20
	-0.29	N/A	N/A	N/A	0.01	0.01	0.06	N/A	N/A	N/A
Mn	-0.04	-0.09	-0.10	-0.05	0.00	0.00	0.00	0.00	0.00	0.00
	0.08	N/A	-0.21	0.10	0.03	-0.17	0.00	-0.22	0.11	0.18
	-0.13	N/A	N/A	-0.12	0.01	0.01	0.25	0.02	0.00	0.00
	-0.29	N/A	N/A	-0.25	N/A	0.00	0.08	0.00	0.00	0.00
Co	0.00	0.08	-0.04	-0.09	0.00	0.00	0.10	0.00	0.00	0.00
	-0.07	-0.20	N/A	-0.04	-0.03	0.03	0.00	N/A	N/A	N/A
	0.01	0.02	-0.05	-0.04	-0.09	0.14	0.00	0.00	0.00	0.00
	-0.03	-0.04	-0.06	N/A	0.03	0.00	0.00	0.00	0.20	0.00
Ni	-0.02	-0.03	0.00	-0.12	-0.01	-0.03	0.13	0.00	0.00	0.00
	0.03	N/A	-0.01	-0.12	-0.01	0.07	0.01	0.01	0.00	N/A
	0.00	0.02	-0.03	-0.03	0.00	0.01	0.00	0.00	0.00	0.23
	-0.11	-0.09	-0.17	-0.26	-0.12	-0.14	0.00	0.00	0.00	0.00
Cu	-0.03	0.03	-0.01	0.02	0.09	0.12	0.13	0.01	0.14	0.17
	0.02	-0.17	0.02	-0.15	0.01	0.13	0.15	0.01	0.00	-0.23
	-0.13	0.02	0.01	0.20	0.01	0.03	-0.01	0.01	0.00	-0.27
	-0.16	-0.34	-0.18	-0.20	-0.19	-0.16	-0.09	0.00	0.00	0.00
Nb	0.09	0.09	0.13	-0.04	0.04	-0.03	-0.04	0.17	0.01	0.00
	0.16	N/A	N/A	-0.21	N/A	0.00	0.04	0.18	N/A	-0.03
	-0.30	N/A	N/A	-0.18	0.03	0.02	-0.17	-0.44	N/A	N/A
	-0.35	-0.34	N/A	-0.53	-0.01	-0.15	-0.21	-0.67	-0.16	-0.02
Mo	0.06	0.09	0.12	-0.09	0.04	-0.07	0.06	0.16	0.15	0.00
	-0.25	N/A	N/A	-0.28	N/A	-0.19	-0.20	-0.26	N/A	N/A
	-0.10	N/A	-0.13	-0.19	0.04	0.02	-0.18	N/A	-0.06	0.07
	-0.36	-0.35	N/A	-0.41	0.02	-0.14	-0.23	-0.64	-0.31	0.00
W	0.04	0.06	0.11	-0.09	0.03	-0.09	0.07	0.13	0.79	0.62
	-0.19	N/A	N/A	-0.15	N/A	N/A	-0.35	-0.23	N/A	N/A
	N/A	N/A	-0.13	-0.08	-0.03	0.28	-0.19	N/A	0.18	0.34
	-0.07	-0.26	N/A	-0.33	-0.02	0.06	-0.29	-0.52	0.15	0.26

Table S50: The heuristic errors (lower left) and configurational variations (upper right) at each favourable configuration in each elemental combination. Greyed values indicate that the segregation of the second atom is unfavourable/X-X pairings (for visual clarity regarding the separation diagonal between the two sets of data). The heuristic errors for the X-X combinations are listed in the grey X-X cells, since configurational variation values do not exist for these combinations.

23. Co-segregation plots

23.1. $E_{\text{seg}}^{\text{inc}}$ vs Voronoi volume

Here, we plot the incremental energy of segregation ($E_{\text{seg}}^{\text{inc}}$) of a solute against the final relaxed Voronoi volume occupied by the solute in the co-segregation study (i.e. pair solute segregation study). Note the schemes used for colours and markers used here are the same as in Fig. 2 in the main text. The colour used here in the marker indicates the element of the prior segregated solute at the GB. The results of this comparison in each minimum energy configuration for each ordered pair are plotted below, in Figs S38-S47.

Note the clear trends of site-preferencing behaviour with respect to solute size, as observed in the single-solute segregation case above, also hold true here. This demonstrates that large solute segregation behaviour is dominated by large-volume site availability, rather than chemical interactions between solutes, as noted in the text. This may be seen in the plots of Ti, Nb, Mo, W, and to a lesser extent, V.

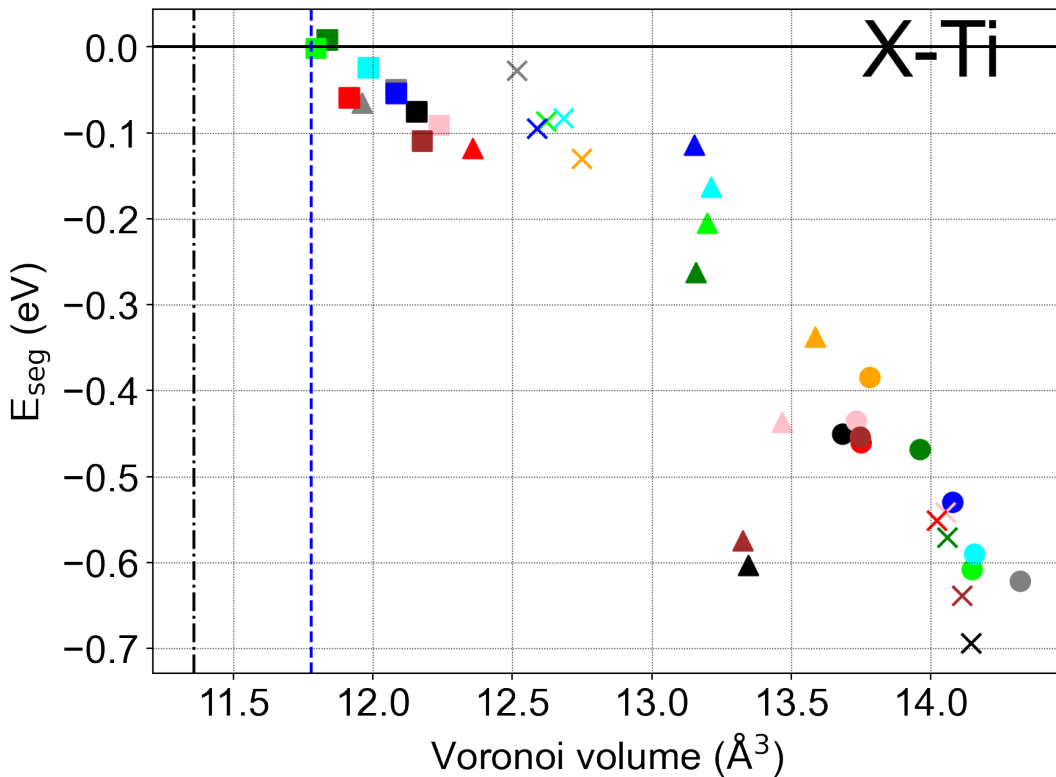


Figure S38: The incremental energy of segregation ($E_{\text{seg}}^{\text{inc}}$) for Ti is plotted against the relaxed Voronoi volume occupied by the solute at that site. The black/coloured dashed lines indicate the respective Voronoi volumes occupied in the bulk by the Fe/solute atoms, respectively.

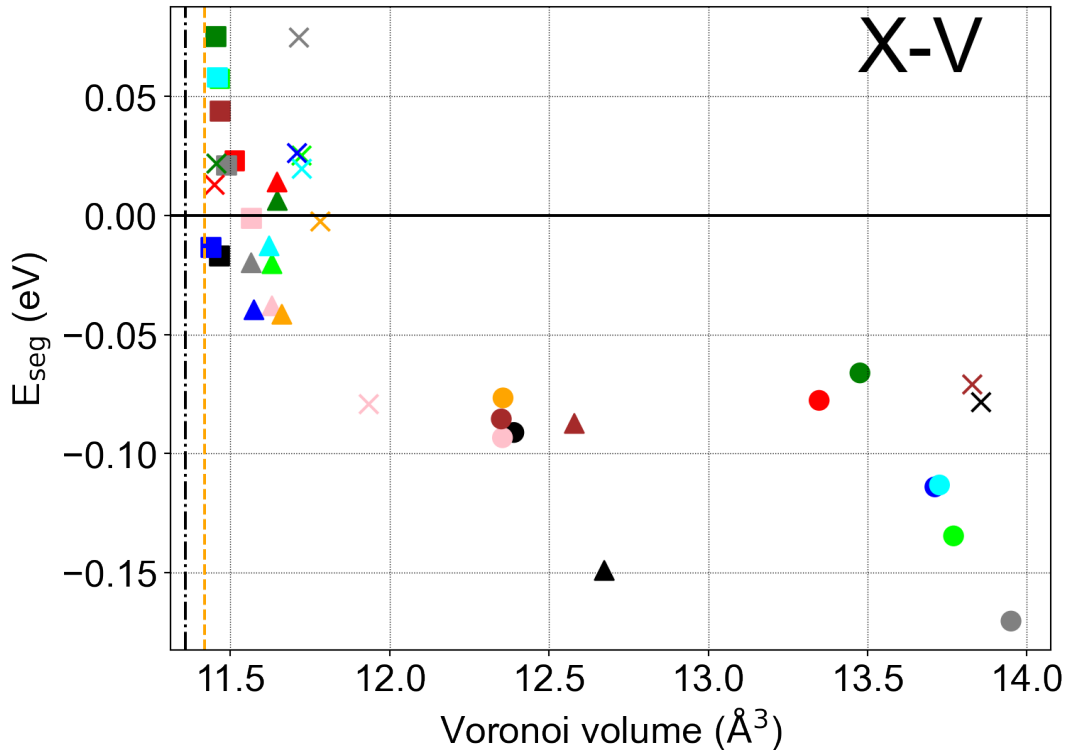


Figure S39: The incremental energy of segregation ($E_{\text{seg}}^{\text{inc}}$) for V is plotted against the relaxed Voronoi volume occupied by the solute at that site. The black/coloured dashed lines indicate the respective Voronoi volumes occupied in the bulk by the Fe/solute atoms, respectively

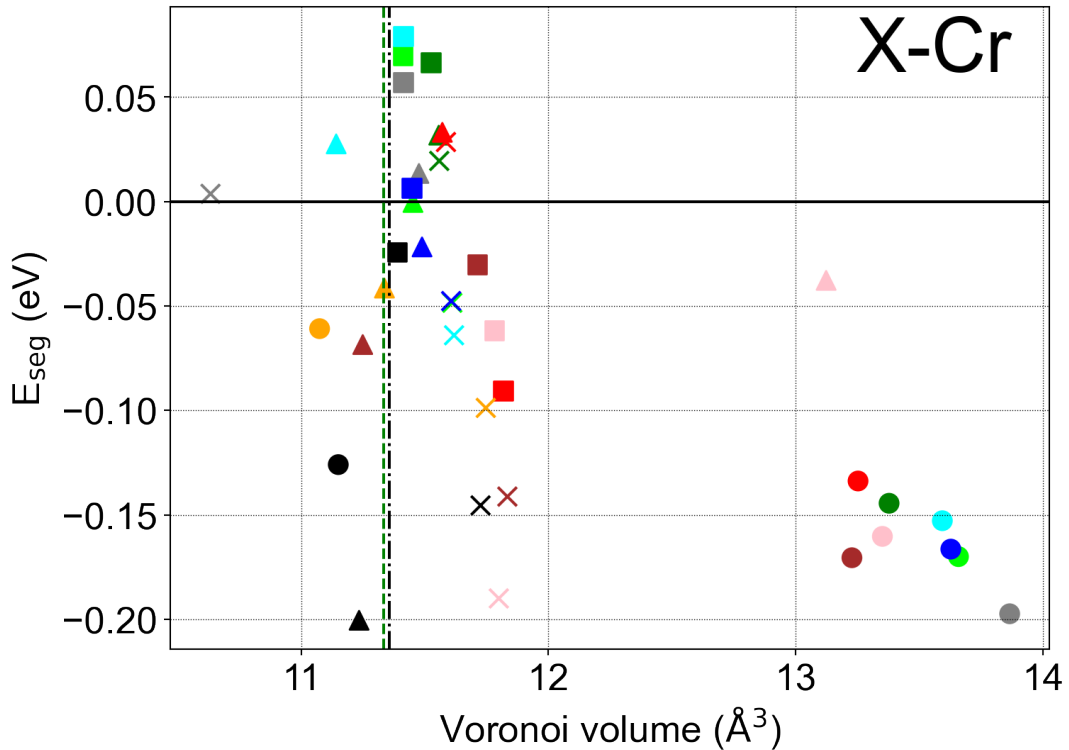


Figure S40: The incremental energy of segregation ($E_{\text{seg}}^{\text{inc}}$) for Cr is plotted against the relaxed Voronoi volume occupied by the solute at that site. The black/coloured dashed lines indicate the respective Voronoi volumes occupied in the bulk by the Fe/solute atoms, respectively

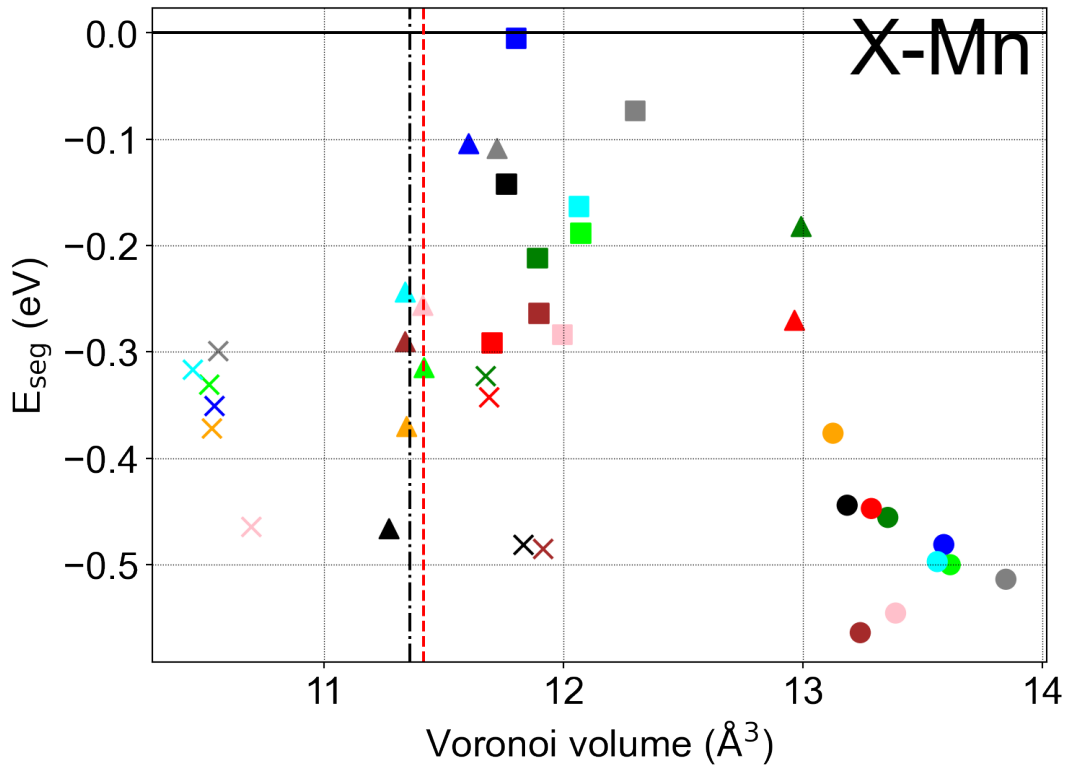


Figure S41: The incremental energy of segregation ($E_{\text{seg}}^{\text{inc}}$) for Mn is plotted against the relaxed Voronoi volume occupied by the solute at that site. The black/coloured dashed lines indicate the respective Voronoi volumes occupied in the bulk by the Fe/solute atoms, respectively

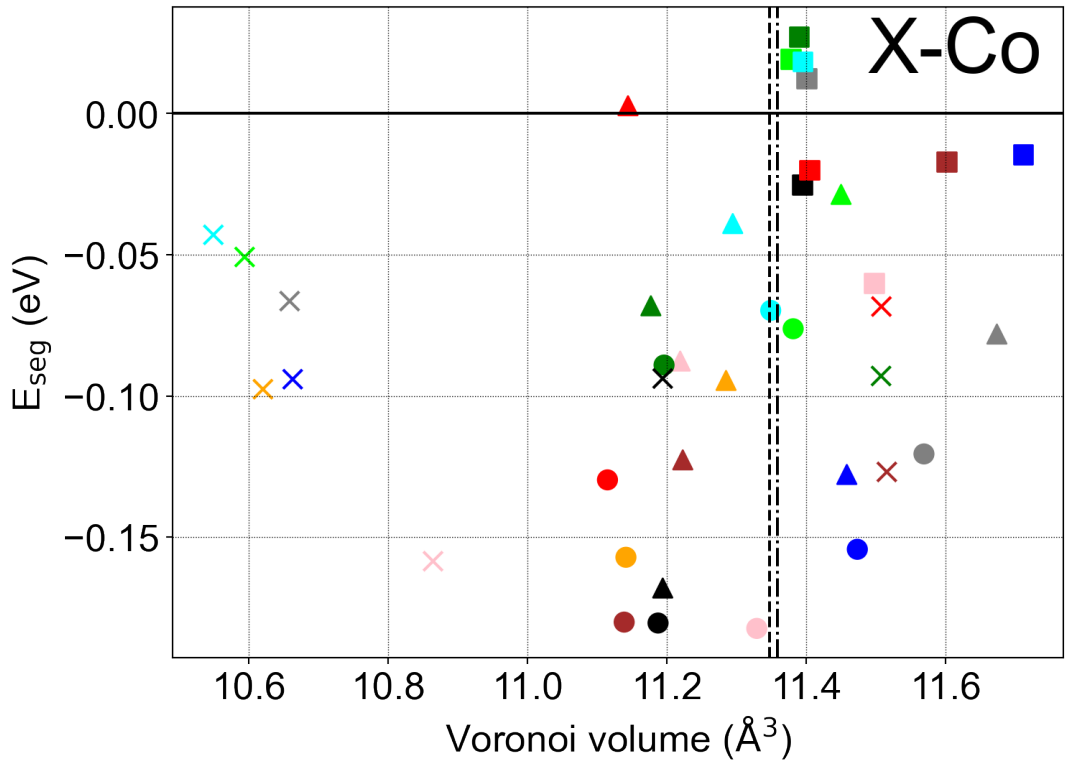


Figure S42: The incremental energy of segregation ($E_{\text{seg}}^{\text{inc}}$) for Co is plotted against the relaxed Voronoi volume occupied by the solute at that site. The black/coloured dashed lines indicate the respective Voronoi volumes occupied in the bulk by the Fe/solute atoms, respectively

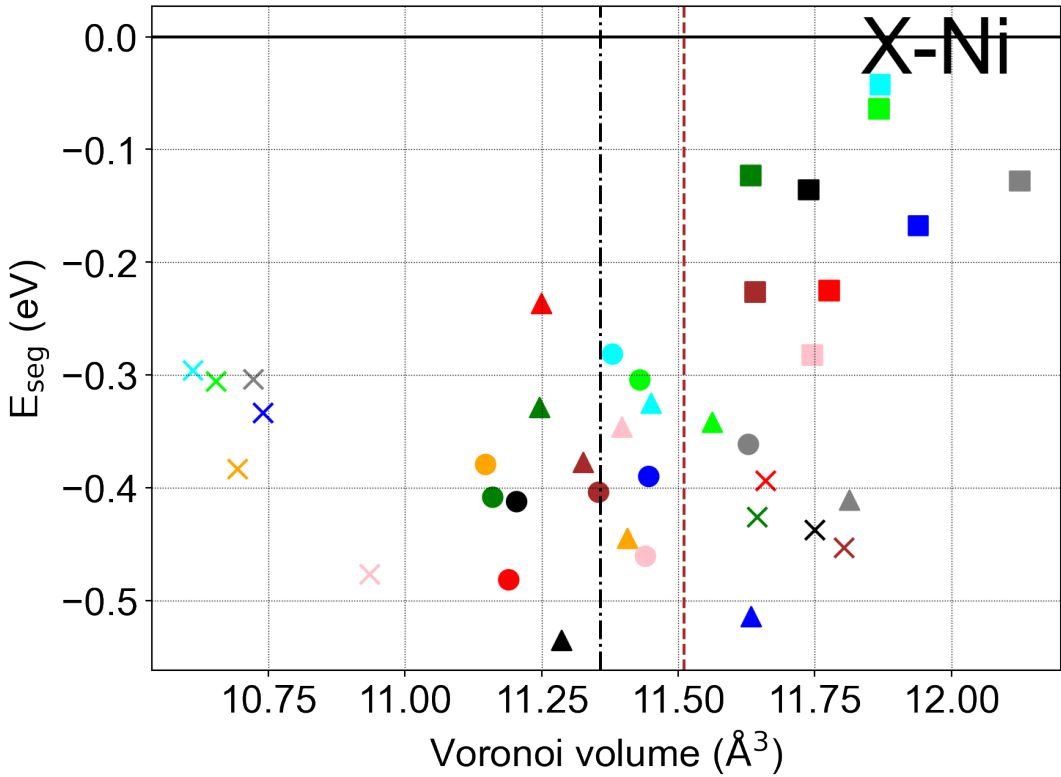


Figure S43: The incremental energy of segregation ($E_{\text{seg}}^{\text{inc}}$) for Ni is plotted against the relaxed Voronoi volume occupied by the solute at that site. The black/coloured dashed lines indicate the respective Voronoi volumes occupied in the bulk by the Fe/solute atoms, respectively

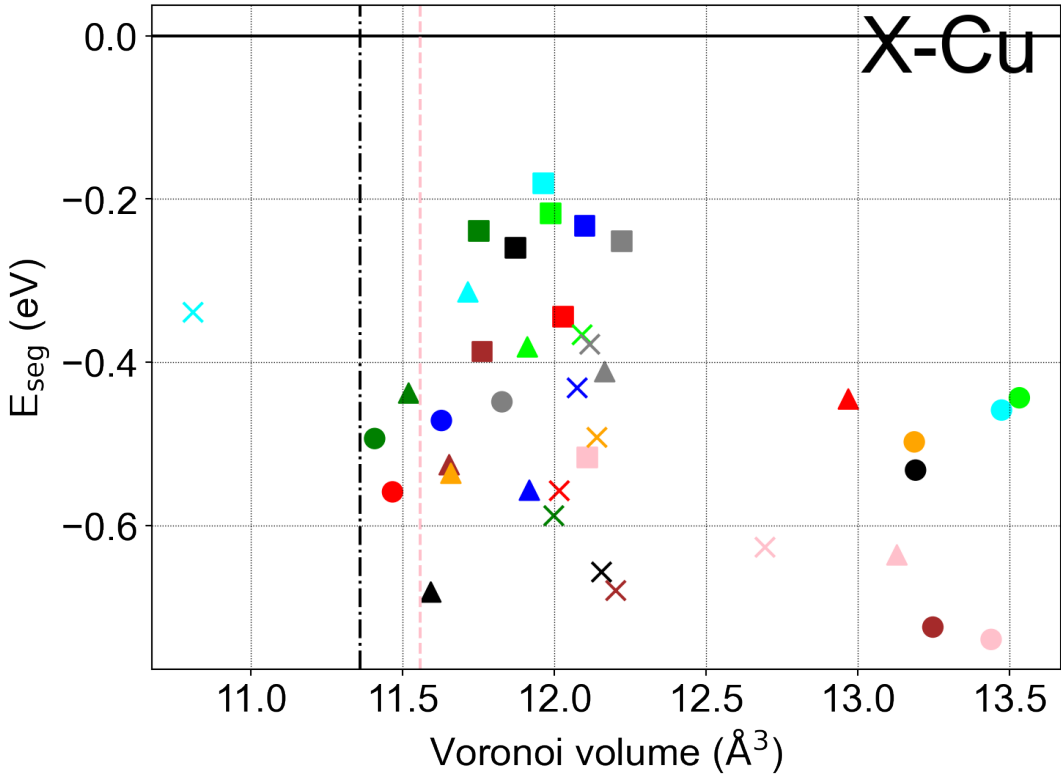


Figure S44: The incremental energy of segregation ($E_{\text{seg}}^{\text{inc}}$) for Cu is plotted against the relaxed Voronoi volume occupied by the solute at that site. The black/coloured dashed lines indicate the respective Voronoi volumes occupied in the bulk by the Fe/solute atoms, respectively

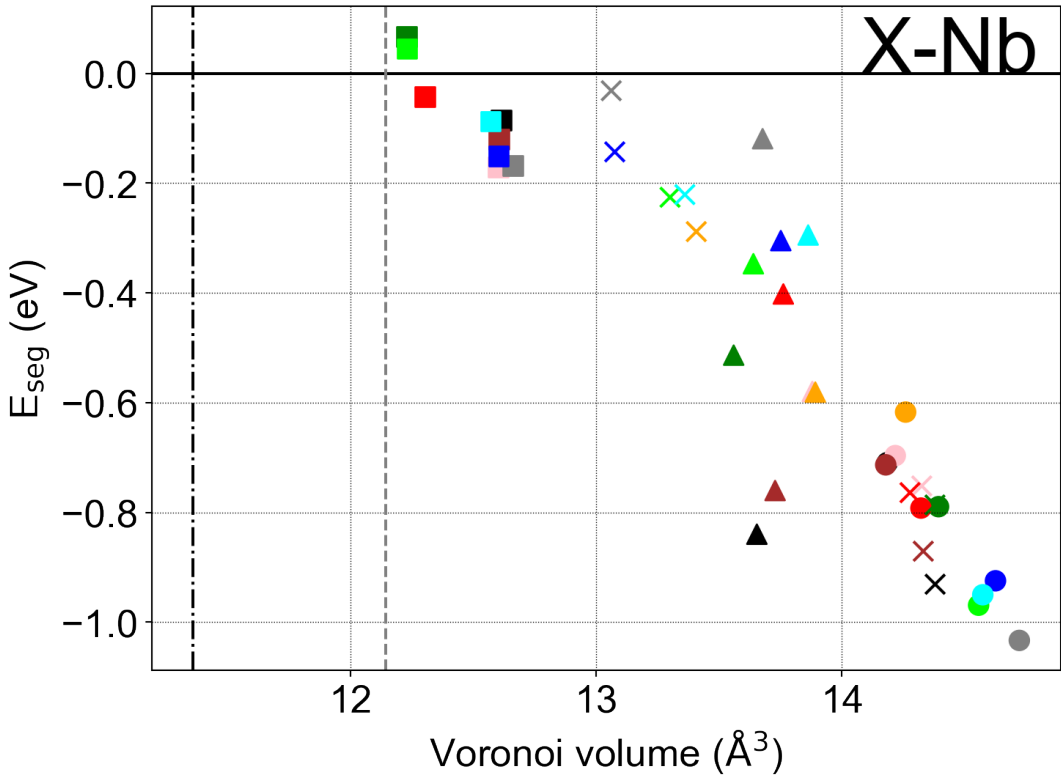


Figure S45: The incremental energy of segregation ($E_{\text{seg}}^{\text{inc}}$) for Nb is plotted against the relaxed Voronoi volume occupied by the solute at that site. The black/coloured dashed lines indicate the respective Voronoi volumes occupied in the bulk by the Fe/solute atoms, respectively

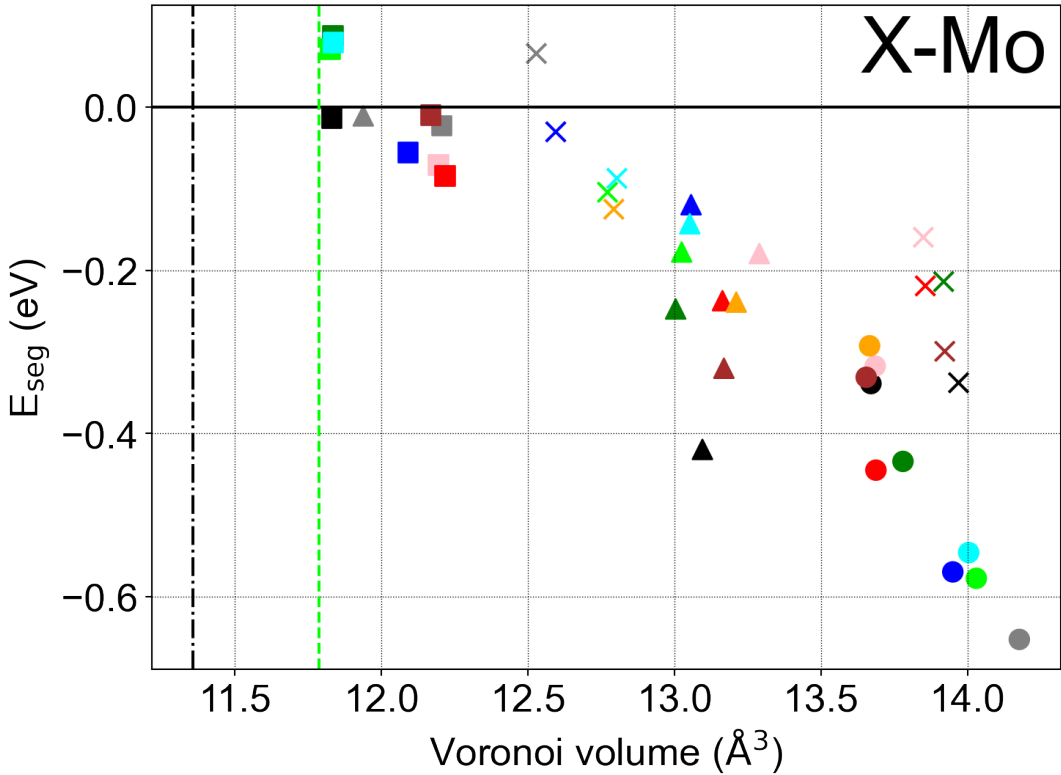


Figure S46: The incremental energy of segregation ($E_{\text{seg}}^{\text{inc}}$) for Mo is plotted against the relaxed Voronoi volume occupied by the solute at that site. The black/coloured dashed lines indicate the respective Voronoi volumes occupied in the bulk by the Fe/solute atoms, respectively

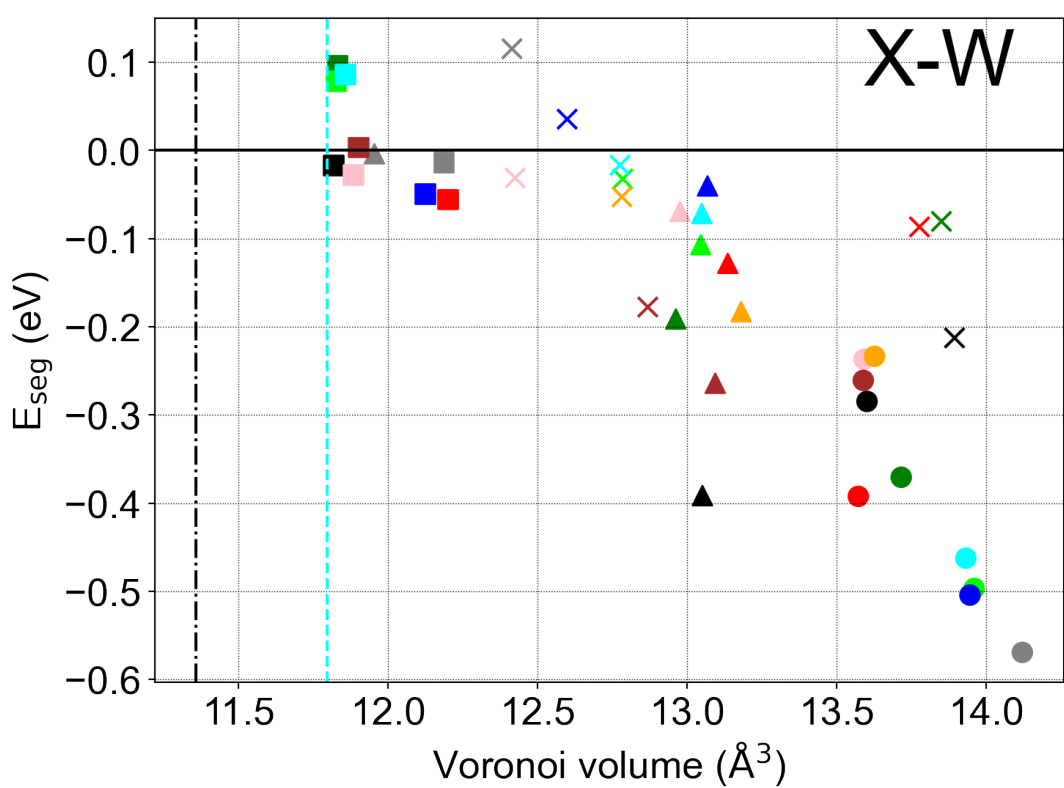


Figure S47: The incremental energy of segregation ($E_{\text{seg}}^{\text{inc}}$) for W is plotted against the relaxed Voronoi volume occupied by the solute at that site. The black/coloured dashed lines indicate the respective Voronoi volumes occupied in the bulk by the Fe/solute atoms, respectively

23.2. $E_{\text{seg}}^{\text{inc}}$ vs magnetic moment

Here, we plot the incremental segregation energy ($E_{\text{seg}}^{\text{inc}}$) of a solute against its final magnetic moment in the co-segregation study (i.e. pair solute segregation study). Note the schemes used for colours and markers used here are the same as in Fig. 2 in the main text. The colour used here in the marker indicates the element of the prior segregated solute at the GB. The results of this comparison are plotted below, in Figs S48-S57.

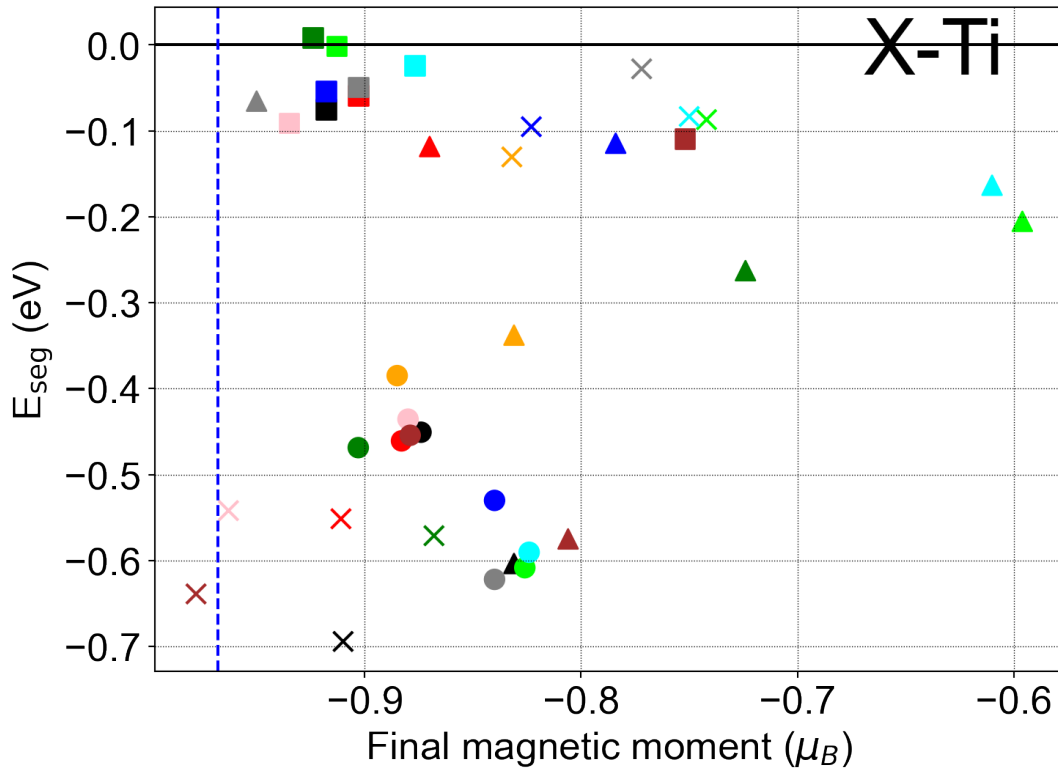


Figure S48: The incremental energy of segregation ($E_{\text{seg}}^{\text{inc}}$) for Ti is plotted against the final magnetic moment of that solute at that site. The coloured dashed line is a reference line indicating the magnetic moment of the solute when in bulk ferrite.

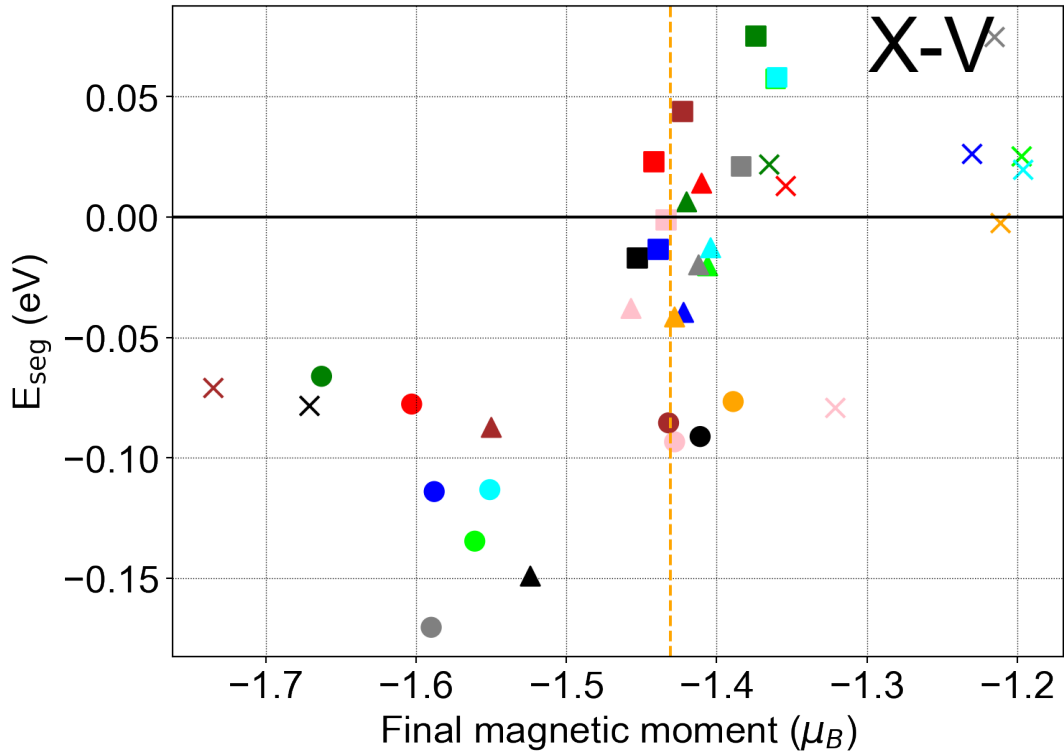


Figure S49: The incremental energy of segregation ($E_{\text{seg}}^{\text{inc}}$) for V is plotted against the final magnetic moment of that solute at that site. The coloured dashed line is a reference line indicating the magnetic moment of the solute when in bulk ferrite.

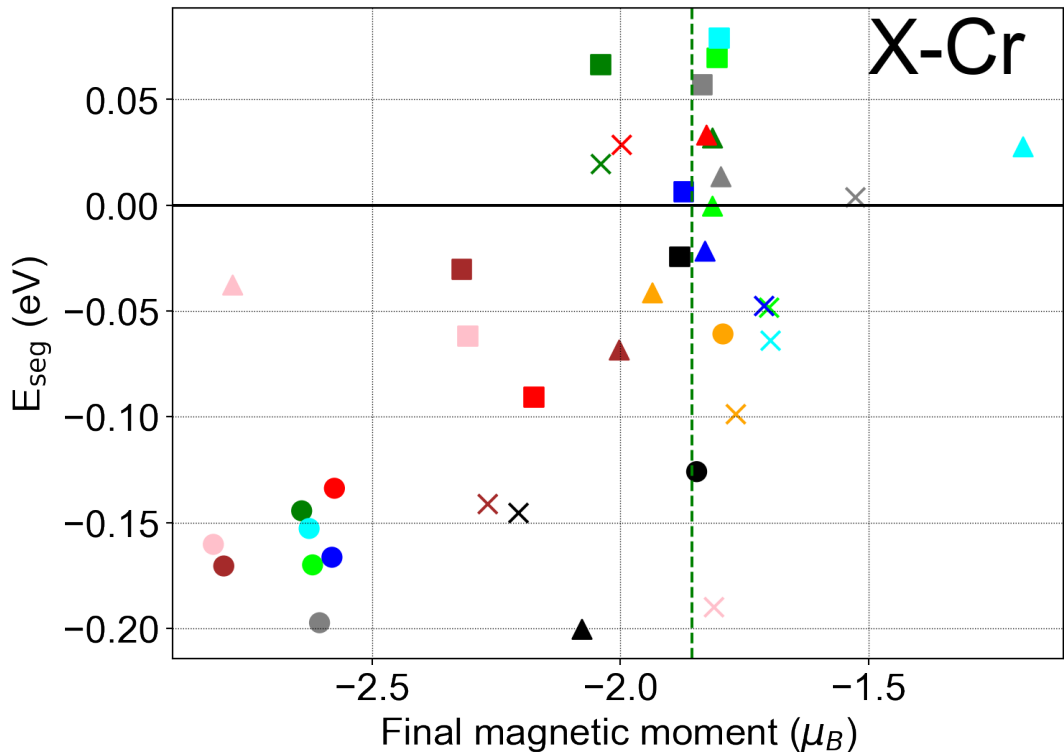


Figure S50: The incremental energy of segregation ($E_{\text{seg}}^{\text{inc}}$) for Cr is plotted against the final magnetic moment of that solute at that site. The coloured dashed line is a reference line indicating the magnetic moment of the solute when in bulk ferrite.

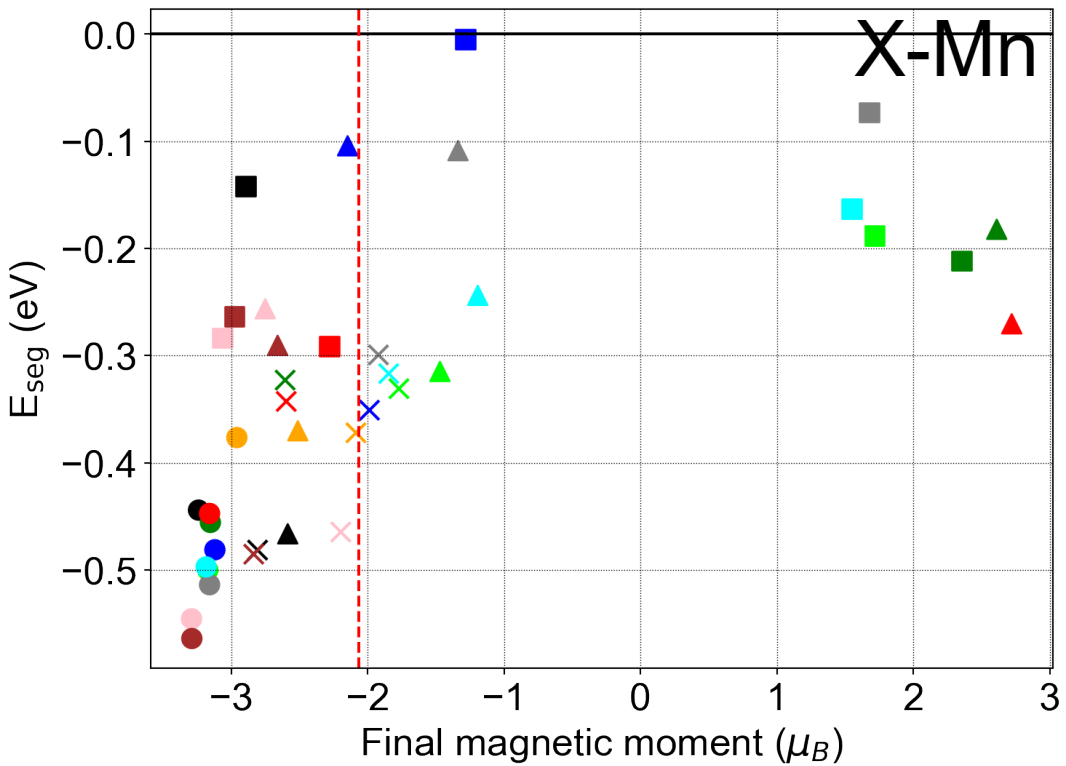


Figure S51: The incremental energy of segregation ($E_{\text{seg}}^{\text{inc}}$) for Mn is plotted against the final magnetic moment of that solute at that site. The coloured dashed line is a reference line indicating the magnetic moment of the solute when in bulk ferrite.

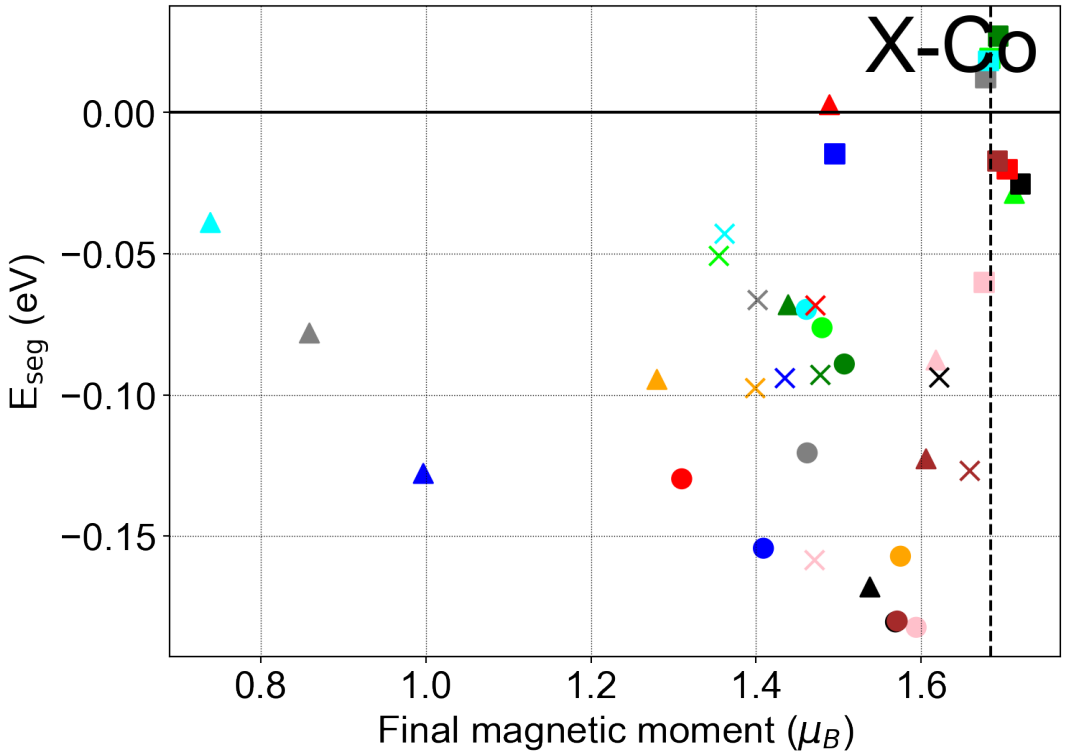


Figure S52: The incremental energy of segregation ($E_{\text{seg}}^{\text{inc}}$) for Co is plotted against the final magnetic moment of that solute at that site. The coloured dashed line is a reference line indicating the magnetic moment of the solute when in bulk ferrite.

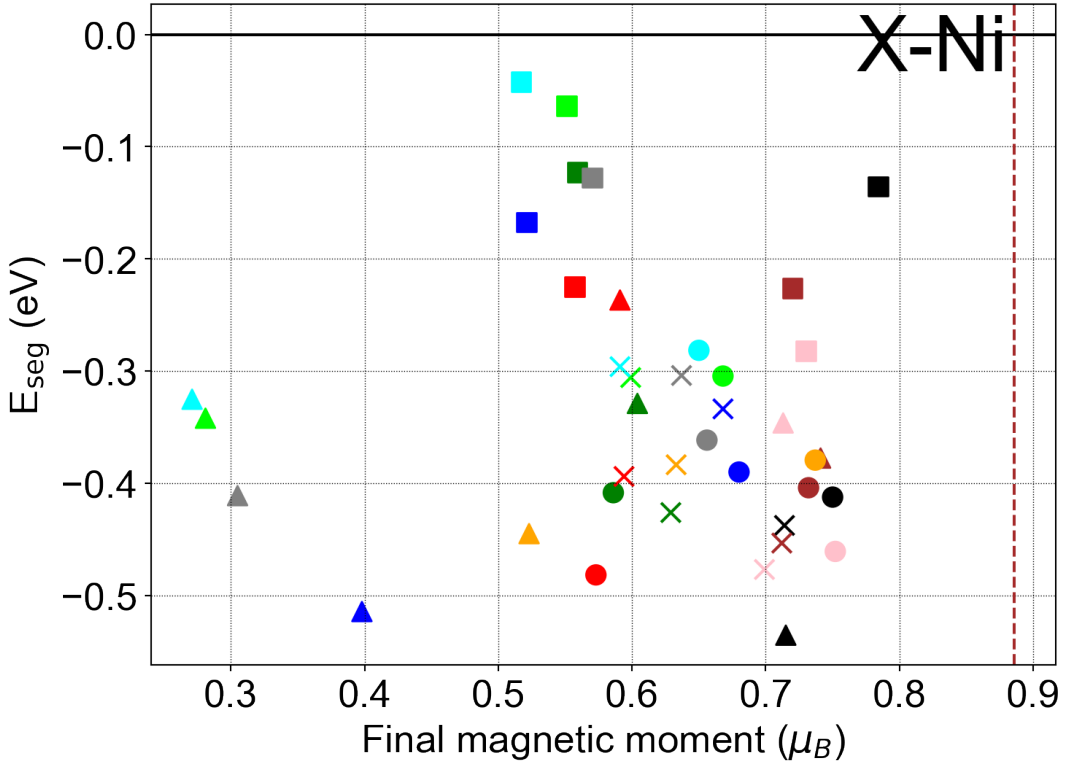


Figure S53: The incremental energy of segregation ($E_{\text{seg}}^{\text{inc}}$) for Ni is plotted against the final magnetic moment of that solute at that site. The coloured dashed line is a reference line indicating the magnetic moment of the solute when in bulk ferrite.

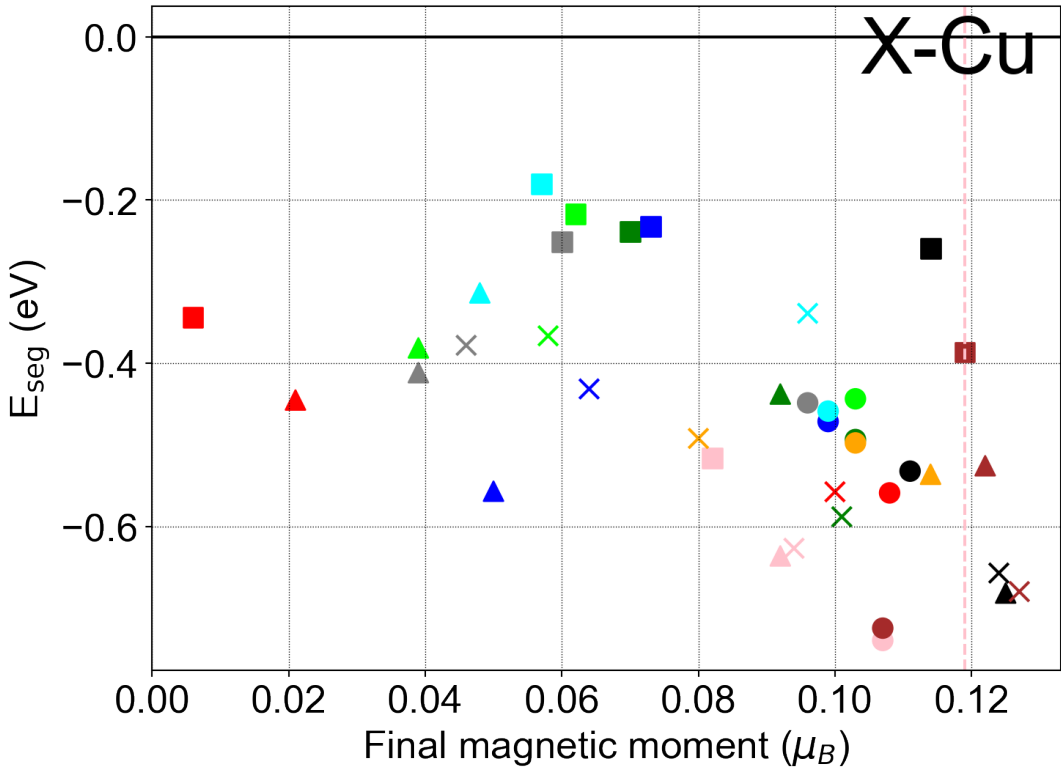


Figure S54: The incremental energy of segregation ($E_{\text{seg}}^{\text{inc}}$) for Cu is plotted against the final magnetic moment of that solute at that site. The coloured dashed line is a reference line indicating the magnetic moment of the solute when in bulk ferrite.

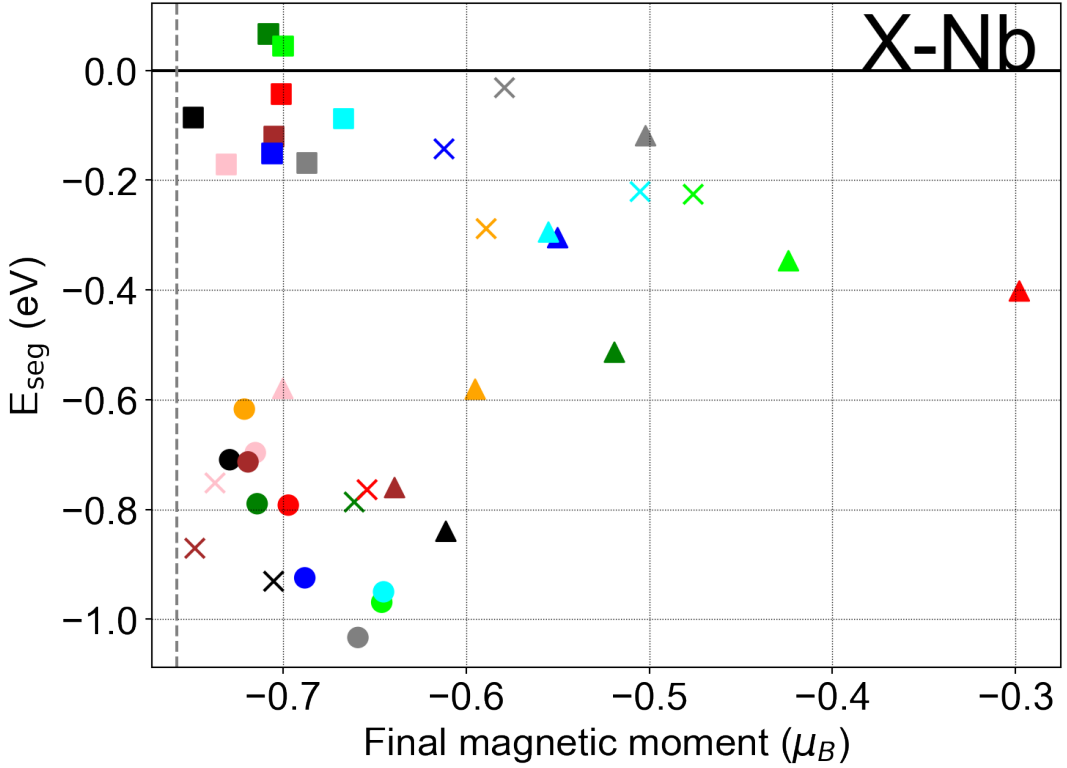


Figure S55: The incremental energy of segregation ($E_{\text{seg}}^{\text{inc}}$) for Nb is plotted against the final magnetic moment of that solute at that site. The coloured dashed line is a reference line indicating the magnetic moment of the solute when in bulk ferrite.

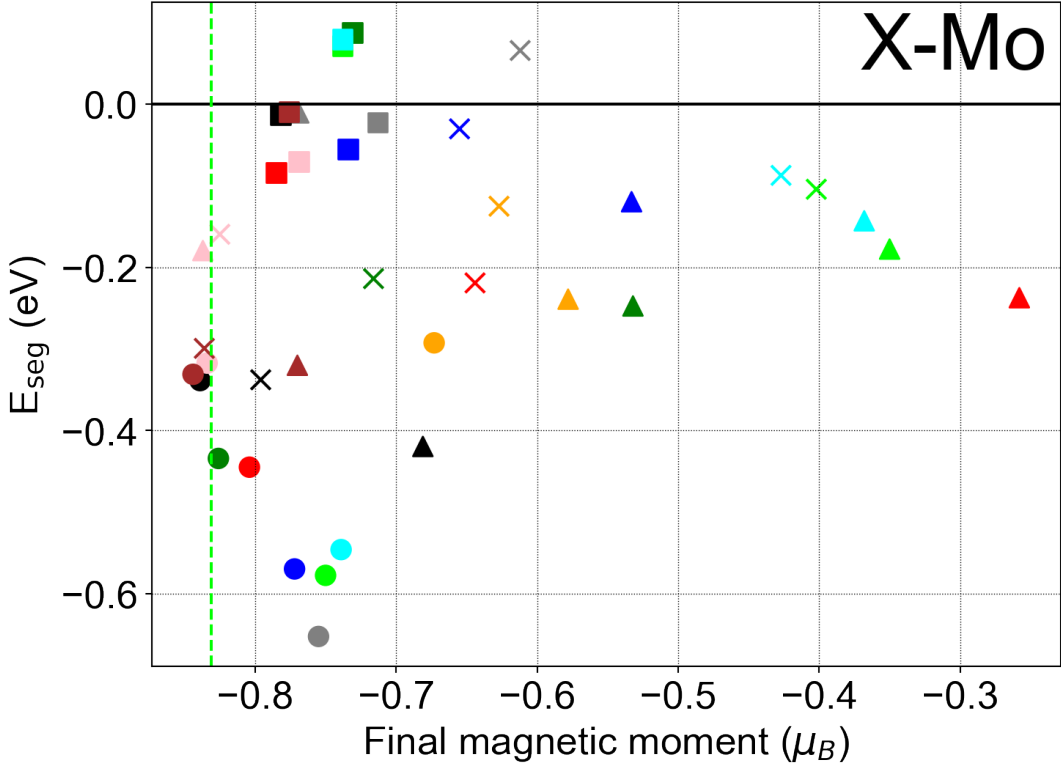


Figure S56: The incremental energy of segregation ($E_{\text{seg}}^{\text{inc}}$) for Mo is plotted against the final magnetic moment of that solute at that site. The coloured dashed line is a reference line indicating the magnetic moment of the solute when in bulk ferrite.

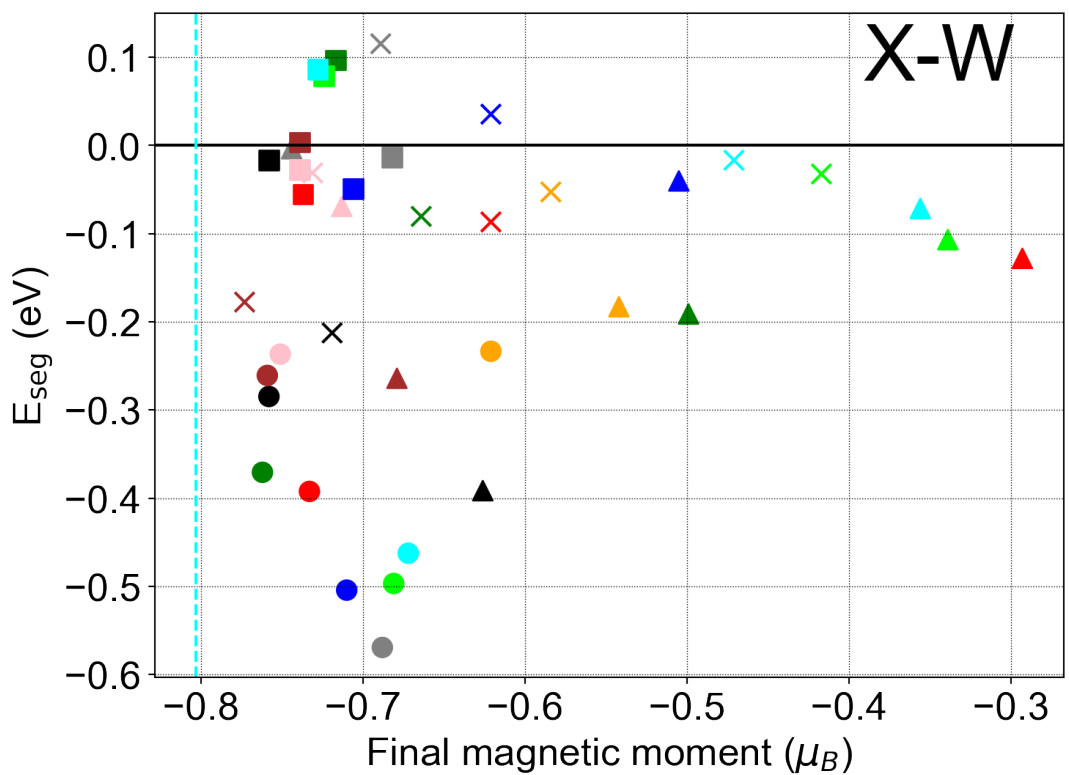


Figure S57: The incremental energy of segregation ($E_{\text{seg}}^{\text{inc}}$) for W is plotted against the final magnetic moment of that solute at that site. The coloured dashed line is a reference line indicating the magnetic moment of the solute when in bulk ferrite.

23.3. Magnetic moment vs Voronoi volume

Here, we plot the magnetic moment (μ_B) of a solute against the final relaxed Voronoi volume occupied by the solute in the co-segregation study (i.e. pair solute segregation study). The plotted data are for the solute in the minimum energy configuration in each ordered elemental pairing, where data is available. Note the schemes used for colours and markers used here are the same as in Fig. 2 in the main text. The colour used here in the marker indicates the element of the prior segregated solute at the GB. The results of this comparison are plotted below, in Figs S58-S67.

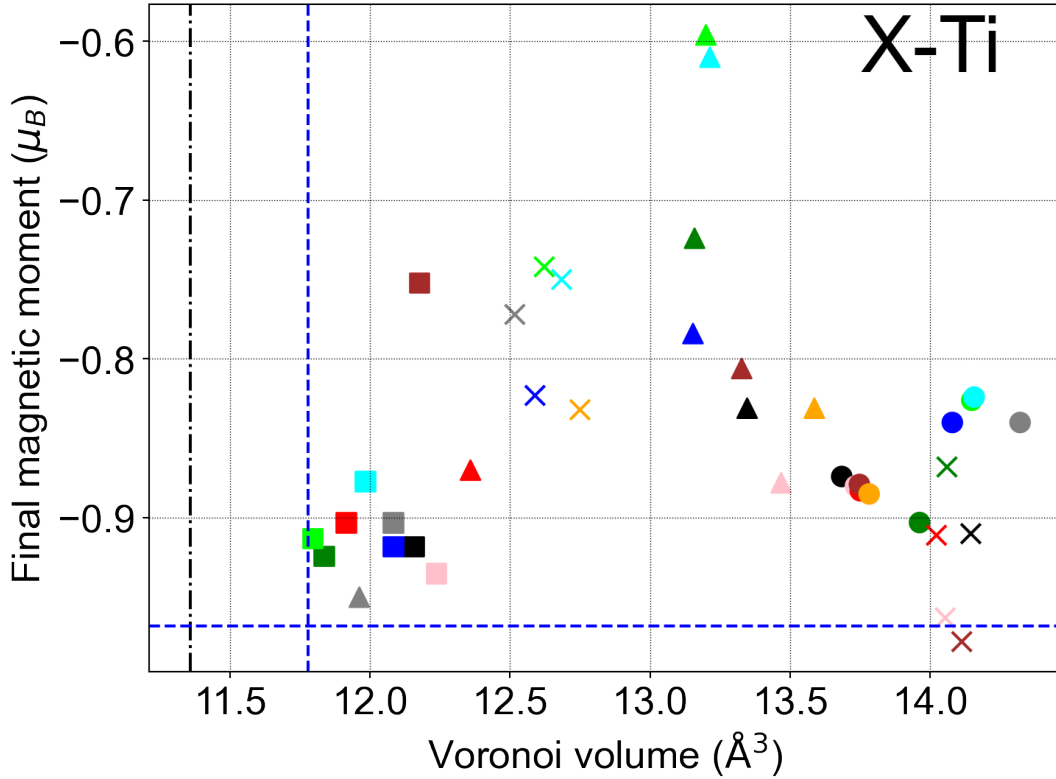


Figure S58: The final magnetic moment (μ_B) for Ti is plotted against the relaxed Voronoi volume occupied by the solute at that site. The black/coloured dashed lines indicate the respective properties for the Fe/solute in the ferrite bulk, respectively.

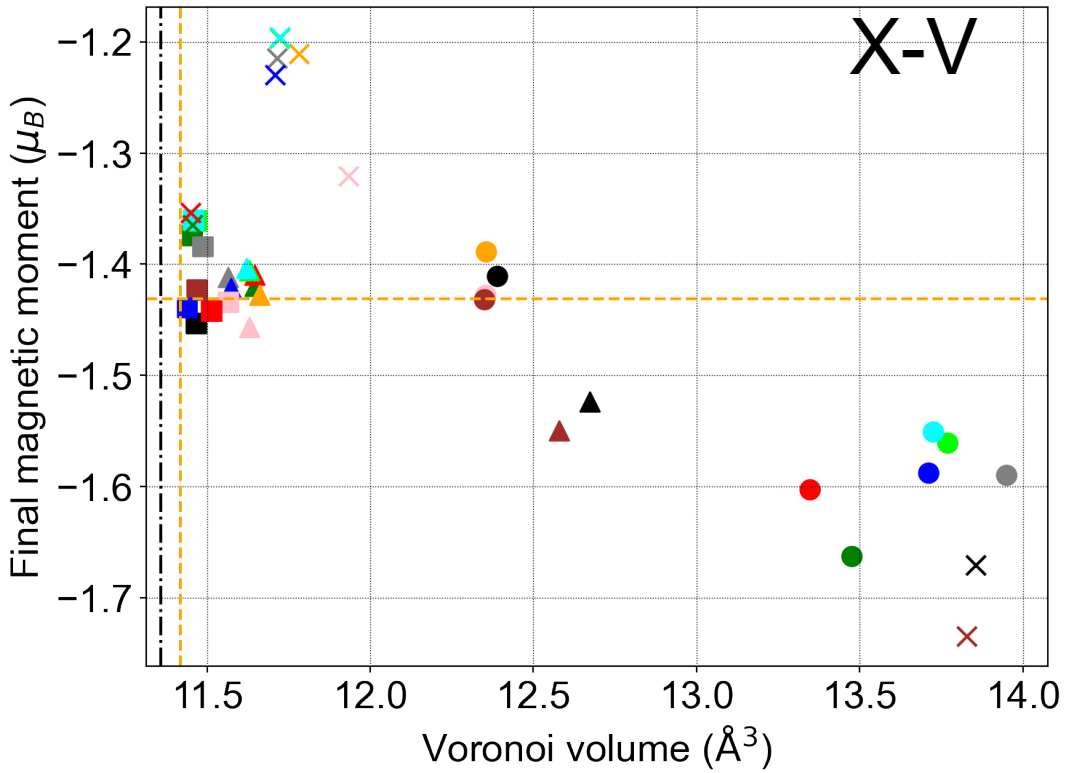


Figure S59: The final magnetic moment (μ_B) for V is plotted against the relaxed Voronoi volume occupied by the solute at that site. The black/coloured dashed lines indicate the respective properties for the Fe/solute in the ferrite bulk, respectively.

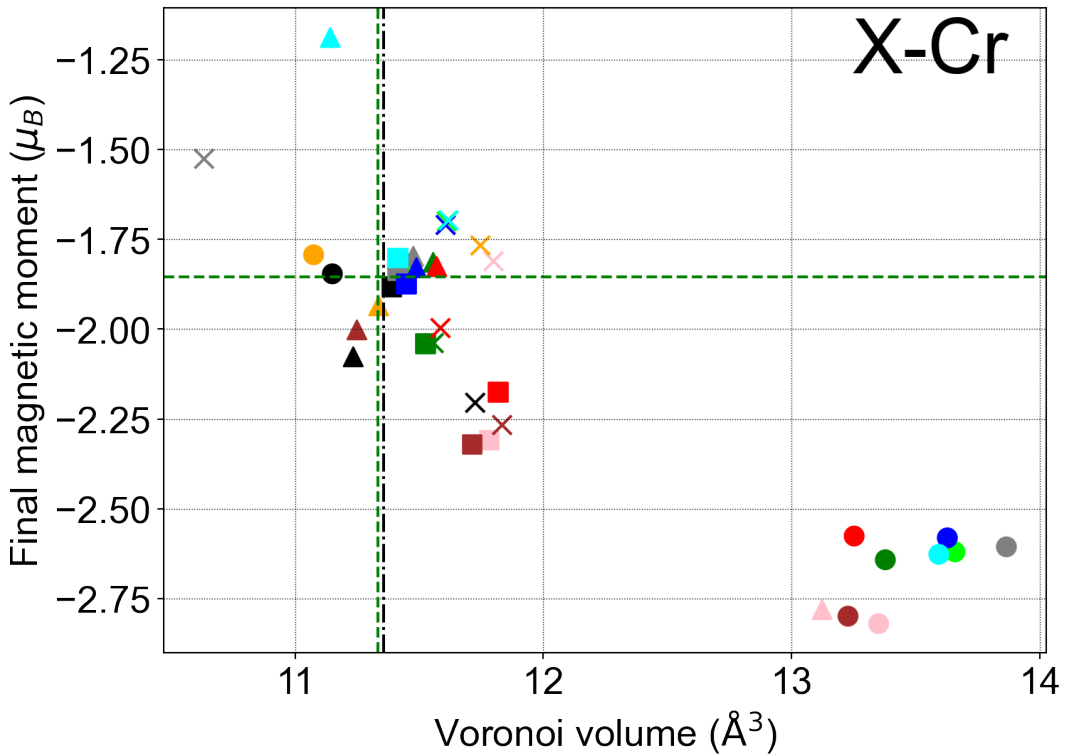


Figure S60: The final magnetic moment (μ_B) for Cr is plotted against the relaxed Voronoi volume occupied by the solute at that site. The black/coloured dashed lines indicate the respective properties for the Fe/solute in the ferrite bulk, respectively.

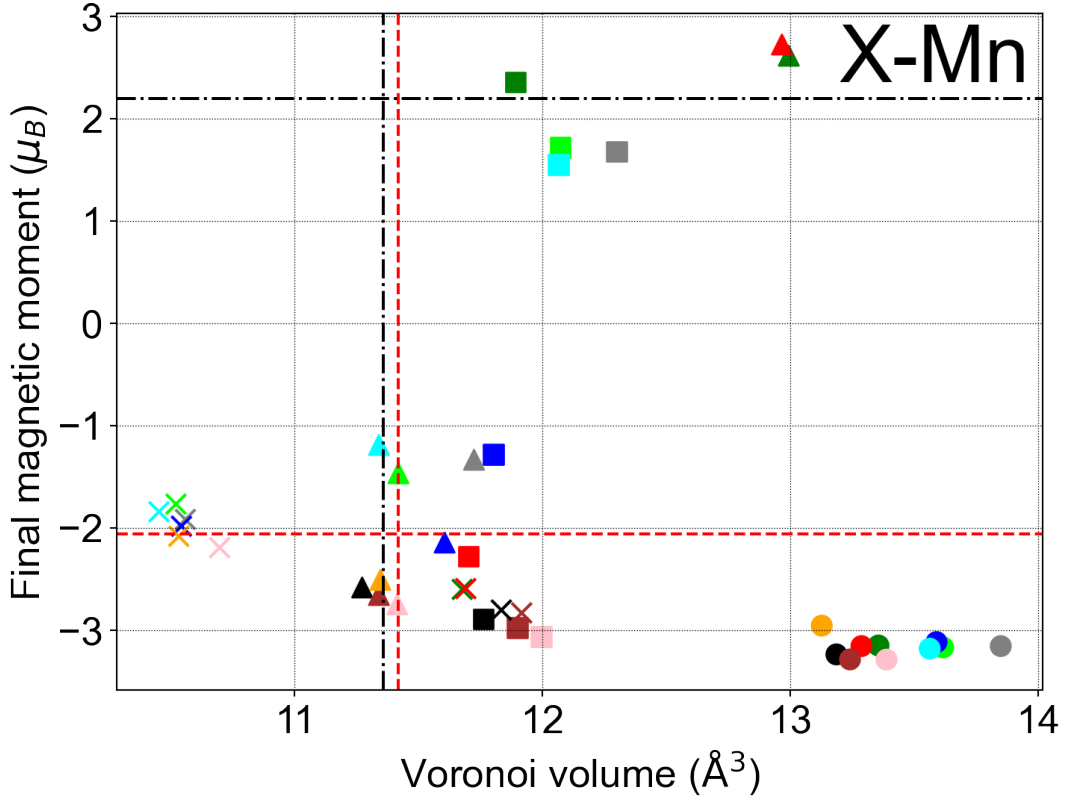


Figure S61: The final magnetic moment (μ_B) for Mn is plotted against the relaxed Voronoi volume occupied by the solute at that site. The black/coloured dashed lines indicate the respective properties for the Fe/solute in the ferrite bulk, respectively.

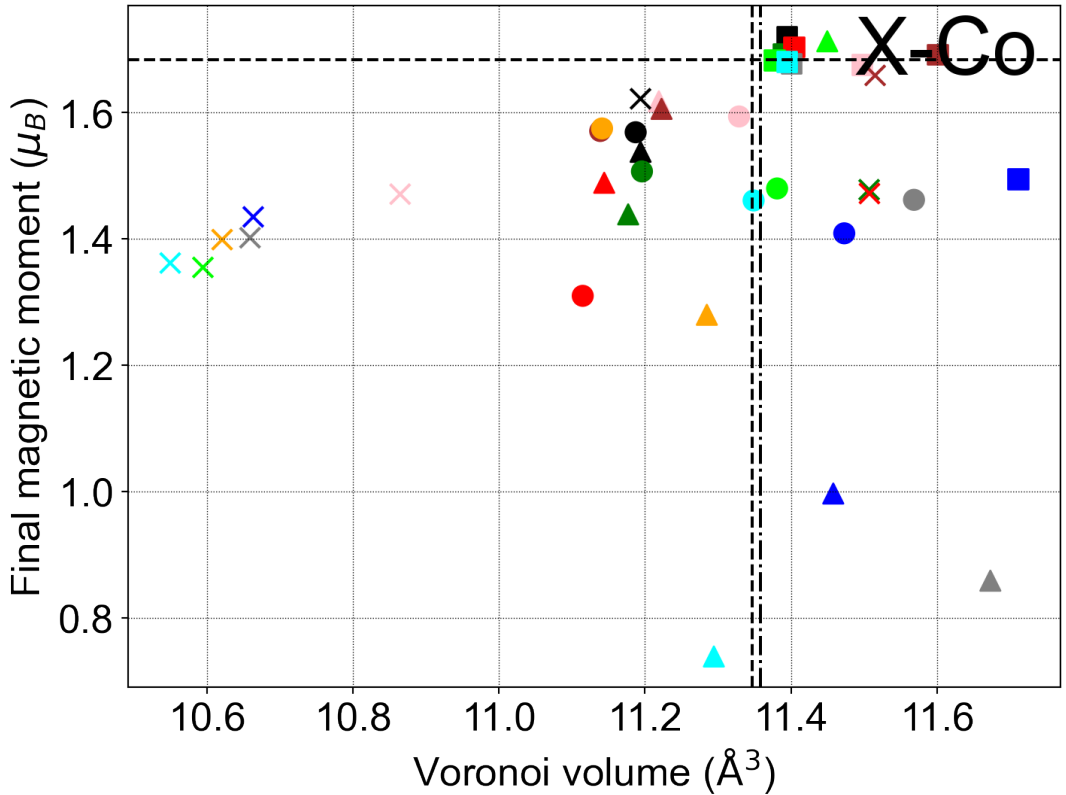


Figure S62: The final magnetic moment (μ_B) for Co is plotted against the relaxed Voronoi volume occupied by the solute at that site. The black/coloured dashed lines indicate the respective bulk properties for the Fe/solute atoms in the bulk, respectively.

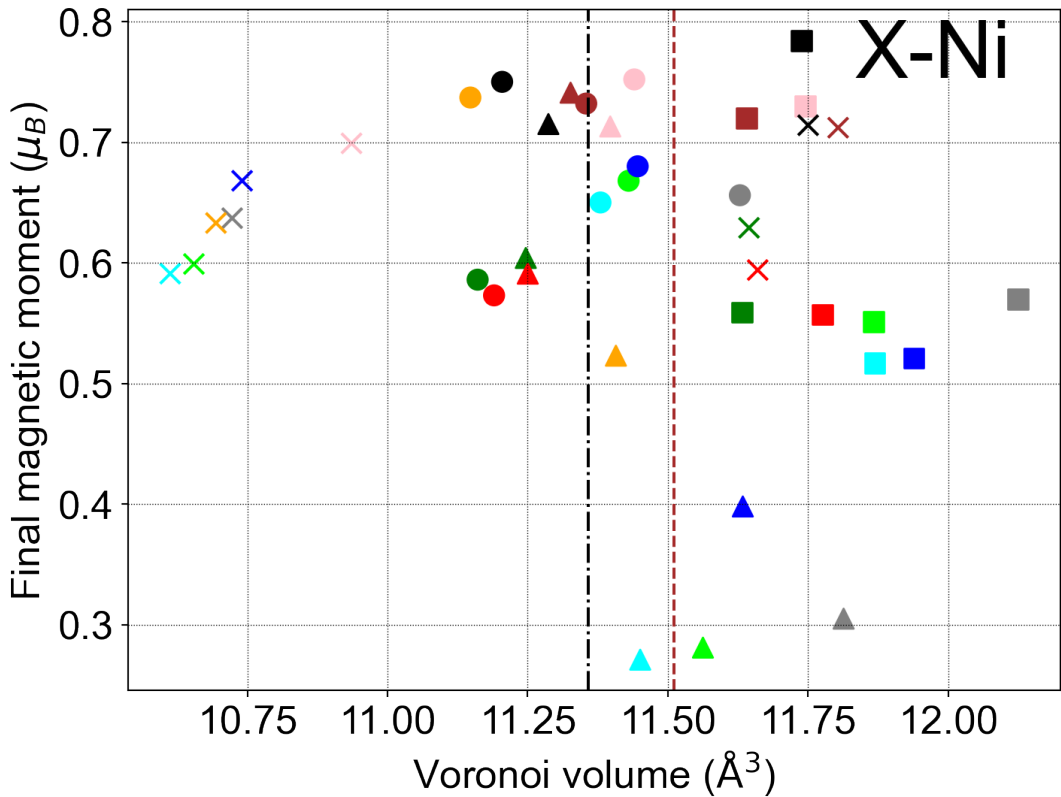


Figure S63: The final magnetic moment (μ_B) for Ni is plotted against the relaxed Voronoi volume occupied by the solute at that site. The black/coloured dashed lines indicate the respective properties for the Fe/solute in the ferrite bulk, respectively.

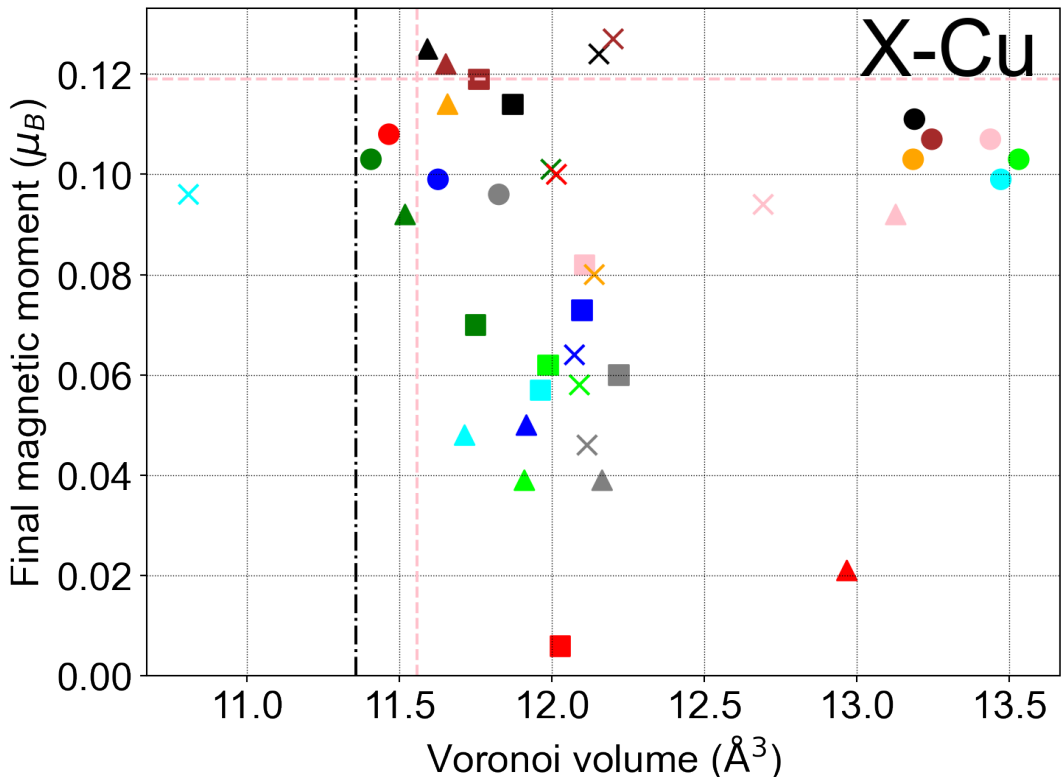


Figure S64: The final magnetic moment (μ_B) for Cu is plotted against the relaxed Voronoi volume occupied by the solute at that site. The black/coloured dashed lines indicate the respective properties for the Fe/solute atoms in the ferrite bulk, respectively.

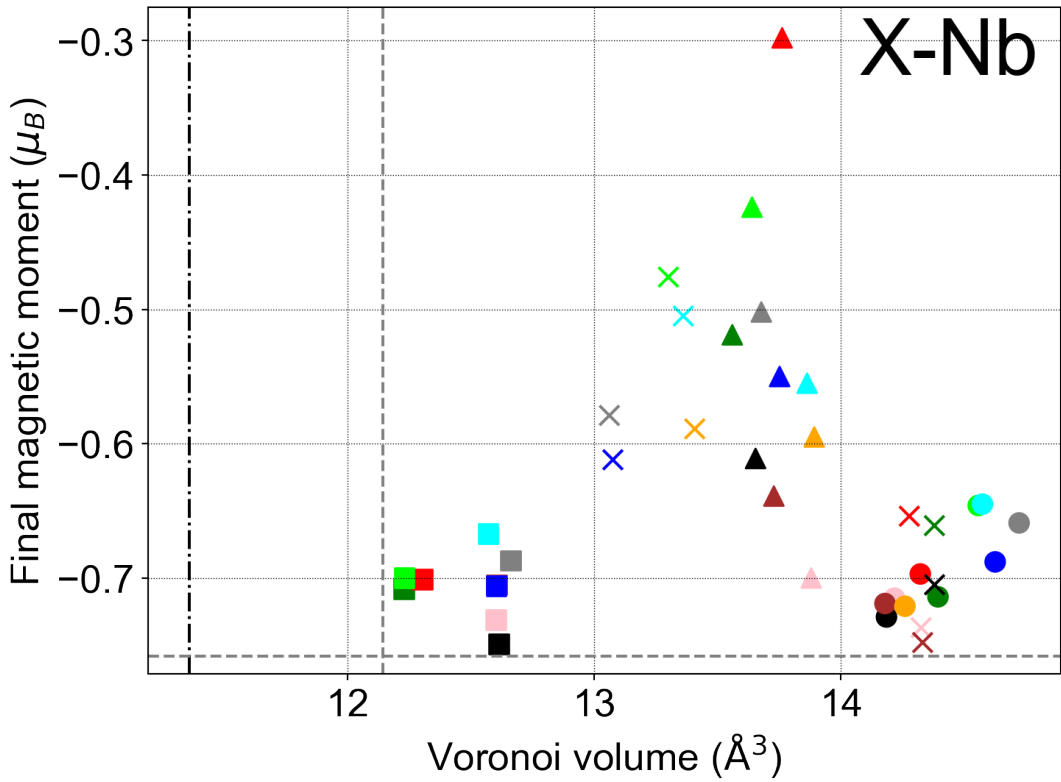


Figure S65: The final magnetic moment (μ_B) for Nb is plotted against the relaxed Voronoi volume occupied by the solute at that site. The black/coloured dashed lines indicate the respective properties for the Fe/solute in the ferrite bulk, respectively.

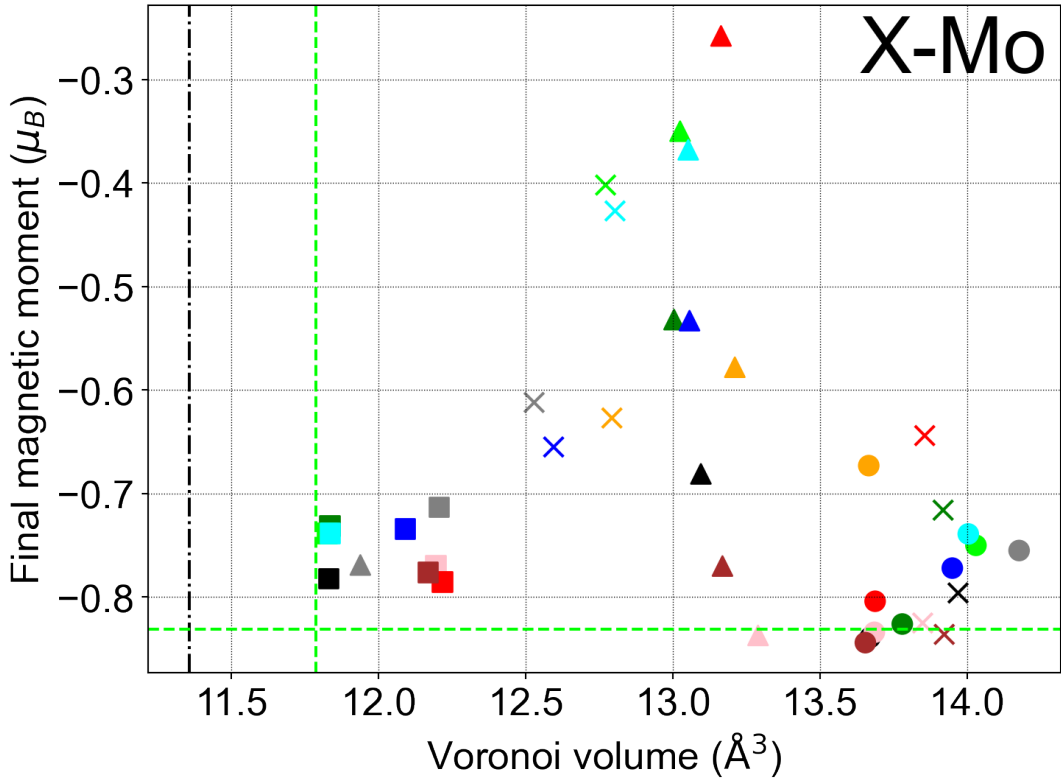


Figure S66: The final magnetic moment (μ_B) for Mo is plotted against the relaxed Voronoi volume occupied by the solute at that site. The black/coloured dashed lines indicate the respective properties for the Fe/solute in the ferrite bulk, respectively.

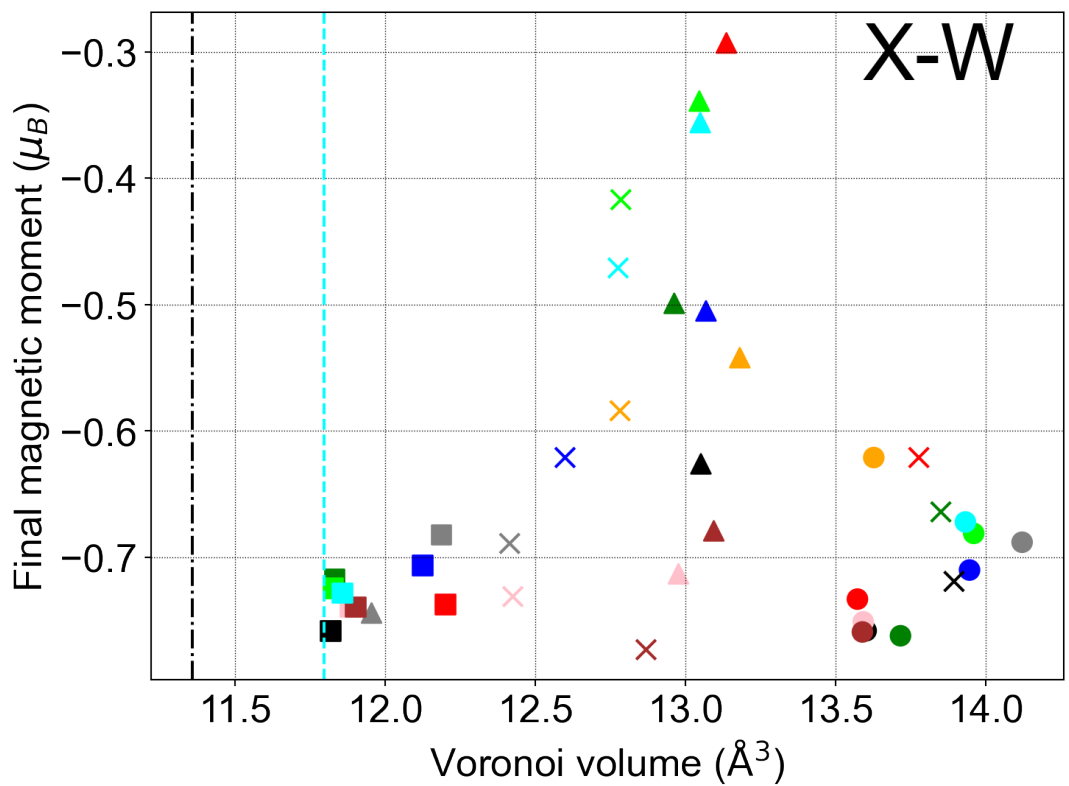


Figure S67: The final magnetic moment (μ_B) for W is plotted against the relaxed Voronoi volume occupied by the solute at that site. The black/coloured dashed lines indicate the respective bulk properties for the Fe/solute atoms in the bulk, respectively.

24. Bond orders vs $W_{\text{sep}}^{\text{RGS}}$

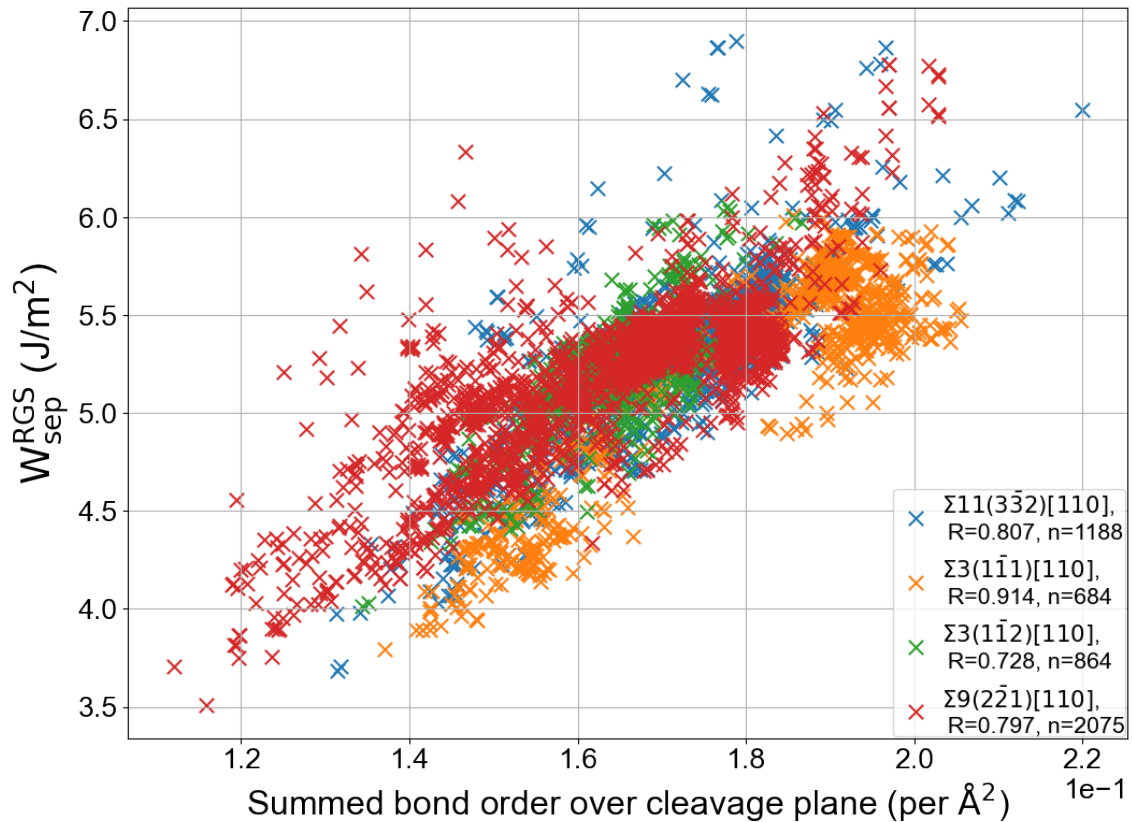


Figure S68: Plots the bond orders against all of the cleavage planes tested in all permutations performed in the study against their corresponding calculated $W_{\text{sep}}^{\text{RGS}}$. This includes values across all cleavage planes in both the 1-solute and 2-solute segregation cases. The correlation coefficients for the GBs range 0.728-0.914, with the overall dataset exhibiting a correlation coefficient of 0.772. For assessing interface cohesion, the quantity of the *minimum* W_{sep} in each case is the most important, which is presented in the text.

25. Bond order data

25.1. Single solute segregation cases

System	W_{sep}^{RGS} (J/m ²)	W_{sep} (J/m ²)	$\sum BO$ (Å ⁻²) DDEC6
Co-34-d-1.1	4.184	3.782	0.1559
Cr-34-d-1.1	4.182	3.871	0.1594
Cr-36-d-0.0	4.265	3.879	0.1545
Cu-34-d-1.1	3.965	3.531	0.1462
Cu-36-d-0.0	3.941	3.524	0.1480
Mn-36-d-0.0	4.331	4.031	0.1538
Mo-36-d-0.0	4.684	4.135	0.1631
Nb-36-d-0.0	4.407	3.980	0.1572
Ni-34-d-1.1	4.128	3.775	0.1502
P-34-d-1.1	3.847	3.599	0.1621
Ti-36-d-0.0	4.193	3.835	0.1539
V-32-d-1.7	4.327	3.925	0.1615
V-36-d-0.0	4.354	3.909	0.1561
W-36-d-0.0	5.013	4.361	0.1690
GB	4.200	3.805	0.1580

Table S51: The cohesion effects for the single-solute segregation cases for the $\Sigma 3(1\bar{1}1)$ GB, calculated in the Rice-Thomson-Wang theory of interfacial embrittlement in the relaxed and rigid calculation methodologies. The corresponding area-normalised summed bond orders calculated in the DDEC6 framework, calculated across the weakest interfacial cleavage plane, as assessed by W_{sep}^{RGS} , are also presented.

System	W_{sep}^{RGS} (J/m ²)	W_{sep} (J/m ²)	$\sum BO$ (Å ⁻²) DDEC6
Co-20-d-2.4	4.930	4.749	0.1546
Co-22-d-1.2	4.945	4.722	0.1531
Cr-24-d-0.0	5.005	4.811	0.1551
Cu-20-d-2.4	4.425	4.217	0.1528
Cu-22-d-1.2	4.474	4.253	0.1520
Cu-24-d-0.0	4.427	4.239	0.1473
Mn-22-d-1.2	5.088	4.889	0.1612
Mn-24-d-0.0	4.962	4.851	0.1593
Mo-24-d-0.0	5.278	5.122	0.1689
Nb-24-d-0.0	4.979	4.672	0.1546
Ni-20-d-2.4	4.687	4.455	0.1522
Ni-22-d-1.2	4.706	4.477	0.1506
Ni-24-d-0.0	4.693	4.466	0.1470
P-20-d-2.4	3.857	3.647	0.1701
P-22-d-1.2	3.921	3.664	0.1612
P-24-d-0.0	3.932	3.661	0.1698
Ti-22-d-1.2	4.983	4.666	0.1625
Ti-24-d-0.0	4.871	4.657	0.1470
V-24-d-0.0	5.139	4.907	0.1549
W-24-d-0.0	5.287	5.130	0.1688
GB	4.880	4.721	0.1547

Table S52: The cohesion effects for the single-solute segregation cases for the $\Sigma 3(1\bar{1}2)$ GB, calculated in the Rice-Thomson-Wang theory of interfacial embrittlement in the relaxed and rigid calculation methodologies. The corresponding area-normalised summed bond orders calculated in the DDEC6 framework, calculated across the weakest interfacial cleavage plane, as assessed by W_{sep}^{RGS} , are also presented.

System	W_{sep}^{RGS} (J/m ²)	W_{sep} (J/m ²)	$\sum BO$ (Å ⁻²) DDEC6
Co-33-d-1.2	4.154	3.599	0.1389
Co-36-d-0.0	4.286	3.719	0.1406
Cr-36-d-0.0	4.406	3.842	0.1432
Cu-33-d-1.2	3.748	3.400	0.1196
Mn-33-d-1.2	4.332	3.863	0.1346
Mn-36-d-0.0	4.638	3.882	0.1451
Mo-34-d-0.0	4.783	3.997	0.1555
Nb-34-d-0.0	4.589	4.038	0.1520
Ni-33-d-1.2	4.032	3.643	0.1218
Ni-36-d-0.0	4.232	3.646	0.1387
P-36-d-0.0	4.162	3.568	0.1478
Ti-34-d-0.0	4.405	3.901	0.1441
V-31-d-2.1	4.156	3.758	0.1366
V-32-d-1.5	4.338	3.869	0.1372
V-34-d-0.0	4.492	3.777	0.1472
W-34-d-0.0	4.967	3.895	0.1493
GB	4.195	3.599	0.1421

Table S53: The cohesion effects for the single-solute segregation cases for the $\Sigma 9(1\bar{1}2)$ GB, calculated in the Rice-Thomson-Wang theory of interfacial embrittlement in the relaxed and rigid calculation methodologies. The corresponding area-normalised summed bond orders calculated in the DDEC6 framework, calculated across the weakest interfacial cleavage plane, as assessed by W_{sep}^{RGS} , are also presented.

System	W_{sep}^{RGS} (J/m ²)	W_{sep} (J/m ²)	$\sum BO$ (Å ⁻²) DDEC6
Co-21-d-0.0	4.433	3.991	0.1515
Cr-21-d-0.0	4.610	4.173	0.1542
Cu-21-d-0.0	4.066	3.670	0.1449
Mn-21-d-0.0	4.882	4.242	0.1562
Mo-19-d-1.5	5.059	4.508	0.1620
Nb-22-d-0.0	4.755	4.405	0.1624
Ni-21-d-0.0	4.378	4.001	0.1491
P-21-d-0.0	3.908	3.453	0.1648
Ti-22-d-0.0	4.527	4.193	0.1534
V-22-d-0.0	4.723	4.176	0.1559
W-22-d-0.0	5.302	4.395	0.1672
GB	4.275	0.1537	3.831

Table S54: The cohesion effects for the single-solute segregation cases for the $\Sigma 11(3\bar{3}2)$ GB, calculated in the Rice-Thomson-Wang theory of interfacial embrittlement in the relaxed and rigid calculation methodologies. The corresponding area-normalised summed bond orders calculated in the DDEC6 framework, calculated across the weakest interfacial cleavage plane, as assessed by W_{sep}^{RGS} , are also presented.

25.2. Summed bond-orders at the minimum RGS cleavage plane $\sum \text{BO}$ (DDEC6) (\AA^{-2})

	Ti	V	Cr	Mn	Co	Ni	Cu	Nb	Mo	W
Ti	0.1458	0.1493	0.1470	0.1465	0.1526	0.1457	0.1408	0.1528	0.1616	0.1675
	0.1469	0.1624	0.1628	0.1682	0.1609	0.1461	0.1505	0.1545	0.1557	0.1560
	0.1393	0.1420	0.1427	0.1476	0.1421	0.1398	0.1246	0.1404	0.1467	0.1528
	0.1449	0.1515	0.1513	0.1577	0.1501	0.1478	0.1451	0.1433	0.1555	0.1592
V	0.1571	0.1631	0.1608	0.1604	0.1585	0.1520	0.1509	0.1615	0.1639	0.1690
	NaN									
	0.1349	0.1398	0.1404	0.1519	0.1453	0.1430	0.1240	0.1294	0.1461	0.1500
	0.1500	0.1494	0.1563	0.1534	0.1452	0.1429	0.1439	0.1572	0.1604	0.1572
Cr	0.1475	0.1527	0.1506	0.1496	0.1518	0.1467	0.1424	0.1570	0.1639	0.1705
	0.1553	0.1555	0.1656	0.1544	0.1550	0.1521	0.1486	0.1567	0.1540	0.1531
	0.1473	0.1343	0.1431	0.1343	0.1297	0.1277	0.1240	0.1549	0.1592	0.1536
	0.1556	0.1493	0.1492	0.1511	0.1469	0.1449	0.1374	0.1637	0.1651	0.1662
Mn	0.1479	0.1520	0.1495	0.1468	0.1547	0.1547	0.1418	0.1551	0.1620	0.1697
	0.1643	0.1598	0.1688	0.1662	0.1606	0.1594	0.1520	0.1743	0.1610	0.1633
	0.1479	0.1359	0.1321	0.1399	0.1335	0.1316	0.1261	0.1560	0.1599	0.1503
	0.1507	0.1571	0.1552	0.1604	0.1603	0.1443	0.1443	0.1668	0.1728	0.1726
Co	0.1529	0.1582	0.1556	0.1551	0.1544	0.1541	0.1465	0.1564	0.1604	0.1657
	0.1606	0.1550	0.1660	0.1605	0.1550	0.1498	0.1505	0.1562	0.1655	0.1655
	0.1420	0.1455	0.1249	0.1339	0.1333	0.1207	0.1197	0.1499	0.1542	0.1491
	0.1502	0.1456	0.1452	0.1503	0.1437	0.1532	0.1424	0.1609	0.1693	0.1657
Ni	0.1459	0.1532	0.1470	0.1549	0.1541	0.1472	0.1424	0.1508	0.1548	0.1600
	0.1454	0.1465	0.1585	0.1514	0.1473	0.1462	0.1426	0.1526	0.1583	0.1532
	0.1402	0.1433	0.1293	0.1331	0.1249	0.1251	0.1195	0.1484	0.1527	0.1317
	0.1491	0.1468	0.1460	0.1460	0.1514	0.1382	0.1313	0.1585	0.1675	0.1631
Cu	0.1416	0.1491	0.1426	0.1427	0.1437	0.1424	0.1370	0.1457	0.1500	0.1556
	0.1459	0.1480	0.1550	0.1430	0.1485	0.1448	0.1344	0.1538	0.1537	0.1491
	0.1236	0.1262	0.1265	0.1347	0.1199	0.1192	0.1158	0.1283	0.1293	0.1244
	0.1455	0.1446	0.1477	0.1388	0.1435	0.1341	0.1314	0.1550	0.1644	0.1534
Nb	0.1508	0.1550	0.1528	0.1517	0.1559	0.1500	0.1454	0.1608	0.1672	0.1739
	0.1551	0.1546	0.1547	0.1547	0.1540	0.1548	0.1544	0.1615	0.1674	0.1678
	0.1458	0.1490	0.1548	0.1559	0.1497	0.1473	0.1292	0.1434	0.1518	0.1456
	0.1612	0.1600	0.1604	0.1663	0.1604	0.1591	0.1556	0.1522	0.1607	0.1599
Mo	0.1578	0.1611	0.1591	0.1581	0.1606	0.1480	0.1522	0.1676	0.1731	0.1979
	0.1622	0.1691	0.1689	0.1651	0.1764	0.1716	0.1661	0.1631	0.1785	0.1783
	0.1457	0.1513	0.1526	0.1596	0.1540	0.1524	0.1302	0.1383	0.1613	0.1620
	0.1556	0.1612	0.1585	0.1658	0.1624	0.1567	0.1464	0.1609	0.1743	0.1735
W	0.1623	0.1664	0.1646	0.1634	0.1661	0.1601	0.1581	0.1720	0.1972	0.1998
	0.1706	0.1693	0.1694	0.1695	0.1693	0.1732	0.1688	0.1660	0.1697	0.1690
	0.1358	0.1541	0.1414	0.1505	0.1491	0.1483	0.1553	0.1394	0.1453	0.1627
	0.1601	0.1682	0.1686	0.1724	0.1654	0.1635	0.1404	0.1564	0.1737	0.1739

Table S55: The area-normalised summed bond orders ($\sum \text{BO}$) are presented in the units of DDEC6 calculated bond orders per unit interface area across all four GBs. The values in each element-element cell are in the order, from top to bottom, $\Sigma 3(1\bar{1}1)[110]$, $\Sigma 3(1\bar{1}2)[110]$, $\Sigma 9(2\bar{2}1)[110]$, $\Sigma 11(3\bar{3}2)[110]$ GBs, respectively. This data was used to plot Fig. 6 in the main text, in combination with the data in Table S41 and S42 for the co-segregation cases.

References

- [1] A. A. Mirzoev, D. A. Mirzaev, A. V. Verkhovykh, Hydrogen–vacancy interactions in ferromagnetic and paramagnetic bcc iron: Ab initio calculations, *physica status solidi (b)* 252 (9) (2015) 1966–1970. doi:[10.1002/pssb.201451757](https://doi.org/10.1002/pssb.201451757).
- [2] M. Yamaguchi, J. Kameda, K.-I. Ebihara, M. Itakura, H. Kaburaki, Mobile effect of hydrogen on intergranular decohesion of iron: First-principles calculations, *Philosophical Magazine* 92 (11) (2012) 1349–1368. doi:[10.1080/14786435.2011.645077](https://doi.org/10.1080/14786435.2011.645077).
- [3] N. Gao, C.-C. Fu, M. Samaras, R. Schäublin, M. Victoria, W. Hoffelner, Multiscale modelling of bi-crystal grain boundaries in bcc iron, *Journal of Nuclear Materials* 385 (2) (2009) 262–267. doi:[10.1016/j.jnucmat.2008.12.016](https://doi.org/10.1016/j.jnucmat.2008.12.016).
- [4] Y.-J. Hu, Y. Wang, W. Y. Wang, K. A. Darling, L. J. Kecskes, Z.-K. Liu, Solute effects on the $\Sigma 3$ 111[11-0] tilt grain boundary in BCC Fe: Grain boundary segregation, stability, and embrittlement, *Computational Materials Science* 171 (2020) 109271. doi:[10.1016/j.commatsci.2019.109271](https://doi.org/10.1016/j.commatsci.2019.109271).
- [5] E. Wachowicz, T. Ossowski, A. Kiejna, Cohesive and magnetic properties of grain boundaries in bcc Fe with Cr additions, *Physical Review B* 81 (9) (2010) 094104. doi:[10.1103/PhysRevB.81.094104](https://doi.org/10.1103/PhysRevB.81.094104).
- [6] J. Wang, G. K. H. Madsen, R. Drautz, Grain boundaries in bcc-Fe: A density-functional theory and tight-binding study, *Modelling and Simulation in Materials Science and Engineering* 26 (2) (2018) 025008. doi:[10.1088/1361-651X/aa9f81](https://doi.org/10.1088/1361-651X/aa9f81).
- [7] Z. Xu, S. Tanaka, M. Kohyama, Grain-boundary segregation of 3d-transition metal solutes in bcc Fe: Ab initio local-energy and d-electron behavior analysis, *Journal of Physics: Condensed Matter* 31 (11) (2019) 115001. doi:[10.1088/1361-648X/aafdf00](https://doi.org/10.1088/1361-648X/aafdf00).
- [8] A. S. Kholtobina, W. Ecker, R. Pippan, V. I. Razumovskiy, Effect of alloying elements on hydrogen enhanced decohesion in bcc iron, *Computational Materials Science* 188 (2021) 110215. doi:[10.1016/j.commatsci.2020.110215](https://doi.org/10.1016/j.commatsci.2020.110215).
- [9] A. S. Kholtobina, R. Pippan, L. Romaner, D. Scheiber, W. Ecker, V. I. Razumovskiy, Hydrogen Trapping in bcc Iron, *Materials* 13 (10) (2020) 2288. doi:[10.3390/ma13102288](https://doi.org/10.3390/ma13102288).
- [10] S. K. Bhattacharya, S. Tanaka, Y. Shiihara, M. Kohyama, Ab initio study of symmetrical tilt grain boundaries in bcc Fe: Structural units, magnetic moments, interfacial bonding, local energy and local stress, *Journal of Physics: Condensed Matter* 25 (13) (2013) 135004. doi:[10.1088/0953-8984/25/13/135004](https://doi.org/10.1088/0953-8984/25/13/135004).

- [11] H. Momida, Y. Asari, Y. Nakamura, Y. Tateyama, T. Ohno, Hydrogen-enhanced vacancy embrittlement of grain boundaries in iron, *Physical Review B* 88 (14) (2013) 144107. doi:10.1103/PhysRevB.88.144107.
- [12] D. Scheiber, R. Pippan, P. Puschnig, L. Romaner, Ab initio calculations of grain boundaries in bcc metals, *Modelling and Simulation in Materials Science and Engineering* 24 (3) (2016) 035013. doi:10.1088/0965-0393/24/3/035013.
- [13] S. K. Bhattacharya, S. Tanaka, Y. Shiihara, M. Kohyama, Ab initio perspective of the ⟨110⟩ symmetrical tilt grain boundaries in bcc Fe: Application of local energy and local stress, *Journal of Materials Science* 49 (11) (2014) 3980–3995. doi:10.1007/s10853-014-8038-1.
- [14] A. A. Guzmán, J. Jeon, A. Hartmaier, R. Janisch, Hydrogen Embrittlement at Cleavage Planes and Grain Boundaries in Bcc Iron—Revisiting the First-Principles Cohesive Zone Model, *Materials* 13 (24) (2020) 5785. doi:10.3390/ma13245785.
- [15] X. Huang, R. Janisch, Partitioning of Interstitial Segregants during Decohesion: A DFT Case Study of the Σ_3 Symmetric Tilt Grain Boundary in Ferritic Steel, *Materials* 12 (18) (2019) 2971. doi:10.3390/ma12182971.
- [16] J. Wang, R. Janisch, G. K. H. Madsen, R. Drautz, First-principles study of carbon segregation in bcc iron symmetrical tilt grain boundaries, *Acta Materialia* 115 (2016) 259–268. doi:10.1016/j.actamat.2016.04.058.
- [17] Y. A. Du, L. Ismer, J. Rogal, T. Hickel, J. Neugebauer, R. Drautz, First-principles study on the interaction of H interstitials with grain boundaries in α - and γ -Fe, *Physical Review B* 84 (14) (2011) 144121. doi:10.1103/PhysRevB.84.144121.
- [18] H. Zheng, X.-G. Li, R. Tran, C. Chen, M. Horton, D. Winston, K. A. Persson, S. P. Ong, Grain boundary properties of elemental metals, *Acta Materialia* 186 (2020) 40–49. doi:10.1016/j.actamat.2019.12.030.
- [19] S. He, W. Ecker, R. Pippan, V. I. Razumovskiy, Hydrogen-enhanced decohesion mechanism of the special $\Sigma_5(012)[100]$ grain boundary in Ni with Mo and C solutes, *Computational Materials Science* 167 (2019) 100–110. doi:10.1016/j.commatsci.2019.05.029.
- [20] H. L. Mai, X.-Y. Cui, D. Scheiber, L. Romaner, S. P. Ringer, An understanding of hydrogen embrittlement in nickel grain boundaries from first principles, *Materials & Design* 212 (2021) 110283. doi:10.1016/j.matdes.2021.110283.

- [21] H. Jin, I. Elfimov, M. Militzer, Study of the interaction of solutes with Σ 5 (013) tilt grain boundaries in iron using density-functional theory, *Journal of Applied Physics* 115 (9) (2014) 093506. doi:10.1063/1.4867400.
- [22] M. Militzer, J. J. Hoyt, N. Provatas, J. Rottler, C. W. Sinclair, H. S. Zurob, Multiscale Modeling of Phase Transformations in Steels, *JOM* 66 (5) (2014) 740–746. doi:10.1007/s11837-014-0919-x.
- [23] M. Yamaguchi, J. Kameda, Multiscale thermodynamic analysis on fracture toughness loss induced by solute segregation in steel, *Philosophical Magazine* 94 (19) (2014) 2131–2149. doi:10.1080/14786435.2014.906757.
- [24] L. Zhong, R. Wu, A. J. Freeman, G. B. Olson, Effects of Mn additions on the P embrittlement of the Fe grain boundary, *Physical Review B* 55 (17) (1997) 11133–11137. doi:10.1103/PhysRevB.55.11133.
- [25] K. Ito, H. Sawada, S. Ogata, First-principles study on the grain boundary embrittlement of bcc-Fe by Mn segregation, *Physical Review Materials* 3 (1) (2019) 013609. doi:10.1103/PhysRevMaterials.3.013609.
- [26] A. P. A. Subramanyam, A. Azócar Guzmán, S. Vincent, A. Hartmaier, R. Janisch, Ab Initio Study of the Combined Effects of Alloying Elements and H on Grain Boundary Cohesion in Ferritic Steels, *Metals* 9 (3) (2019) 291. doi:10.3390/met9030291.
- [27] Z. X. Tian, J. X. Yan, W. Hao, W. Xiao, Effect of alloying additions on the hydrogen-induced grain boundary embrittlement in iron, *Journal of Physics: Condensed Matter* 23 (1) (2010) 015501. doi:10.1088/0953-8984/23/1/015501.
- [28] Z.-Z. Chen, C.-Y. Wang, First-principles study on the effects of co-segregation of Ti, B and O on the cohesion of the α -Fe grain boundary, *Journal of Physics: Condensed Matter* 17 (42) (2005) 6645–6652. doi:10.1088/0953-8984/17/42/005.
- [29] S. Kim, S.-G. Kim, M. F. Horstemeyer, H. Rhee, The effects of Vanadium on the strength of a bcc Fe Σ 3(111)[1-10] grain boundary, arXiv:1201.5915 [cond-mat] (Jan. 2012). arXiv: 1201.5915.
- [30] P. Lejcek, *Grain Boundary Segregation in Metals*, Vol. 136, Springer Science & Business Media, 2010.
- [31] P. Lejček, M. Šob, V. Paidar, Interfacial segregation and grain boundary embrittlement: An overview and critical assessment of experimental data and calculated results, *Progress in Materials Science* 87 (2017) 83–139. doi:10.1016/j.pmatsci.2016.11.001.

- [32] Y. S. Ng, T. T. Tsong, ToF atom-probe fim investigation of surface segregation in dilute alloys, *Surface Science* 78 (2) (1978) 419–438. doi:10.1016/0039-6028(78)90089-4.
- [33] M. Menyhard, C. J. McMahon, On the effect of molybdenum in the embrittlement of phosphorus-doped iron, *Acta Metallurgica* 37 (8) (1989) 2287–2295. doi:10.1016/0001-6160(89)90156-9.
- [34] J. Wu, S. H. Song, L. Q. Weng, T. H. Xi, Z. X. Yuan, An Auger electron spectroscopy study of phosphorus and molybdenum grain boundary segregation in a 2.25Cr1Mo steel, *Materials Characterization* 59 (3) (2008) 261–265. doi:10.1016/j.matchar.2007.01.003.
- [35] N. Maruyama, G. D. W. Smith, A. Cerezo, Interaction of the solute niobium or molybdenum with grain boundaries in α -iron, *Materials Science and Engineering: A* 353 (1) (2003) 126–132. doi:10.1016/S0921-5093(02)00678-0.
- [36] P. Lejček, J. Pokluda, P. Šandera, J. Horníková, M. Jenko, Solute segregation at $46.8^\circ(111)$ twist grain boundary of a phosphorus doped Fe–2.3%V alloy, *Surface Science* 606 (3) (2012) 258–262. doi:10.1016/j.susc.2011.10.002.
- [37] D. Scheiber, L. Romaner, R. Pippan, P. Puschnig, Impact of solute-solute interactions on grain boundary segregation and cohesion in molybdenum, *Physical Review Materials* 2 (9) (2018) 093609. doi:10.1103/PhysRevMaterials.2.093609.
- [38] C.-X. Li, S.-H. Dang, L.-P. Wang, C.-L. Zhang, P.-D. Han, Effect of Cr, Mo, and Nb additions on intergranular cohesion of ferritic stainless steel: First-principles determination, *Chinese Physics B* 23 (3) (2014) 037102. doi:10.1088/1674-1056/23/3/037102.
- [39] M. Yuasa, M. Mabuchi, First-principles study in Fe grain boundary with Al segregation: Variation in electronic structures with straining, *Philosophical Magazine* 93 (6) (2013) 635–647. doi:10.1080/14786435.2012.726749.
- [40] M. Yuasa, M. Mabuchi, Effects of segregated Cu on an Fe grain boundary by first-principles tensile tests, *Journal of Physics: Condensed Matter* 22 (50) (2010) 505705. doi:10.1088/0953-8984/22/50/505705.
- [41] J.-X. Shang, X.-D. Zhao, F.-H. Wang, C.-Y. Wang, H.-B. Xu, Effects of Co and Cr on bcc Fe grain boundaries cohesion from first-principles study, *Computational Materials Science* 38 (1) (2006) 217–222. doi:10.1016/j.commatsci.2006.02.010.
- [42] W. T. Geng, A. J. Freeman, R. Wu, G. B. Olson, Effect of Mo and Pd on the grain-boundary cohesion of Fe, *Physical Review B* 62 (10) (2000) 6208–6214. doi:10.1103/PhysRevB.62.6208.

- [43] M. Yuasa, M. Hakamada, Y. Chino, M. Mabuchi, First-principles Study of Hydrogen-induced Embrittlement in Fe Grain Boundary with Cr Segregation, *ISIJ International* 55 (5) (2015) 1131–1134. doi:10.2355/isijinternational.55.1131.
- [44] Li Chunxia, Dang Suihu, Han Peide, First-principles study on the effects of co-segregation of Al, Cr on the cohesion of the α -Fe grain boundary, *Journal of Atomic and Molecular Physics* 31 (3) (2014) 470–474.
- [45] W. T. Geng, A. J. Freeman, G. B. Olson, Influence of alloying additions on grain boundary cohesion of transition metals: First-principles determination and its phenomenological extension, *Physical Review B* 63 (16) (2001) 165415. doi:10.1103/PhysRevB.63.165415.
- [46] J.-X. Shang, C.-Y. Wang, Electronic effects of alloying elements Nb and V on body-centred-cubic Fe grain boundary cohesion, *Journal of Physics: Condensed Matter* 13 (42) (2001) 9635–9644. doi:10.1088/0953-8984/13/42/320.
- [47] J.-X. Shang, X.-D. Zhao, C.-Y. Wang, Effect of titanium on bcc Fe grain boundary cohesion, *Acta Metallurgica Sinica* 37 (8) (2001) 893–896.
- [48] T. Moriya, Ferro- and Antiferromagnetism of Transition Metals and Alloys, *Progress of Theoretical Physics* 33 (2) (1965) 157–183. doi:10.1143/PTP.33.157.
- [49] P. Olsson, T. P. C. Klaver, C. Domain, Ab initio study of solute transition-metal interactions with point defects in bcc Fe, *Physical Review B* 81 (5) (2010) 054102. doi:10.1103/PhysRevB.81.054102.